Université du Québec
Institut National de la Recherche Scientifique
Centre Énergie Matériaux Télécommunications

Study and Design of Frequency Selective Surfaces and their Applications for Beam-Switching Antennas with Gain Enhancement

Par

Ghada Hussain Elzwawi

Thése présentée pour l'obtention du grade de
Philosophiae doctor, Ph.D.
en télécommunications

Jury d'évaluation

Examinateur externe	Prof. Chan-Wang Park Université de Québec à Rimouski
Examinateur externe	Prof. Khelifa Hettak Communications Research Centre (CRC)
Examinateur interne	Prof. Serioja Ovidiu Tatu INRS- EMT
Directeur de recherche	Prof. Tayeb A. Denidni INRS-EMT

ACKNOWLEDGEMENT

I would like to express my sincere gratitude to my research supervisor Prof. Tayeb A. Denidni for his vital support and sound advice he rendered throughout my Ph.D. period and all research activities associated therein.

My deep appreciation and gratitude to the government of my beloved country for sponsoring me during my Ph.D. study.

I deeply indebted to my beloved parents and siblings especially my dear brother Wael and sister Hifa for their unlimited encouragement, constant moral, and financial support.

I am so thankful to my dear Fiance, Othman Berrwin for being with me in the same boat, sharing me my ups and downs through rough seas and calms, and patiently supporting me in every way.

My deep appreciation is to all my colleagues at INRS-EMT especially Dr. Arun Kesavan for his generous help and constructive discussions.

ABSTRACT

This dissertation proposes new active frequency selective surface (AFSS) elements. These unit cells have simple structures and can convert the omnidirectional radiation pattern of the antenna source into a directional one to enhance the gain and forming a new class of beam-switching antennas.

A new switched beamforming antenna using a novel active triangular frequency selective surfaces (ATFSSs) is introduced. This design consists of a source of electromagnetic waves (EM waves) and a novel active triangular frequency selective surface (ATFSS) surrounding the source. By switching the embedded pin-diode between ON and OFF the omnidirectional radiation pattern of the source will be converted into a directional one. By using this design, the main beam can be steered in different directions in the azimuth plane with 120º radiation beamwidth.

A novel corner-reflector antenna with a tunable gain based on AFSSs is proposed. This structure contains a dipole antenna as a source with an omnidirectional radiation pattern, and three reconfigurable AFSS layers with different sizes. The AFSS layers are arranged on the same side of the dipole and form a corner reflector. By using this design, the omnidirectional radiation pattern of the source can be converted into a directional radiation pattern with a tunable gain. To our best knowledge, it is the first time to propose a corner-reflector antenna with a tunable and variable gain directional pattern.

A reconfigurable reflector antenna with beam-tilting capability (RRA) operating in the WLAN band is also presented. An array of AFSS elements and a WLAN-band patch antenna are used to design this structure. A mechanical beam tilting technique is also applied to the proposed antenna. This technique has the ability to tilt the main beam without adding any extra layers or setups to the main structure. As far as we know, this structure is the first design where AFSS is used to provide the beam reconfigurability when AFSS is arranged in a parabolic shape.

To validate the concept of all the proposed antennas, the prototypes of these antennas are fabricated and measured. A good agreement between simulations and measurements in terms of beam directions, reflection coefficient, and gain has been achieved.

TABLE OF CONTENTS

Acknowledgement ..... **II**

Abstract ..... **III**

Table of Contents ..... **IV**

List of Tables ..... **VIII**

List of Figures ..... **IX**

List of Abbreviations ..... **XIV**

1. Chapter one: introduction **1**

1.1 Motivation 1

1.2 Problem identification 2

1.3 Research objectives 2

1.4 Organization of the thesis 2

1.5 List of publications 4

1.6 Awards 6

1.7 Affiliations 6

2. Chapter two: Frequency selective surface **7**

2.1 Introduction 7

2.2 Filtering characteristics of FSS 7

2.3 Design parameters of FSS 8

2.3.1 FSS elements' types 8

2.3.2 Dielectric loading 9

2.3.3 Periodic array lattice and grating lobe responses 10

2.4 FSS applications 10

2.4.1 Traditional applications 10

2.4.2 More recent applications 11

2.5 Conclusion 12

3. Chapter three: Reconfigurable antennas **13**

3.1 Introduction 13

3.1.1 Frequency reconfigurable antennas 13

3.1.2 Polarization reconfigurable antennas 15

3.1.3 Radiation pattern reconfigurable antennas 16
3.2 Conclusion 17
4. Chapter four (Article 1): Frequency Selective Surface-Based Switched-Beamforming Antenna…. 18
4.1 Abstract 18
4.2 Index terms 18
4.3 Introduction 18
4.4 Switched-beamforming antenna design 20
4.4.1 ATFSS element design 21
4.4.2 Feed design 25
4.4.3 Switched beamforming antenna 27
4.4.4 Swithed beamforming antenna design using dipole as a source. 28
4.5 Fabrication and measurement results 34
4.6 Conclusion 38
4.7 References 38
5. Chapter five (Article 2): A New Corner-Reflector Antenna with Tunable Gain Based on Active Frequency Selective Surfaces 40
5.1 Abstract 40
5.2 Index terms 40
5.3 Introduction 41
5.4 Design of AFSS unit-cell 42
5.5 Design and operational mechanism of the proposed antenna 44
5.5.1 Design of the Proposed Antenna 44
5.5.2 The Operating Mechanism of the Proposed Anten 46
5.5.2.1 Case-I (ON-OFF-OFF State) 47
5.5.2.2 Case-II (OFF-ON-OFF State) 48
5.5.2.3 Case-III (OFF-OFF-ON State) 48
5.6 Fabrication and measurement results 50
5.7 Conclusion 54
5.8 References 55
6. Chapter six (Article 3): Reconfigurable Reflector Antenna with Beam-Tilting Capability 58
6.1 Abstract 58
6.2 Keywords 58
6.3 Introduction 59

6.4 Design of an Active FSS Unit Cell 61
6.5 Reconfigurable Reflector Antenna Design 63
6.5.1 Feed Design 63
6.5.2 RR Surface Design 65
6.6 Beam-tilting mechanism of the proposed RRA 65
6.7 Prototyping and Measurement Results 68
6.8 Conclusion 72
6.9 References 73
7. Chapter seven: Conclusion and Future Work 76
7.1 Conclusion 76
7.2 Future work 77
8. Chapter eight: RÉSUMÉ 79
8.1 Introduction 79
8.2 Motivation 79
8.3 Identification des problèmes 80
8.4 Objectifs de la recherche 80
8.5 Antenne à formation de faisceaux commutée basée sur des surfaces sélectives en fréquence 81
8.5.1 Conception d'élements ATFSS 81
8.5.2 Conception d'une antenne à formation de faisceau commutée 83
8.5.3 Le mécanisme opérationnel de l'antenne à formation de faisceaux commutée 85
8.5.4 Résultats de la fabrication et des mesures 85
8.6 Une nouvelle antenne à réflecteur en coin avec un gain accordable basé sur des surfaces actives sélectives en fréquence 89
8.6.1 Conception de la cellule unitaire AFSS 90
8.6.2 Conception de l'antenne 92
8.7 Mécanisme de fonctionnement de l'antenne 92
8.7.1 Résultats de la fabrication et des mesures 94
8.8 Antenne à réflecteur reconfigurable à inclinaison de faisceau, basée sur des surfaces actives sélectives en fréquence 97
8.8.1 Conception d'une cellule unitaire FSS active 98
8.8.2 Conception d'une antenne à réflecteur reconfigurable 99
8.8.3 Conception de l'alimentation 99
8.8.4 Conception de la surface RR 101

8.9 Mécanisme d'inclinaison du faisceau de l'RRA ……..……..102
8.10 Prototype et résultats de mesures ……..……..102
8.11 Conclusion ……..……..106
8.12 Travaux futurs……..……..108
References 109

LIST OF TABLES

Table 4.1: The proposed ATFSS element design…….....….....22

Table 4.2: The feed dimensions…….....26

Table 4.3: Simulated gain comparison in three used combinations along with the dipole used as a source (at 5.8GHz). ……..……...……..…….....….....33

Table 4.4: Gain comparison in three used combinations along with the patch used as a source (at 5.8 GHz). ……..……..……...……..…...…….....37

Table 5.1: Dimension of the improved AFSS unit cell……..……...…..…….…….....43

Table 5.2: The simulated and measured gain of the proposed antenna……..…….....…..…….…….....53

Table 5.3: Comparison of the proposed design with previous works. ……..……...…….…….....54

Table 6.1: Comparison of the proposed antenna performance with recent publications……..……....72

Table 8.1: Les dimensions de l'élément ATFSS proposé..……...……..……...…….....82

Table 8.2: Dimension de la cellule unitaire AFSS améliorée. ……...…….....91

LIST OF FIGURES

Figure 2.1: The frequency response of the FSS……..….....7

Figure 2.2: FSS element types……..…….....9

Figure 2.3: FSS symmetry……..……..…….....10

Figure 2.4: Sketch diagram of FSS works as a sub-reflector…….….....11

Figure 2.5: Designing a reconfigurable pattern antenna by using AFSS ……..…….….....11

Figure 3.1: (a) Designing a reconfigurable bow-tie antenna using pin-diodes (b) equivalent circuit of the biasing circuit ……..…….....14

Figure 3.2: Different configurations of a mechanical frequency reconfigurable antenna…….....15

Figure 3.3: Designing of a single-feed polarization reconfigurable antenna……..….....16

Figure.3.4. Using AFSS IN designing a reconfigurable pattern antenna……..…….….....17

Figure 4.1. Basic principle of the AFSS in two diode states: (a) reflection, (b) transmission…….….....20

Figure 4.2. The proposed AFSS element with an equivalent circuit model of the diode's ON/OFF states…….....21

Figure 4.3. Scattering characteristics of the proposed unit cell in diode's ON/OFF states: (a), (b) The effect of dielectric permittivity, (c), (d) The impact of the substrate thickness, and (e) reflection and transmission coefficients of the proposed element. ……..…….....23

Figure 4.4. Effect of element size on the scattering performance in diode's ON states..…….....24

Figure 4.5. Effect of radiating patch size on the scattering performance in diode's ON states. …….....24

Figure 4.6. Near field analysis on the proposed AFSS element surface: reflection state. (b) transmission state.……..…….....25

Figure 4.7. Simulated and fabricated feed antenna model to excite ATFSS elements. …..…….....26

Figure 4. 8. Simulated and measured reflection coefficient of the feed. …….....26

Figure 4.9. Simulated and measured radiation patterns in the H plane of the monopole patch antenna.....27

Figure 4.10. Simulated model of the proposed ATFSS antenna in, top and side 3-D view.....28

Figure 4. 11. Sketch of the proposed ATFSS antenna, (a) with multiple combinations of the diodes for steering the beam in various directions, and (b) the simulation results in each combination.....29

Figure 4.12. Effect of feed offset 'd1' in 'Combination C' on the simulated reflection coefficient.....30

Figure 4.13. Effect of feed offset 'd1' in 'Combination C' on the simulated realized gain. 30

Figure 4.14. Effect of feed offset 'd1' in 'Combination C' on the simulated radiation patterns in H-plane.....31

Figure 4.15. Top view of the proposed active triangular FSS antenna using dipole as a source of EM waves. 31

Figure 4.16. Simulated reflection coefficient of the proposed ATFSS antenna. 32

Figure 4.17. Simulated gain of the proposed ATFSS antenna. 32

Figure 4.18. Simulated radiation pattern of the proposed switched beamforming ATFSS antenna with dipole feed (in combination C). 33

Figure 4.19. Prototyping steps and measurement picture of the fabricated ATFSS antenna in an anechoic chamber.....35

Figure 4. 20. Simulated and measured reflection coefficient of the proposed switched beamforming ATFSS antenna.....36

Figure 4. 21. Simulated and measured gain of the proposed switched beamforming ATFSS antenna. 36

Figure 4.22. Simulated and measured radiation patterns of the proposed switched beamforming ATFSS antenna (in combination C).....37

Figure 5. 1. (a) Structure of the proposed AFSS unit-cell, (b) equivalent circuit of the diode's ON/OFF states, (c) configuration of the AFSS element simulation. 43

Figure 5. 2. Simulated scattering parameters of the proposed unit-cell under normal and oblique wave incidence (Ψ/2=30º).....44

Figure 5. 3. Sketch of the proposed antenna. (a) top view, and (b) side 3-D view. 45

Figure 5. 4. Operational mechanism of the proposed antenna, (a) Case-I (ON-OFF-OFF State), (b) Case-II (OFF-ON-OFF State), (C) Case-III (OFF-OFF-ON State). 46

Figure 5. 5. Effect of feeding space (Fp), and rotating angle of the AFSS Screen (θ) on the simulated gain of the proposed antenna, when just one AFSS layer (Screen-1) is used.....47

Figure 5. 6. Effect of space between layers (Sp) on the simulated gain of the proposed antenna, when two AFSS layers (Screen-1, Screen-2) are used. θ=60º, Fs=0.3λ.....48

Figure 5.7. Simulated reflection coefficient of the proposed antenna, where θ=60º, Fs=0.3λ, and Sp=0.5λ. ……..49

Figure 5. 8. Simulated gain of the proposed antenna, where θ=60º, Fs=0.3λ, and Sp=λ/2……..…….....49

Figure 5. 9. Simulated radiation pattern of the proposed antenna in the H plane. where θ=60º, Fs=0.3λ, and Sp=λ/2……..…….....50

Figure 5. 10. A picture of the proposed prototype in an anechoic chamber……....51

Figure 5. 11. Simulated and measured reflection coefficient of the proposed antenna, where θ=60º, Fs=0.3λ, and Sp=0.5λ. ……..…….....52

Figure 5.12. Simulated and measured gain of the proposed antenna, where θ=60º, Fs=0.3λ, and Sp=λ/2. ……..…….....52

Figure 5. 13. Simulated and measured radiation pattern of Case-I and Case-II of the proposed antenna in the H plane. Where θ=60º, Fs=0.3λ, and Sp=λ/2. ……..…….....53

Figure 6. 1. AFSS unit cell: (a) front view, (b) equivalent circuit model of the ideal and non-ideal diode in ON/OFF states, and (c) transmission and reflection coefficients of the unit-cell for ideal and non-ideal diode ON/OFF states……..…….....62

Figure 6. 2. Top view of the proposed RRA.……..…….....63

Figure 6. 3. Feed antenna structure, (a) Top view, (b) side view……..…….....64

Figure 6. 4. Simulated and measured results of the patch antenna: (a) reflection coefficient, (b) gain, and (c) radiation pattern in the H plane……..…….....64

Figure 6. 5. Effect of (θ_1, and θ_2) on the proposed RRA performance: (a) reflection coefficient, (b) realized gain, (c) radiation patterns of the OFF state RRA in the H plane, (d) radiation patterns of the ON state RRA in the H plane……..…….....66

Figure 6. 6. Sketch of the proposed beam-tilting mechanism: (a) rotating the left sub-screen towards the feed by θ_1, (b) rotating the right sub-screen towards the feed by θ_2.……..…….....67

Figure 6. 7. Simulated radiation patterns of the proposed RRA in the H-plane: (a) with different values of θ_1, when θ_2=0º, (b) with different values of θ_2, when θ_1=0º.……..…….....68

Figure 6. 8. Prototyping and measurement steps: (a) A picture of the proposed RRA prototype in an anechoic chamber, (b) Plexiglas base. ……..…….....69

Figure 6. 9. Simulated and measured results of the proposed RRA, where θ_1=θ_2=15º: (a) reflection coefficient of (b) gain, (c) radiation pattern in the H plane……..….70

Figure 6. 10. Simulated and measured radiation patterns of the proposed non-ideal beam-tilting RRA in H-plane: (a) with different values of θ1, when θ_2=0º, (b) with different values of θ2, when θ_1=0º.…….....71

Figure 8.1 L'élément AFSS proposé avec un modèle de circuit équivalent des états ON/OFF de la diode……..…….....82

Figure 8.2 Coefficient de réflexion de la cellule unitaire AFSS proposée…….…….....83

Figure 8. 3 Modèle simulé de l'antenne ATFSS proposée en vue 3D, supérieure et latérale.. …….....83

Figure 8. 4. Modèle d'antenne d'alimentation simulé et fabriqué pour exciter les éléments ATFSS.…….....84

Figure 8. 5. Croquis de l'antenne ATFSS proposée, (a) avec de multiples combinaisons de diodes pour orienter le faisceau dans différentes directions, et (b) les résultats de la simulation pour chaque combinaison.....84

Figure 8. 6. Étapes de prototypage et image de mesure de l'antenne ATFSS fabriquée dans une chambre anéchoïque.……..……..…….....86

Figure 8. 7. Simulation et mesure du coefficient de réflexion de l'alimentation..…….....87

Figure 8.8. Simulation et mesure des diagrammes de rayonnement dans le plan H de l'antenne planaire unipolaire……..…….....87

Figure 8. 9. Simulation et mesure du coefficient de réflexion de l'antenne ATFSS à formation de faisceau commutée proposée.……..……..…….....88

Figure 8. 10. Simulation et mesure du gain de l'antenne ATFSS à formation de faisceau commutée proposée.……..……..…….....88

Figure 8. 11. Simulation et mesure des diagrammes de rayonnement de l'antenne ATFSS à formation de faisceaux commutée proposée (en combinaison C)…..……..……..…….....89

Figure 8. 12. (a) Structure de la cellule unitaire AFSS proposée, (b) circuit équivalent des états ON/OFF de la diode, (c) configuration de la simulation de l'élément AFSS.……..…….....91

Figure 8. 13. Paramètres de diffusion simulés de la cellule unitaire proposée sous une onde incidente normale et oblique (Ψ/2=30º).……..…….....91

Figure 8. 14. Croquis de l'antenne proposée. (a) vue de dessus, et (b) vue latérale en 3-D. …….....92

Figure 8.15. Mécanisme opérationnel de l'antenne proposée, (a) Cas I (État ON-OFF-OFF), (b) Cas II (État OFF-ON-OFF), (C) Cas III (État OFF-OFF-ON)……..……..…….....93

Figure 8. 16. Une photo du prototype offerte dans une chambre anéchoïque.....….…….....95

Figure 8.17. Coefficient de réflexion simulé et mesuré de l'antenne proposée (θ=60º, Fs=0.3λ, and Sp=0.5λ)..……..…….....95

Figure 8. 18. Gain simulé et mesuré de l'antenne proposée (θ=60º, Fs=0.3λ, and Sp=λ/2).…….....96

Figure 8. 19. Simulation et mesure du diagramme de rayonnement de l'antenne proposée dans le plan H (θ = 60 °, Fs = 0,3λ et Sp = λ / 2)…….....96

Figure 8. 20. Cellule unitaire AFSS : (a) vue de face, (b) modèle de circuit équivalent de la diode idéale et non idéale dans les états ON/OFF, et (c) coefficients de transmission et de réflexion de la cellule unitaire pour les états ON/OFF de la diode idéale et non idéale.…….....99

Figure 8. 21. Vue de dessus de la RRA proposée.…….....100

Figure 8. 22. Structure de l'antenne d'alimentation, (a) vue de dessus, (b) vue de côté.……...100

Figure 8. 23. Simulation et mesure des résultats de l'antenne planaire : (a) coefficient de réflexion, (b) gain, et (c) diagramme de rayonnement dans le plan H.……..….....101

Figure 8. 24. Croquis du mécanisme d'inclinaison du faisceau proposé : (a) rotation du sous-écran de gauche vers l'alimentation par θ_1, (b) rotation du sous-écran de droite vers l'alimentation par θ_2.….....103

Figure 8. 25. Étapes de prototypage et de mesure : (a) photos des prototypes du RRA proposé dans une chambre, (b) base en plexiglas.…….…….....104

Figure 8. 26. Coefficient de réflexion simulé et mesuré de la RRA idéale proposée, où θ1=θ2=15º.....104

Figure 8. 27. Gain simulé et mesuré de la RRA proposée, où $\theta_1=\theta_2=15º$.……..….....105

Figure 8. 28. Simulation et mesure du diagramme de rayonnement de la RRA proposée dans le plan H, où $\theta_1=\theta_2=15º$: (a) ON, (b) OFF.……..….....105

Figure 8. 29. Diagrammes de rayonnement simulés et mesurés du RRA à inclinaison de faisceau non idéal proposé dans le plan H: (a) avec différentes valeurs de θ_1, lorsque $\theta_2=0º$, (b) avec différentes valeurs de θ_2, lorsque $\theta_1=0º$.……..…..…….....106

LIST OF ABBREVIATIONS

AFSS	Active Frequency Selective Surface.
AMC	Artificial Magnetic Conductor
AMPBG	Active Metallic Photonic Band Gap.
ATFSS	Active Triangular Frequency Selective Surface.
DOA	Determining the Direction of Arrival
EBG	Electromagnetic Bandgap structures
EM	Electro Magnetic.
FSS	Frequency Selective Surface.
FPV	First-Person View
GHz	Giga Hertz.
GPS	Global Positioning System.
HIS	High Impedance Surface
HPBW	Half Power Beamwidth
ILAS	Integrated Lens Antennas.
LOS	Line Of Sight
PTP	Point To Point
RF-MEMS	Radio Frequency Microelectromechanical Systems
RA	Reflectarray.
RRA	Reconfigurable Reflector Antenna.
WLAN	Wireless Local Area Network.
WI-Fi	Wireless Fidelity.

CHAPTER 1

INTRODUCTION

1.1 Motivation

Wireless communication systems have recently become one of the most vital and fastest developing technological areas. In this technique, the information is transmitted from the transmitter to the receiver in a flexible, easy, and low-cost way. Wireless fidelity (Wi-Fi), the new generation of mobile communications, GPS receivers, military, and civil radars are some examples of the widely used wireless communication systems in our daily life. In recent years, miniaturization, multifunction, less cost, and robustness have become the most important requirements in modern communication systems. Accordingly, there is a need for designing an antenna with various functionalities by integrating a few functions in a single element. To overcome the problems of radiation interference, this element should have a capability to direct the beam towards the desired direction, while suppressing the unwanted beam in other directions. For this reason, beam-switching antennas (which is the most extended application of the pattern reconfigurable antenna) have obtained significant attention in wireless communication systems. These antennas can significantly decrease interfering signals and improve system capacity. More flexible properties and additional functionalities can be achieved by using these antennas. Also, this type occupies the same or smaller physical volume compared with traditional smart antenna arrays [1].

The spacious applications and remarkable characteristics of frequency selective surfaces (FSSs) and beam-switching antennas for modern communication systems have motivated us to establish comprehensive research in this area. Therefore, this project aims to design and fabricate several new beam-switching antennas based on active frequency selective surfaces (AFSSs).

1.2 Problem identification

Various techniques have been used to steer the radiation pattern beam, such as integrated lens antennas (ILAs) [2-4], traveling-wave antennas [5-6], adaptive arrays [7], phased arrays [8], and active metallic photonic bandgap (AMPBG) [9]. Each of these technologies has some advantages as well as some disadvantages. For example, traveling wave antennas used for beam steering, hold a large size. For phased antenna arrays, the amplitude and phase of each element must be controlled to steer the beam in a specific direction, which complicates the structure and increases the fabrication cost. The AMPBG is a bulky structure and suffers from higher side-lobe levels (SLL) and cross-polarization. To overcome the design complexity, larger size, and expensiveness of the above-mentioned techniques, AFSSs have recently been used for achieving beam steering capability. Due to the partial reflection /transmission behaviour of the frequency selective surface (FSS), the radiation pattern can either be transmitted or reflected in a specific desired direction.

1.3 Research objectives

In this thesis, a new active frequency selective surface (AFSS) unit-cells with simple structures are proposed. These elements are used to convert the omnidirectional radiation pattern of the antenna source into a directional one forming a new class of beam-switching antennas. A new switched beamforming antenna using a novel active triangular frequency selective surfaces (ATFSSs) is presented. This antenna can steer the beam in different directions in the azimuth plane with 120º radiation beamwidth. Moreover, AFSS arrays are used to design a new corner reflector antenna with a tunable gain for the first time. Furthermore, this thesis presents a reconfigurable reflector antenna (RRA)with beam-tilting capability operating in the WLAN band. According to our knowledge, the proposed structure is the first design where AFSS is used to provide the beam reconfigurability when AFSS is arranged in a parabolic shape.

1.4 Organization of the thesis

This thesis is organized as follows:

- Chapter 2 tackles a general overview of FSS, including the FSS operational concept, filtering characteristics, elements' type, design parameters of the element, and its applications. AFSS is also introduced in this chapter.

- Chapter 3 represents an introduction to reconfigurable antennas, their types, and their applications.

- Chapter 4 expresses a novel frequency selective surface-based switched-beamforming antenna. This antenna contains an excitation source with an omnidirectional radiation pattern and a novel active triangular frequency selective surface (ATFSS) surrounding the source. Design each of the proposed unit-cell, feed antenna, and the proposed antenna are illustrated in this chapter. The operation mechanism of the proposed switched beamforming ATFSS antenna and parametric studies are discussed as well. The proposed design can effectively steer the beam in different directions in the azimuth plane with 120º radiation beamwidth at 5.8 GHz. By using the proposed design, the maximum gain has been enhanced by 4dBi. In this design, the number of active elements is minimized to decrease the antenna cost and enhance its radiation performance in terms of gain.

- Chapter 5 presents a new corner-reflector antenna with a tunable gain based on active frequency selective surfaces (AFSSs). The proposed structure comprises a dipole antenna as an excitation source, and three reconfigurable AFSS layers. These layers have different sizes and are arranged on the same side of the dipole form a V-shaped corner reflector. This design modifies the omnidirectional radiation pattern of the source into a directional radiation pattern with a tunable gain. Details regarding the AFSS unit-cell design, the design, operational mechanism, and parametric studies of the proposed antenna, fabrication and measurement results are given in this chapter.

- Chapter 6 introduces details regarding the design and fabrication of a novel reconfigurable reflector antenna with beam-tilting capability (RRA) operating in the WLAN band. The proposed antenna is designed using an array of AFSS elements and a WLAN-band patch antenna (excitation source). A mechanical beam tilting technique is also applied. This mechanical beam tilting method can tilt the main beam without adding any extra layers or setups to the main antenna structure. A good agreement between the simulated and measured results has been achieved. As it is well known in the literature that the main disadvantage in parabolic reflector designs is the minimum beam scanning ability, while using the proposed technique, a high gain antenna can be designed (when the size of the antenna is increased based on any given specification).

- Chapter 7 summarizes the accomplishments of this thesis and proposes future work in the research orientation.

- Chapter 8 produces a French summary of this dissertation.

1.5 List of publications

Journals:

1) **G. H. Elzwawi**, H. H. Elzwawi, M. M. Tahseen and T. A. Denidni, "Frequency Selective Surface-Based Switched-Beamforming Antenna," *IEEE Access*, vol. 6, pp. 48042-48050, July 2018.

2) H. H. Elzuwawi, M. M. Tahseen, **G. H. Elzwawi**, and T. A. Denidni, "A new RFID monopole antenna using a compact AMC structure," Microwave and optical technology letters, vol. 61, no.7, pp. 1835-1840, April 2019.

3) **G. H. Elzwawi**, A. Kesavan, R. Alwahishi and T. A. Denidni, " A New Corner-Reflector Antenna with Tunable Gain Based on Active Frequency Selective Surfaces," IEEE Open Journal of Antennas and Propagation, vol. 1, pp. 88-94, 2020.

4) **G. H. Elzwawi**, M. M. Tahseen and T. A. Denidni, " Reconfigurable Reflector Antenna with Beam-Tilting Capability," International Journal of Electronics and Communications. Submitted.

5) **G. H. Elzwawi,** and T. A. Denidni, " A Double-Beam Double-Band Reconfiguration Antenna," Microwave and optical technology letters. In progress

Conferences:

6) **G. H. Elzwawi**, M. Mantash and T. A. Denidni, "Improving the gain and directivity of CPW antenna by using a novel AMC surface," *IEEE International Symposium on Antennes and Propagation & USNC/URSI National Radio Science Meeting*, San Diego, CA, 2017, pp. 2651-2652.

7) **G. H. Elzwawi**, M. Mantash and T. A. Denidni, "WLAN Band Beam-Switching Antenna Using Active Frequency Selective Surfaces," *STARaCOM,* Montreal, Canada, Conference, 2018. Poster

8) **G. H. Elzwawi**, H. H. Elzuwawi, and T. A. Denidni, "Beam Switching Antenna Using a Novel Triangular Active Frequency Selective Surface," *European Conference on Antenna and Propagation EUCAP*, London, UK., 2018.

9) **G. H. Elzwawi**, M. M. Tahseen and T. A. Denidni, " Directivity Enhancement in FSS- Based Reconfiguration Antenna," IEEE International Symposium on Antennas and Propagation and USNC-URSI Radio Science Meeting, Boston, Massachusetts, USA. July, 2018. Poster

10) **G. H. Elzwawi**, M. M. Tahseen and T. A. Denidni, "Novel Reconfiguration Antennas using Frequency Selective Surfaces," International Symposium on Antenna Technology and Applied Electromagnetics (ANTEM), Waterloo, ON., Canada, 19-22 August 2018.

11) **G. H. Elzwawi**, M. M. Tahseen and T. A. Denidni, "Reflecto Transmitive Antenna using Frequency Selective Surfaces," International Symposium on Antenna Technology and Applied Electromagnetics (ANTEM), Waterloo, ON., Canada, 19-22 August 2018.

12) M. S. Bizan, **G. H. Elzwawi,** M. M. Tahseen and T. A. Denidni, "Bandwidth Enhancement by Position Perturbations in Stacked Dielectric Resonator Antenna," IEEE International Symposium on Antennas and Propagation & USNC/URSI National Radio Science Meeting, Boston, MA, 2018, pp. 2091-2092.

13) H. Houssein, **G. Elzwawi** and T. A. Denidni, "A Dual-Band Beam-Switching Antenna Using Square Active Frequency Selective Surfaces," 2019 IEEE International Symposium on Antennas and Propagation and USNC-URSI Radio Science Meeting, Atlanta, GA, USA, 2019, pp. 685-686.

14) **G. H. Elzwawi**, R. Alwahishi, and T. A. Denidni, " A New Beam-Steering Antenna with Variable Gain"," European Conference on Antenna and Propagation EUCAP, Copenhagen, Denmark, 2020. Accepted

15) **G. H. Elzwawi**, M. Mantash and T. A. Denidni, " A Flower Shaped Beam-Steering Antenna for Wireless communication system Applications," *IEEE International Symposium on Antennes and Propagation & USNC/URSI National Radio Science Meeting*, Montreal, CA, 2020. Accepted.

1.6 Awards

- I was a Promotional Prize Winner for the 2018 IEEE Access Best Multimedia Award Part 1.
- I was awarded a scholarship by the Ministry of High Education in my country (Libya) to obtain a Ph.D. degree in telecommunications in Canada.

1.7 Affiliations

- Member of the IEEE (Institute of Electrical and Electronics Engineers).
- Member of IEEE Student branch INRS-emt

CHAPTER 2

Frequency selective surfaces

2.1 Introduction

Frequency selective surface, known as FSS, is a kind of a periodic array of metal patches or perforated conductors mounted on a substrate. FSS is mainly used as a partial reflector surface, and it is characterized by its response to the incident electromagnetic waves, as it transmits approximately all the incident electromagnetic waves at specific frequencies, while reflects these waves at other frequencies as shown in Figure 2. 1. The frequency response of the FSS screen mainly depends on the shape of elements, the space between elements, and the parameters of the dielectric material [10].

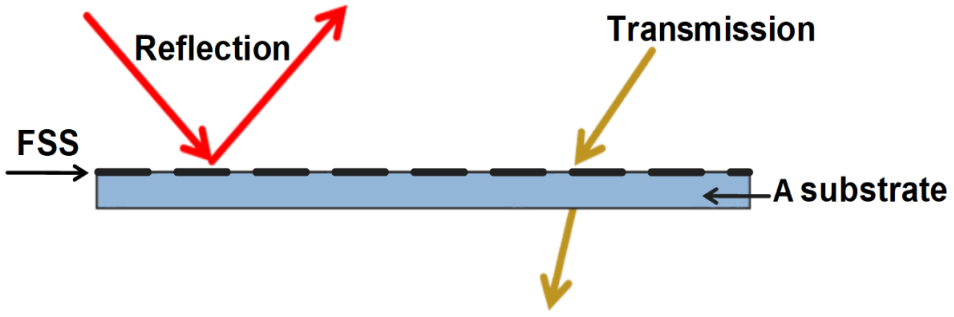

Figure 2. 1. The frequency response of the FSS.

2.2 Filtering characteristics of FSS

- **Band-pass filter:** Generally; aperture types offer transmission band response.
- **Stopband Filter**: Resonant patch elements introduce stopband response.

2.3 Design parameters of FSS

It is an essential matter to design an FSS with appropriate parameters that meet the design requirements. For example, the element shape and lattice pattern greatly affect the center frequency, the transmission and reflection bandwidth, the polarization response, and the onset of the grating lobe. While the number of FSS layers, the spacing between them, and the dielectrics can control the stability of center frequency, and bandwidth with incident angle [10, 11].

2.3.1 FSS elements' types

The choice of the proper element is a vital and critical issue in designing FSS. So, elements type must be chosen to meet the desired bandwidth and cross-polarization. There are four different groups of elements [10]. The most typical elements used in FSS are:

- **Group-1**: The center connected or N-poles, such as the simple straight element, three-legged element; anchor elements; the Jerusalem cross; and the square spiral. As shown in Figure 2 .2. a. At the first dominant resonance, the length of these elements is about a half wavelength. These elements produce moderate bandwidth, but because of their shapes, they can be backed together to produce a broadband response, as when the spacing element becomes smaller the bandwidth increases. This also contributes to pushing the grating response to higher frequencies.

- **Group 2:** The loop types such as the three- and four-legged loaded elements; the circular loops; the square and hexagonal loops are shown in Figure 2. 2. b. The length of this type is about a wavelength. This type of element is the most recommended element for both stop and band-pass applications, as it is characteristic by its ability to offer broadband. it is a small element with stable resonant frequency in response to different angles of incident.

- **Group 3:** Solid interior or plate types of various shapes are shown in Figure 2. 2. c. The element dimension of this group is about half wavelength, this leads to inter element spacing larger than half wavelength, this increases the sensitivity to the incident angle and causes early onset of grating lobes. This group is used for a certain purpose application.

- **Group 4:** Combination elements. This group constructed by a combination of other types and it is the biggest one. Therefore, different types of transmission/ reflection responses can be obtained by combining different shapes.

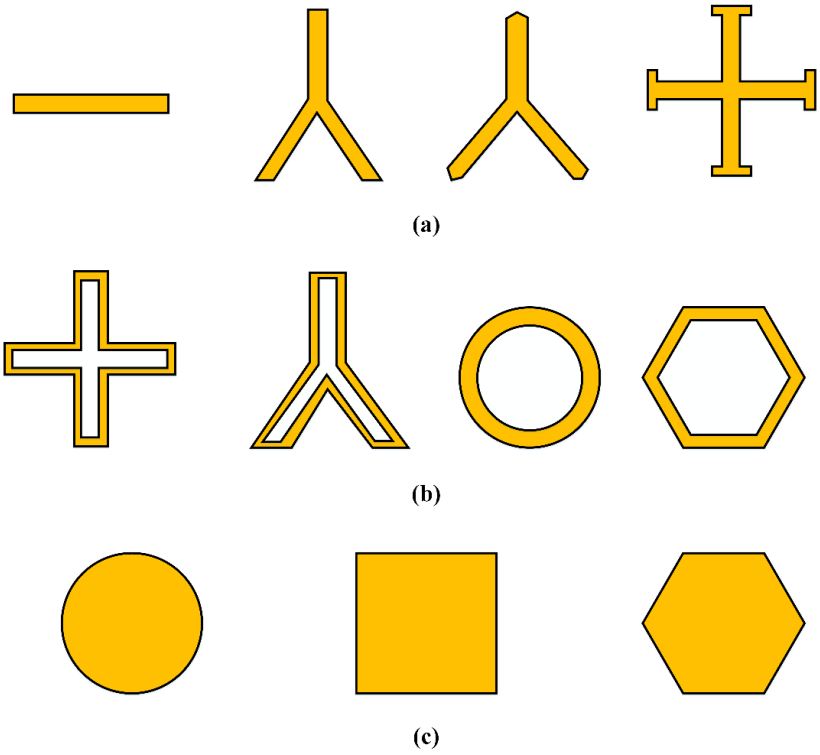

Figure 2. 2. FSS element types.

2.3.2 Dielectric loading

FSS screen must be mounted on a dielectric substrate, which controls the roll-off and the rate of flatness of bandwidth. When the thickness of the substrate increases the bandwidth increases and the reflection increases. This thickness also causes a change in the incident angle and polarization. The number of dielectric substrates significantly changes the transmission and reflection response of the FSS screen. The resonant frequency of the FSS will decrease by the factor of $\frac{1}{\sqrt{\epsilon_r}}$, when it is mounted on a dielectric substrate, the thickness of dielectric in middle must be chosen accurately to achieve a flat top response, while the other dielectric layers (the outer ones) should be a quarter wavelength to reduce the transmission loss.

2.3.3 Periodic array lattice and grating lobe responses

The lattice pattern is a considerable parameter in terms of the transmission reflection response of the FSS, so lattice geometry should be chosen accurately to meet the design requirement. The center frequency, bandwidth, angular sensitivity, and cross-polarization level are largely affected by the distance between elements and the geometrical position of adjacent elements. The most popular types of the grid are shown in Figure 2. 3. The overall degree of FSS summitry depends on the combination of elements and grid geometry. for the normal angle of incident, the spacing between elements should be less than one half of wavelength, to delay the undesired grating lobe to higher frequencies. By reducing the grid spacing the grating lobe will delay, and the bandwidth will increase. Where the real part of array self impedance is increased, but the imaginary part remains almost the same, and the transmission coefficient is close to unity over a large frequency band.

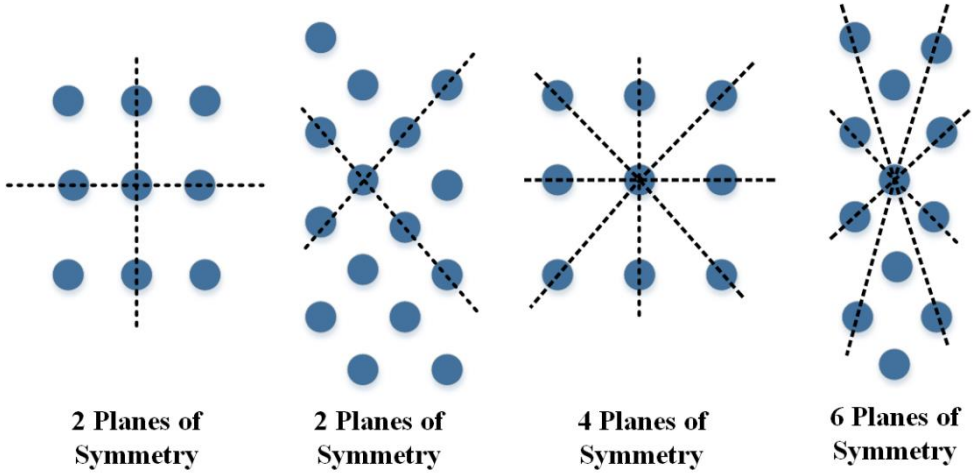

Figure 2. 3. FSS symmetry.

2.4 FSS applications

Frequency selective surfaces have plenty of uses over a gigantic scope of electromagnetic range, from below UHF to above-infrared regions.

2.4.1 Traditional applications: Band-stop filter, dichoric reflectors, hybrid radomes, and polarizers are some of the traditional applications of FSS. FSS is used in a radome structure to reduce the radar cross-section. Moreover, FSS operates as sub and main reflectors in quasi-optical antenna systems to create multi-frequency operation [10]. FSS can also be used to change or filter the electromagnetic wave polarization [12].

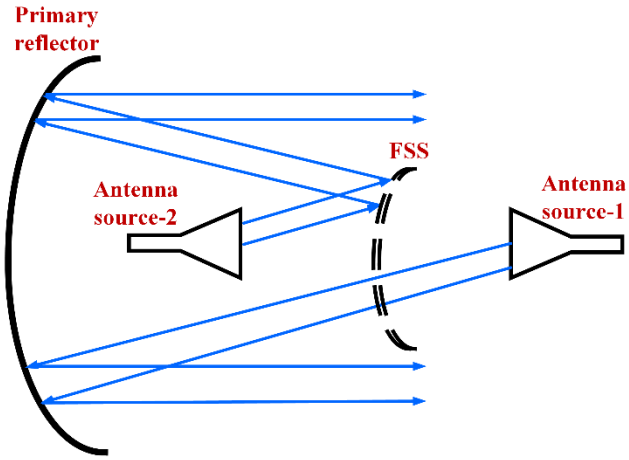

Figure 2. 4. Sketch diagram of FSS works as a sub-reflector [13].

2.4.2 More recent applications: Active frequency selective surface (AFSS) is formed by integrated active components into a passive FSS. AFSS provides extended control in the behaviour of the structure, such as variable reflectivity, transparency or even signal absorption characteristics. Recently, AFSS has been widely used in designing reconfigurable antennas which produce more functionality. By biasing the embedded high-frequency switches inside an antenna aperture constructed of the periodic elements, the radiation parameters of the antenna can be controlled.

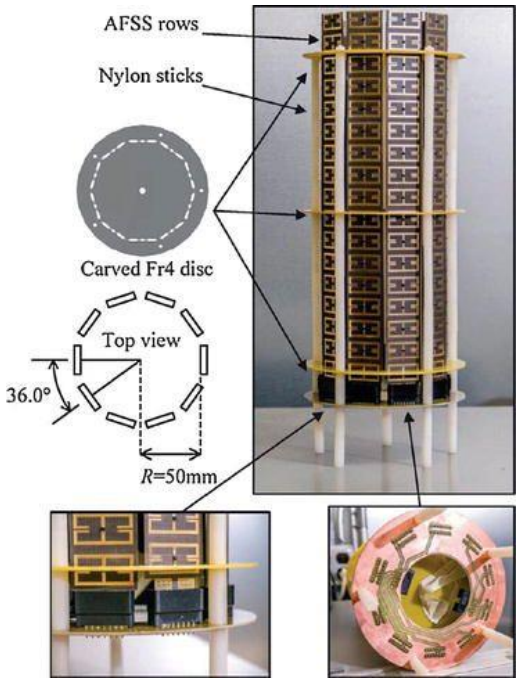

Figure 2. 5. Designing a reconfigurable pattern antenna by using AFSS [14].

2.5 Conclusion

According to the study of the basics of FSS that has been produced in this chapter, it is concluded that the frequency selective surface has an important role in communication systems and it is considered to be as one of the most vital versatile creating smart/tunable structures. To obtain the best performance of the FSS, a careful study is required. It is worthy to mention that, both the type of elements and their arranged in the proper grid are very critical issues in designing the FSS unit-cell.

CHAPTER 3

Reconfigurable antennas

3.1 Introduction

The reconfigurable antenna is a type of antenna that has the capability to modify its radiation properties by using some electrical or mechanical assistance. The key principle in designing reconfigurable antennas is based on the theory of conventional antennas [15]. Moreover, this antenna provides additional levels of functionality to improve wireless communication systems. Reconfigurable antennas are classified according to the antenna parameter that is dynamically adjusted, which typically is operation frequency, radiation pattern, polarization, or multi-performance reconfigurable antennas [16, 17].

3.1.1 Frequency Reconfigurable antennas

Recently, frequency reconfiguration has become a fundamental factor in advanced communication systems. By using this reconfiguration, a single element can replace multiple antennas for various operating frequencies. This will reduce the cost and complexity of the overall system. The principle key in the frequency reconfigurable antenna is changing the effective electrical length or the effective current distribution of the radiator. This change can be controlled electrically or mechanically. The frequency reconfigurability can be achieved smoothly over a specific bandwidth using a continuous variation. However, the discontinuous variation is achieved by switching between different bands. Optical switches, PIN-Diodes, varactor-Diodes, and radio-frequency micro-machined (RF-MEMS) switches are some popularly used methods of the discontinuous frequency reconfiguration approaches. However, the mechanical mechanism is obtained by changing the structure of the antenna and material properties. Changing the size and shape of the structure is one of the common problems in this method. For example, a frequency-reconfiguration bow-tie antenna for Bluetooth, WiMAX, and WLAN applications are proposed in

[18]. In which, pin-Diodes are used to change the effective electrical length of the antenna leading to an electrically tunable operating band as shown in Figure 3.1. Authors in [19] proposed a mechanical frequency reconfiguration technique in microstrip patch antennas for wireless sensor networks. In this structure, the dielectric properties of the antenna have been changed mechanically and a tunable frequency range from 2442 MHz to 2716 MHz is achieved. This design is presented in Figure 3. 2.

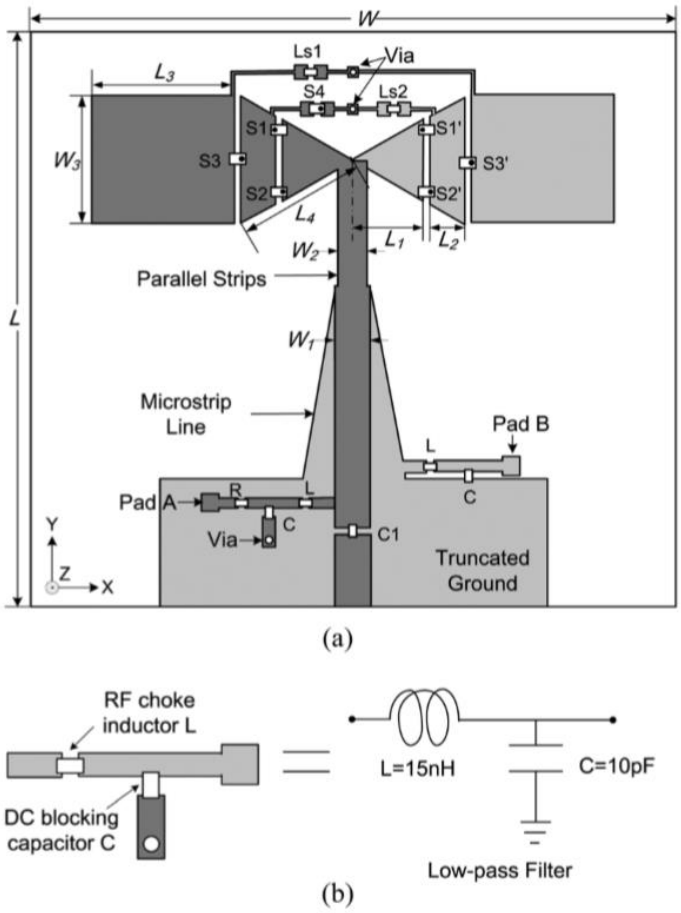

Figure 3.1. (a) Designing a reconfigurable bow-tie antenna using pin-diodes (b) equivalent circuit of the biasing circuit [18].

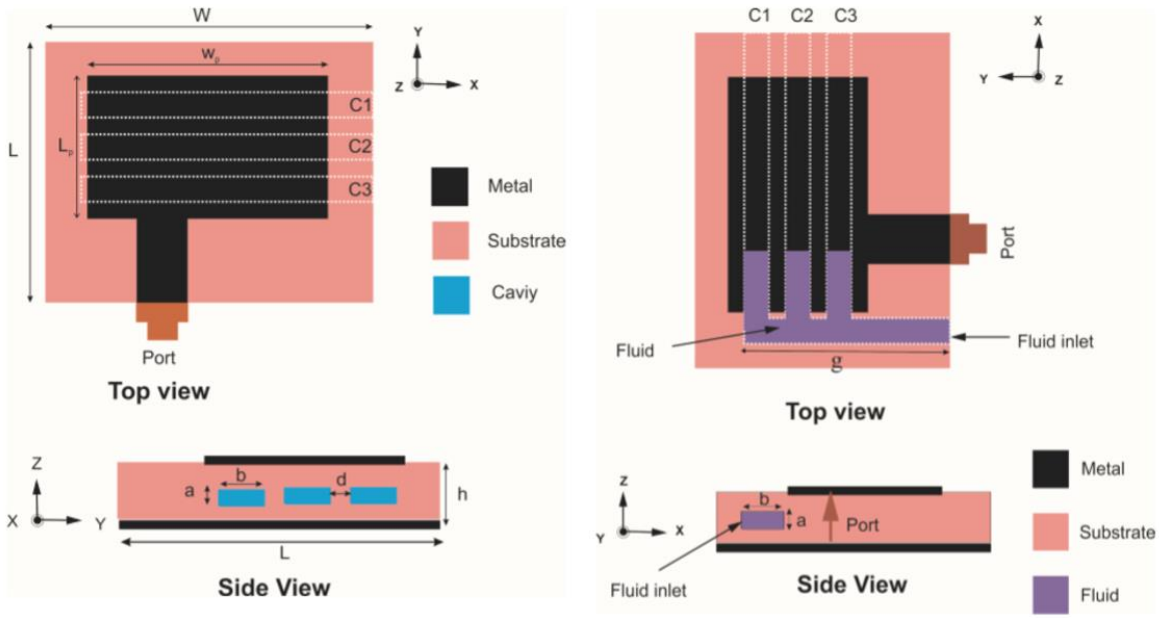

Figure 3.2. Different configurations of a mechanical frequency reconfigurable antenna [19].

3.1.2 Polarisation reconfigurable antennas

The polarization reconfiguration can be achieved by managing the direction of current distribution. This approach can be achieved by changing the antenna structure, feed reconfiguration, or changing the material properties. This reconfiguration can reduce signal interference, improve interface quality, and relieve the polarization mismatch losses in different versatile devices. The switching strategies are the foremost well-known approach for polarization reconfigurations. In [20], F. Wu and K. M. Luk propose a single-feed polarization reconfiguration as shown in Figure 3. 3. In this work, diodes are used to provide three states of polarization control (one linear polarization and two orthogonal circular polarizations). By using this technique, the effective bandwidth, antenna efficiency, and front-to-back ratio are improved.

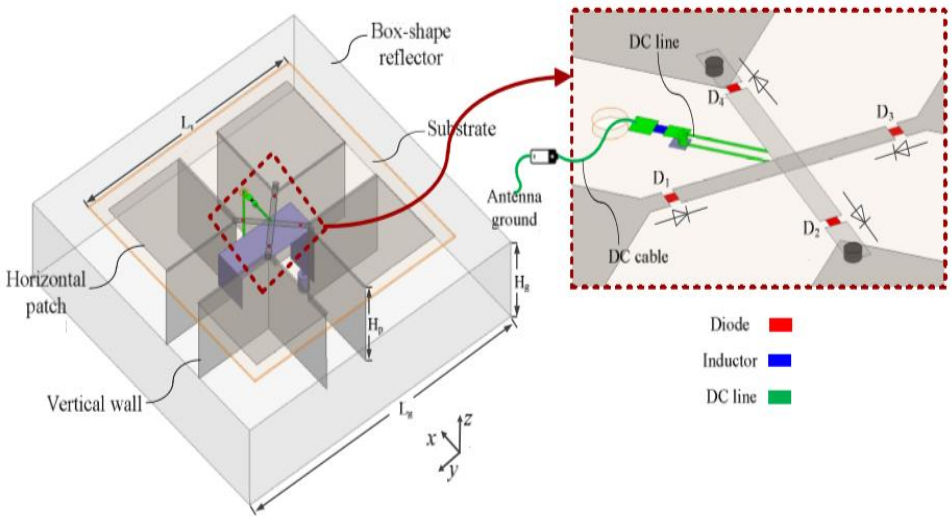

Figure 3. 3. Designing of a single-feed polarization reconfigurable antenna [20].

3.1.3 Radiation pattern reconfigurable antennas

In recent years, radiation pattern reconfigurable antennas have obtained significant attention in wireless communication systems. More flexible properties and additional functionalities can be achieved by using these antennas. The pattern reconfiguration can be realized by changing the amplitude and phase of the electric or magnetic currents of the radiating structure. The change in the current distribution can cause some variation in the frequency response of the antenna. This is the essential issue that should be considered in the design process. Different methods have been reported in the literature for achieving radiation pattern reconfiguration. For instance, the mechanical approach is accomplished by repositioning and moving the antenna to reach the expected characteristics. Low speed and complexity of the system are the main disadvantages of this technic [21-23].

The electrical method is another technique that is used to control the radiation pattern using RF switching (pin-diodes and radiofrequency micro-electromechanical systems (RF-MEMS) switches) and variable reactance devices (varactor diodes) [24-28].

Changing material properties is also proposed for designing the radiation-pattern reconfiguration antennas. However, using this method require a specific biasing structure. Moreover, high cross-polarization and more loss are expected [29-33].

Electromagnetic bandgap structures (EBG), artificial magnetic conductor (AMC), high impedance surface (HIS) and frequency selective surface (FSS) have recently received considerable attention from researchers in designing reconfigurable radiation pattern antennas. FSS is mainly used as a band-stop or band-pass filter according to its structure. AFSS element is formed by soldering active components in the FSS. These active components could be pin-diodes, varactor diodes, or MEMS switches [34- 38]. A beam-steering antenna using active frequency selective surfaces (AFSS) has been presented in [14]. In this design beam sweeping in the whole azimuth plane for both the single beam modes and the dual-beam modes is achieved. Authors in [39] have proposed a reconfigurable antenna using an AFSS as shown in Figure 3. 3. In this structure, pin-diodes are soldered in the FSS unit-cells to form the AFSS that controls the radiation pattern of the antenna.

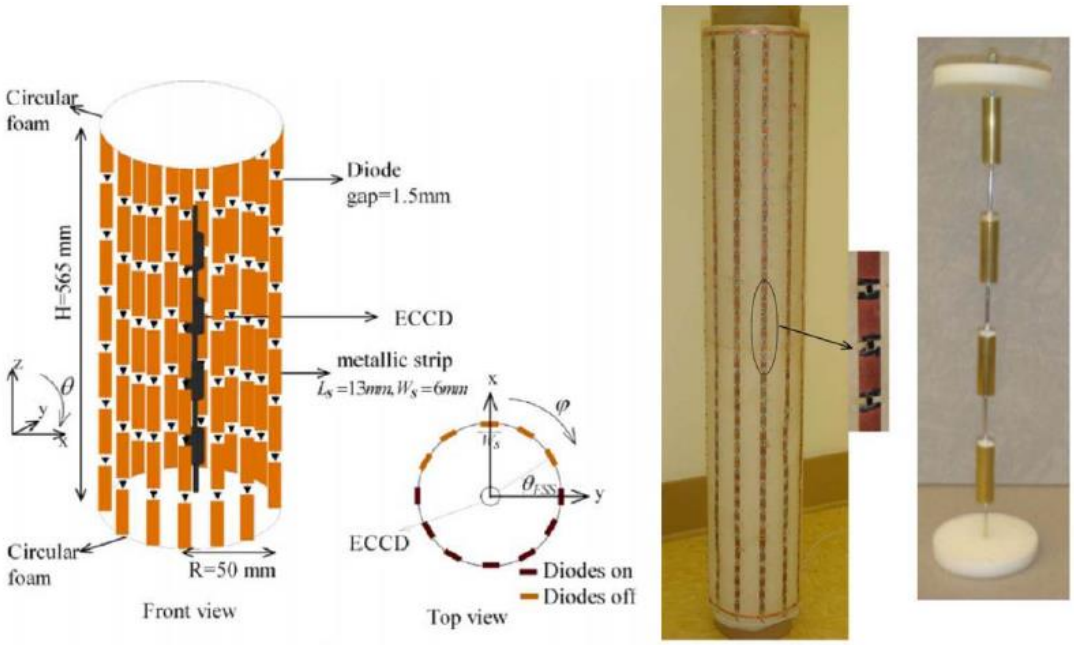

Figure 3. 4. Using AFSS in designing a reconfigurable pattern antenna [39].

3.2 Conclusion

This chapter has casted a light upon reconfigurable antennas. The definition of this type of antennas, its types, and its applications have been introduced. From the study of this topic, it is found that more research is required. Proposing new reconfiguration methodologies and designing more novel reconfigurable structures can develop and enhance the radiation reconfigurable antennas' performance in terms of gain and radiation pattern.

CHAPTER 4 :(ARTICLE 1)

Frequency Selective Surface-Based Switched-Beamforming Antenna

Ghada Hussain Elzwawi, Hifa Houssein Elzuwawi, Muhammad M. Tahseen,
and Tayeb A. Denidni

IEEE Access, vol. 6, pp. 48042-48050, 2018.

4.1 Abstract

A novel switched-beamforming antenna designed using active frequency selective surfaces (AFSS) is presented. The antenna consists of two parts: a source with an omnidirectional radiation pattern and a novel active triangular frequency selective surface (ATFSS) surrounding the source. Each unit cell in the ATFSS structure contains two diamond-shaped patches connected with each other by a high- frequency pin-diode. The ATFSS elements are designed using CST microwave studio. The pin-diodes are applied to achieve beam switching. By switching the applied biasing voltage, the ON and OFF states of the ATFSS exhibit reflection and transmission characteristics in the operating WLAN band. By arranging the AFSS unit cells in a triangular structure with three panels and choosing different combinations of the diode states, the beam switching at various azimuthal directions is achieved. To validate this concept, the proposed antenna is fabricated and measured. A good agreement between simulations and measurements in terms of beam directions, reflection coefficient, and gain has been achieved @5.8 GHz.

4.2 Index terms

Active frequency selective surface, directional radiation pattern, frequency selective surface, omnidirectional radiation pattern, switched-beamforming antenna, pin diode.

4.3 Introduction

The reconfigurable antenna is often characterized by its ability to adapt its behavior with changing system requirements and to provide additional levels of functionality for wireless communications.

By using a reconfigurable antenna, the overall system performance can get rid of the restrictions that arise from the fixed characteristics of the conventional antennas [1]. The reconfigurable antenna concept based on determining the direction of arrival (DOA) of the incoming waves was introduced in [2-3]. Achieving multiple reconfigurable beams by using parabolic reflectors for satellite communication has been discussed in [4]. There are various techniques that can be used to steer the radiation pattern beam, such as integrated lens antennas (ILAs) [5-6], traveling-wave antennas [7-8], adaptive arrays [9], phased arrays [10], and active metallic photonic bandgap (AMPBG) [11].

Each of these technologies has some advantages as well as some disadvantages. For example, traveling wave antennas used for beam steering, hold a large size. For phased antenna arrays, the amplitude and phase of each element must be controlled to steer the beam in a specific direction, which complicates the structure and increases the fabrication cost. The AMPBG is a bulky structure and suffers from higher side-lobe levels (SLL) and cross polarization. To overcome the design complexity, larger size, and expensiveness of the above-mentioned techniques, AFSSs have recently been used for achieving beam steering capability. Due to partial reflection /transmission behavior of the frequency selective surface (FSS), the radiation can either be transmitted or reflected in a specific desired direction.

In [12] an electrical beam steerable antenna has been proposed using an AFSS. The AFSS structure is connected with varactor diodes. By controlling the bias voltage, a 360º radiation pattern sweep is achieved for a single-beam mode and also for dual-beam modes. In spite of nonlinear behavior of the pin-diodes, these are the most common components used to reconfigure the electromagnetic (EM) response of an FSS texture. The transmission/reflection characteristics of the pin-diodes allow AFSS to control the direction of the incident EM waves [13-15]. For instance, in [13], 48 pin- diodes have been used in AFSSs to achieve beam-steering. This large number of active elements in the AFSS increases the complexity of the design and leads to higher fabrication cost. An AFSS-based beam-steering antenna with less number of active elements inserted in a cylindrical geometry has been proposed in [15], where the antenna can sweep the entire azimuth plane with 60º radiation beamwidth in six steps, operating at 2.45 GHz.

This paper presents a new switched beamforming antenna using a novel ATFSS. The antenna comprises multiple AFSS, arranged in an equilateral triangle with three panels, and a feed placed in the middle of the structure to excite the ATFSS. By applying multiple combinations of the diodes (ON and OFF) on each ATFSS panel, the beam-steering is achieved in various directions. The proposed beam-steering antenna can steer the beam in different directions in the azimuth plane

with 120º radiation beamwidth. The proposed switched beamforming antenna provides a maximum realized gain of 7 dBi, which is almost 4 dBi higher than the feed gain. The antenna is fabricated and measured. The obtained results show a good agreement between simulations and measurements in terms of reflection coefficient, beam direction, and realized gain at 5.8 GHz.

The proposed antenna can be used in the upper WLAN WI-FI band (at 5.8 GHz), fixed satellites, radiolocation, first-person view (FPV), and other similar applications.

4.4 Switched-beamforming antenna design

The basic principle for an AFSS is shown in Figure 4. 1, where the surface can control the wave propagation by changing the features of the active components embedded in the FSS. By switching the diodes ON/OFF states, the reflection characteristic of the incident wave is achieved. The AFSS exhibits maximum reflection in the diode's ON state while maximum transmission in OFF state.

The proposed antenna consists of two main parts: first part comprises of three ATFSS panels arranged in an equilateral triangular configuration, while the second part is a patch with monopole radiation pattern used as a feed and placed in the middle of the structure.

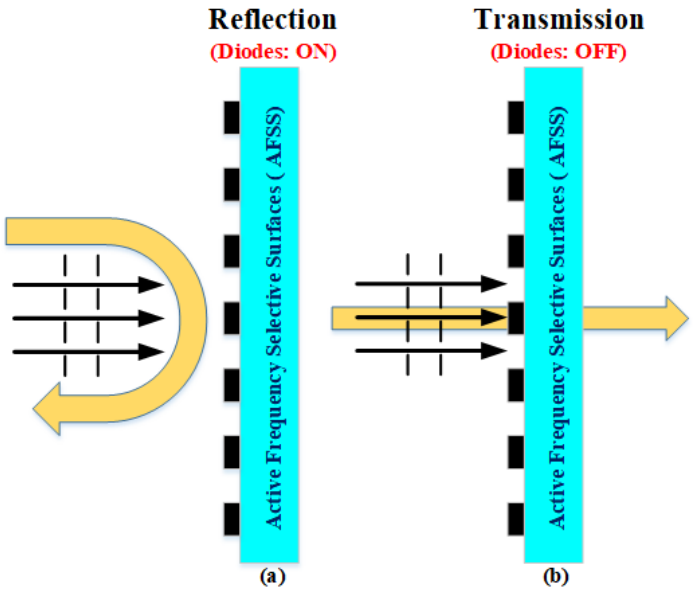

Figure 4. 1. Basic principle of the AFSS in two diode states: (a) reflection, (b) transmission.

4.4.1. ATFSS element design

Each panel in the proposed AFSS consists of two unit cells as shown in Figure 4. 2. Each unit cell is a subject to either transmit or reflect the incoming waves in diode's ON or OFF state. To achieve this objective, an ATFSS element has been designed using CST Microwave Studio considering an infinite number of elements exist along the X- and Y-direction. Each element consists of two diamond-shaped patches, which are electrically connected /disconnected from each other by the pin-diode.

The high-frequency pin-diode (GMP4202-GM1) is modeled as a series RLC circuit. A small resistance of Rs = 1.8 Ω represents the diode's forward bias (state ON), while a series capacitance of Cp = 0.09 pF and inductance of Lp = 0.5 nH exhibit the OFF state, as illustrated in the equivalent circuits shown in Figure 4. 2 [14]. A Y-polarized plane wave incidence is used to obtain the scattering characteristics from the element. The element is designed on Roger's RT/Duroid 5880 substrate with a thickness of 0.127 mm, a permittivity of 2.2, and loss tangent of 0.0009.

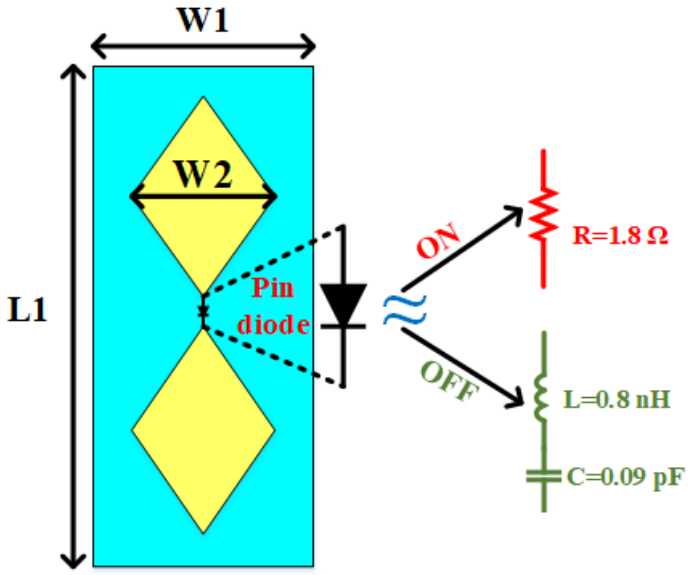

Figure 4. 2. The proposed AFSS element with an equivalent circuit model of the diode's ON/OFF states.

Table (4. 1): The proposed ATFSS element design.

Parameter	L1	W1	W2
Value (mm)	24	11	10

The effect of dielectric permittivity and substrate thickness on the scattering performance of the element in the ON/OFF states of the diode has been analyzed, as shown in Figures 4. 3 (a) to (e). From this analysis, it is visible that dielectric permittivity as well as the thickness result in shifting the resonant frequency of the element. The dimensions of the ATFSS unit cell are summarized in Table 4. 1. The results show that in the forward bias (ON state) the element exhibits maximum reflection, while in the OFF state depicts transmitting characteristics at the operating frequency of 5.8 GHz. It has been observed that the proposed element exhibits a -5 dB difference in magnitude of the reflected wave, while a -21 dB magnitude difference in the transmitted wave in both diode's ON and OFF states (at 5.8 GHz).

Effect of the element size as well as the size of radiating patches on the scattering performance have also been analyzed. Figure 4. 4 depicts that when the element size 'W1' is increased, the resonance frequency shifts to lower frequency band. The effect of radiating patch size 'W2' on the scattering performance is shown in Figure 4. 5, which shows that change in the size of the diamond-shaped patch also shifts the resonant frequency. These parameters were optimized to operate in the desired frequency band.

For deeper investigation, a near field analysis at the AFSS is performed. Figure 4. 6 (a), (b) illustrate the magnitude of electric field distribution on the proposed AFSS element at Z=0 plane at 5.8 GHz. It is evident that the intensity of electric field magnitude is maximum in ON state (reflection) while it is minimum in the diode's OFF state (transmission). The highest field strength of 4500 V/m is observed at the radiating edges at the center as well as at the vertical edges near the cell boundary. This higher field strength near the cell boundary is mainly due to coupling between adjacent elements. The minimum field intensity is observed in most central part of the element in diode's OFF state, which allows the incident waves to transmit to the other side.

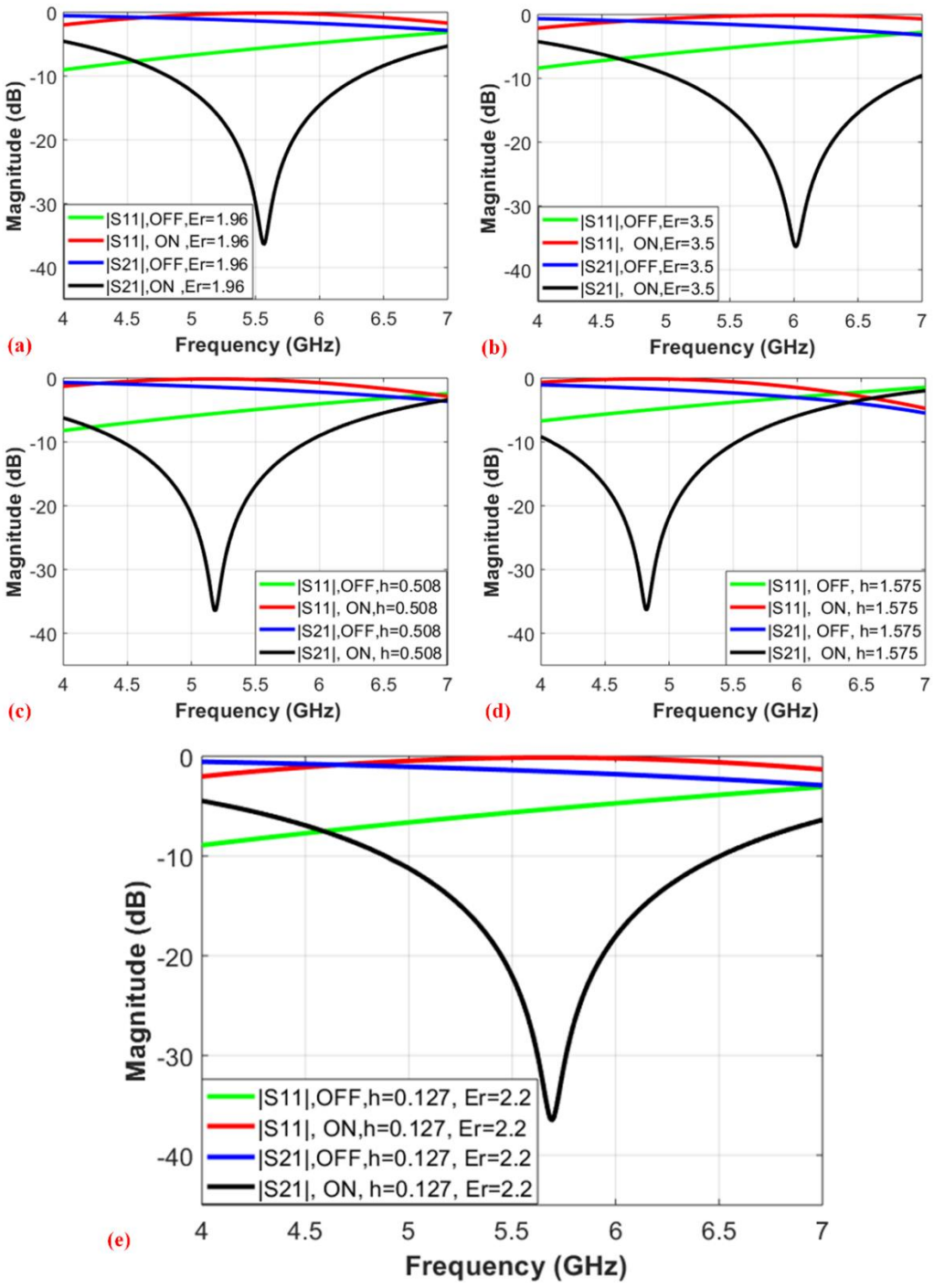

Figure 4. 3. Scattering characteristics of the proposed unit cell in diode's ON/OFF states: (a), (b) The effect of dielectric permittivity, (c), (d) The impact of the substrate thickness, and (e) reflection and transmission coefficients of the proposed element.

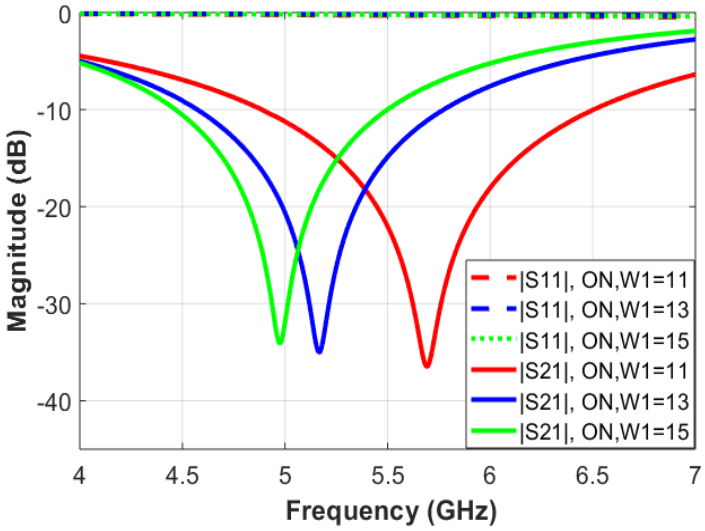

Figure 4. 4. Effect of element size on the scattering performance in diode's ON states.

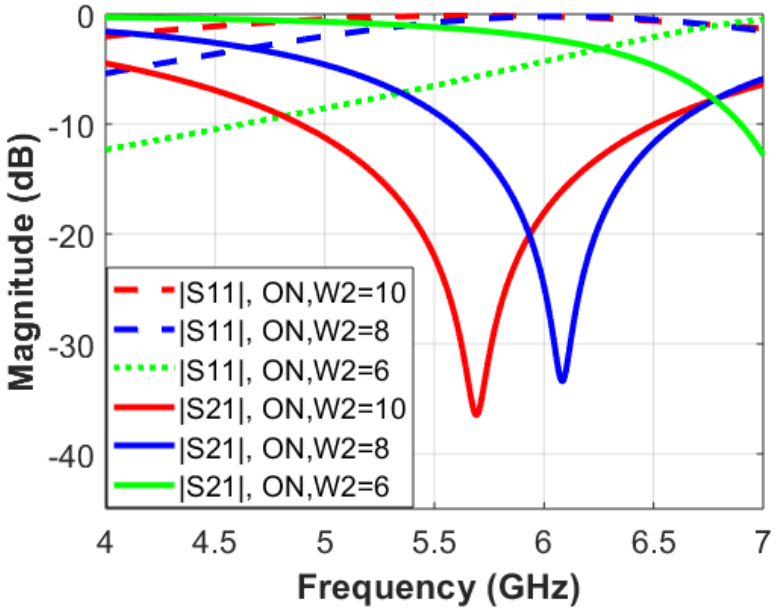

Figure 4. 5. Effect of radiating patch size on the scattering performance in diode's ON states.

4.4.2. Feed design

To excite the AFSS elements from all directions, an antenna with monopole radiation pattern is required. To achieve this objective, a rectangular patch antenna, shown in Figure 4. 7, is designed on Rogers RO-3006 substrate with a relative dielectric permittivity of 6.15, thickness of 1.27 mm, and a loss tangent of 0.002. The feed parameters are optimized to provide a better antenna performance in the operating band, as well as achieving compactness for minimum blockage. Table 4. 2 shows the optimized parameters of this monopole antenna. The feed has the size of 18 mm x 10 mm. The feed is fabricated and measured, as shown in Figure 4. 7 (b). The simulated and measured reflection coefficient and radiation pattern show reasonably good agreement, as shown in Figure 4. 8, and Figure 4. 9, respectively.

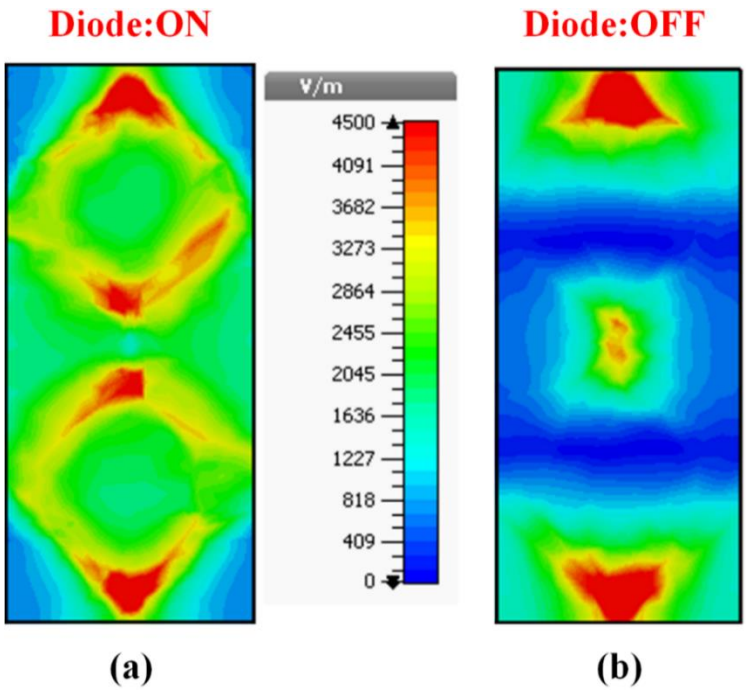

Figure 4. 6. Near field analysis on the proposed AFSS element surface: (a) reflection state. (b) transmission state.

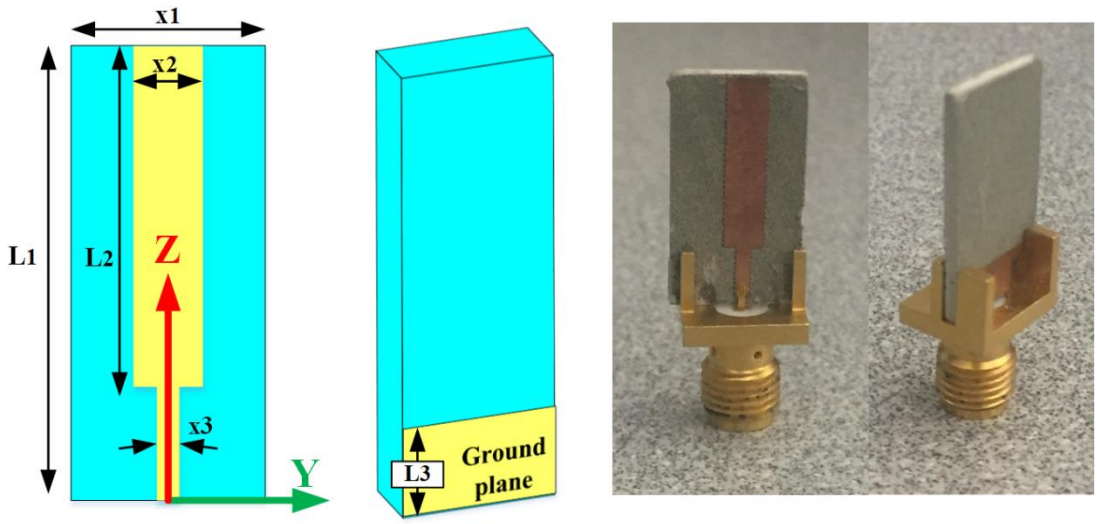

Figure 4. 7. Simulated and fabricated feed antenna model to excite ATFSS elements.

Table (4. 2): The feed dimensions.

Parameter	L1	L2	L3	x1	x2	x3
Value(mm)	18	13.15	3.5	10	3.0	1.2

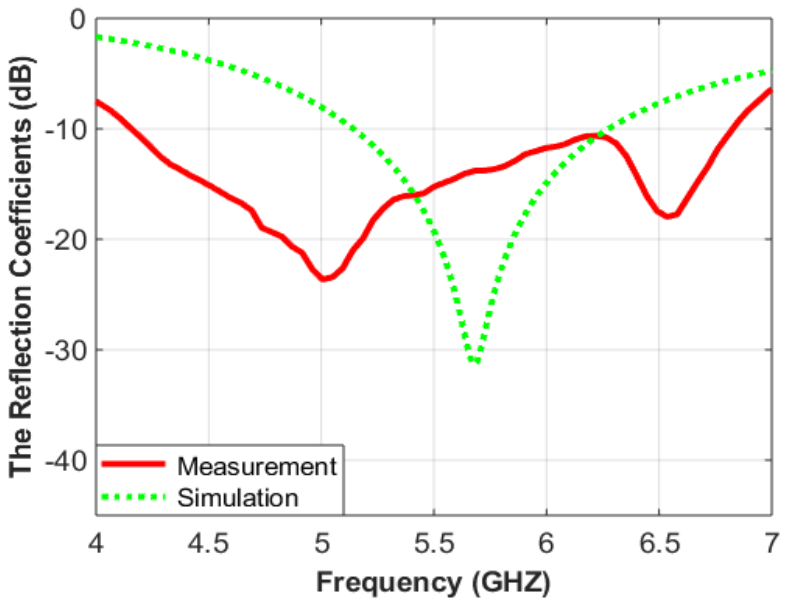

Figure 4. 8. Simulated and measured reflection coefficient of the feed.

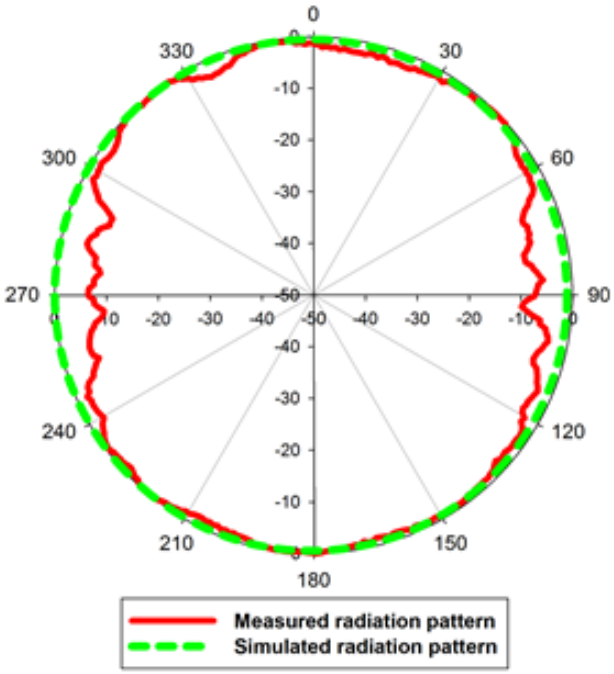

Figure 4. 9. Simulated and measured radiation patterns in the H plane of the monopole patch antenna.

4.4.3. Switched beamforming antenna

The operational mechanism of the proposed switched beamforming antenna is based on converting the omnidirectional radiation pattern of the source into the directional one by using the proposed ATFSS. When the pin-diodes of ATFSS are switched OFF, the ATFSS behaves like a transmitting surface, while in the ON state, it acts as a reflecting surface. The ATFSS screens are arranged in an equilateral triangle to switch the beam in multiple directions using different combinations of the ATFSS diodes. Figure 4. 10 shows the top and side 3-D view of the proposed antenna. In this design, each step sweeps the beam 120º in the azimuth direction. The schematic diagrams illustrating the operating mechanism of the proposed antenna and the simulated results of three beam steering steps (different combinations) are shown in Figure 4. 11 (a), (b).

The effect of feed position offset ‘d1’ on the performance of the proposed antenna in terms of reflection coefficient, realized gain, and the radiation pattern has also been investigated, and results are presented in Figure 4. 12 to Figure 4. 14. The presented results exhibit that as the feed moves away from the central position (for example, away from Side 3 towards positive X-axis), the resonant frequency shifts towards the upper band. This shift in the resonant frequency also effects on reducing the realized gain, as well as narrows the half power beamwidth (HPBW)

of the antenna. It is also evident that the feed position of d1=4 mm gives the best antenna performance, justifying the selection of this distance.

4.4.4 Swithed beamforming antenna design using a dipole as a source.

To evaluate the effect of feeding source on the proposed antenna performance, the patch antenna is replaced by a dipole as shown in Figure 4. 15. The same previous three combinations of the diodes shown in Figure 4. 11, are re-applied on the proposed ATFSS antenna. The simulated reflection coefficient gain and radiation patterns of the proposed antenna using dipole source for different diode states are shown in Figure 4. 16 to Figure 4. 18. The comparison of the proposed antenna gain using two different feed sources is summarized in Table 4. 3 and Table 4. 4. Based on the compared results, it is visible that both feeds result almost similar performance. However, the patch antenna with monopole radiation pattern is selected for fabrication and measurements due to its ease in fabrication and better handling during measurements.

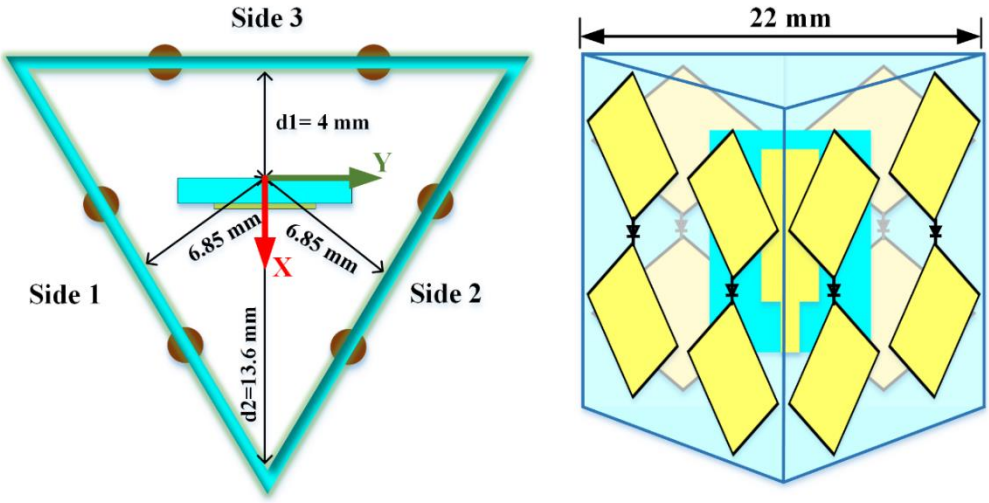

Figure 4. 10. Simulated model of the proposed ATFSS antenna in, top and side 3-D view.

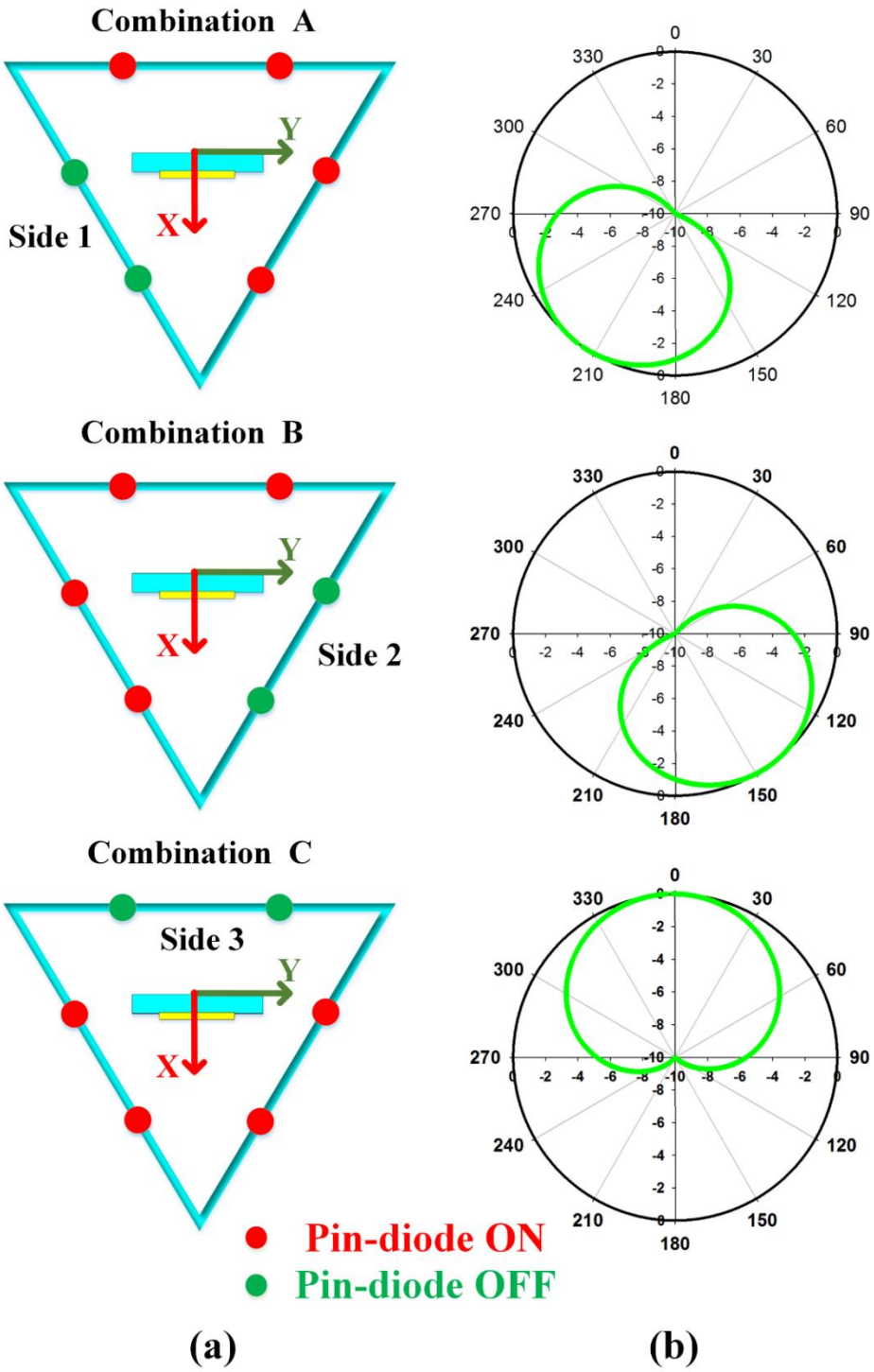

Figure 4. 11. Sketch of the proposed ATFSS antenna, (a) with multiple combinations of the diodes for steering the beam in various directions, and (b) the simulation results in each combination.

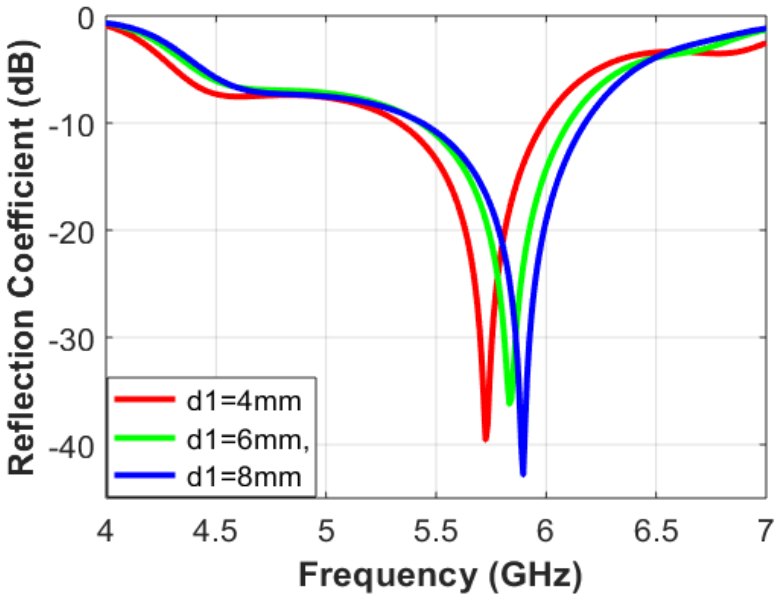

Figure 4. 12. Effect of feed offset ‘d1’ in ‘Combination C’ on the simulated reflection coefficient.

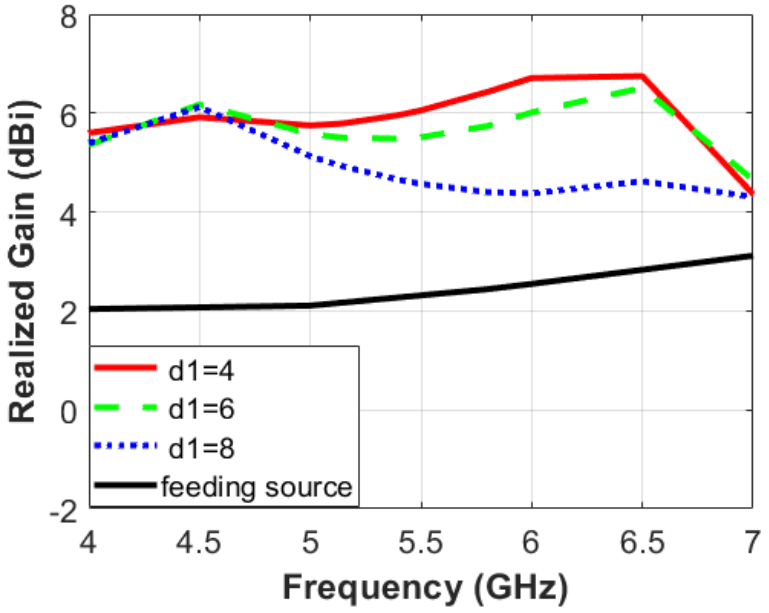

Figure 4. 13. Effect of feed offset ‘d1’ in ‘Combination C’ on the simulated realized gain.

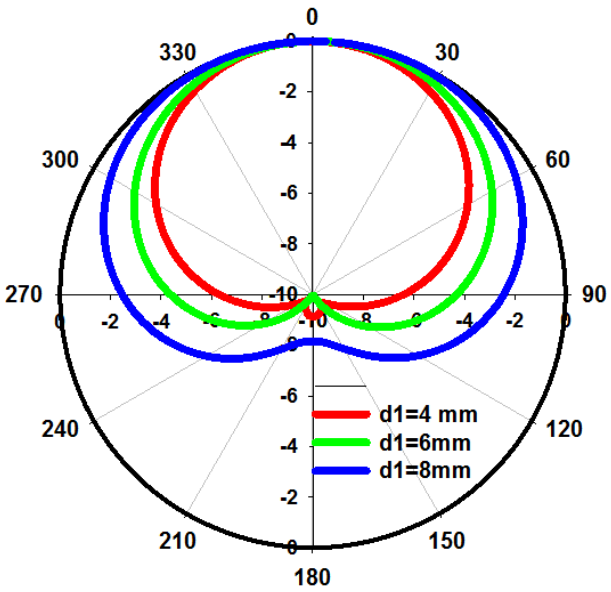

Figure 4. 14. Effect of feed offset ‘d1’ in ‘Combination C’ on the simulated radiation patterns in H-plane.

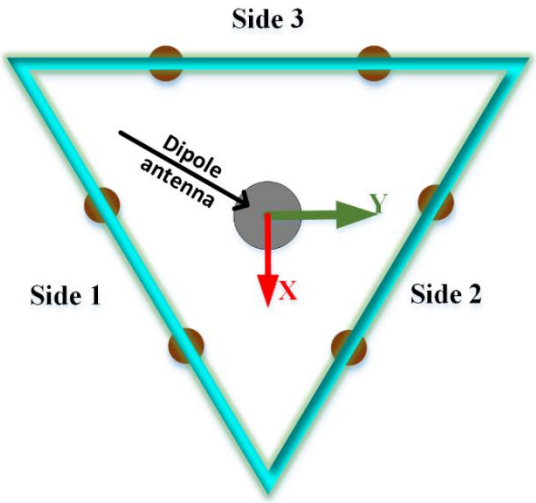

Figure 4. 15. Top view of the proposed active triangular FSS antenna using dipole as a source of EM waves.

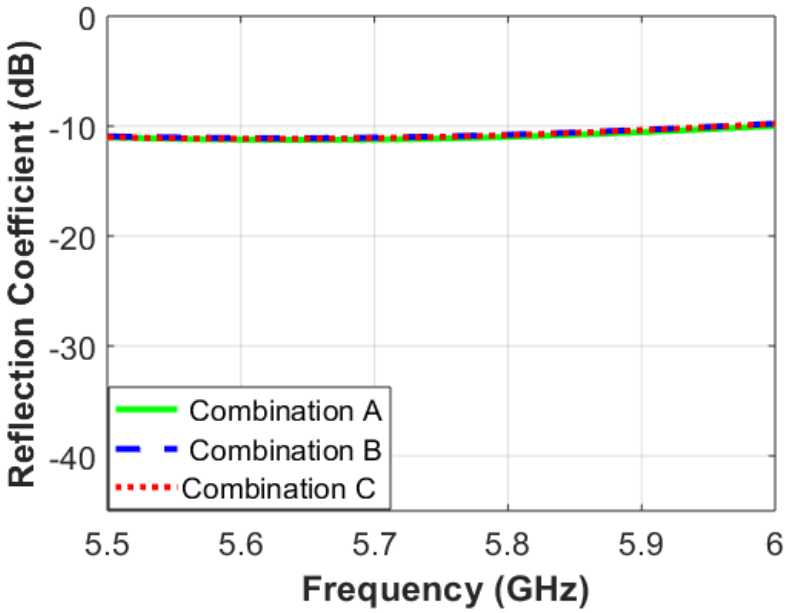

Figure 4. 16. Simulated reflection coefficient of the proposed ATFSS antenna.

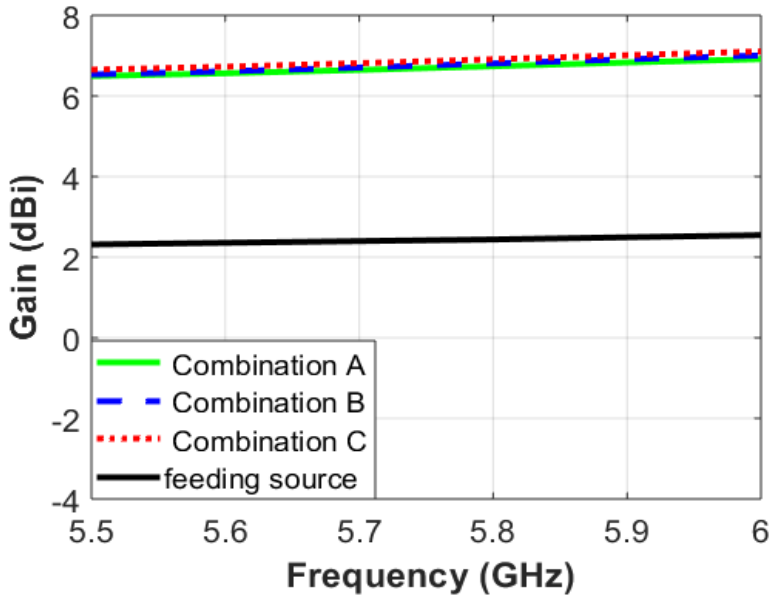

Figure 4. 17. Simulated gain of the proposed ATFSS antenna.

Table (4. 3): Simulated gain comparison in three used combinations along with the dipole used as a source (at 5.8GHz).

Combination	Gain (dBi)
Comb. A	6.7364
Comb. B	6.8074
Comb. C	6.9122
Dipole	2.1870

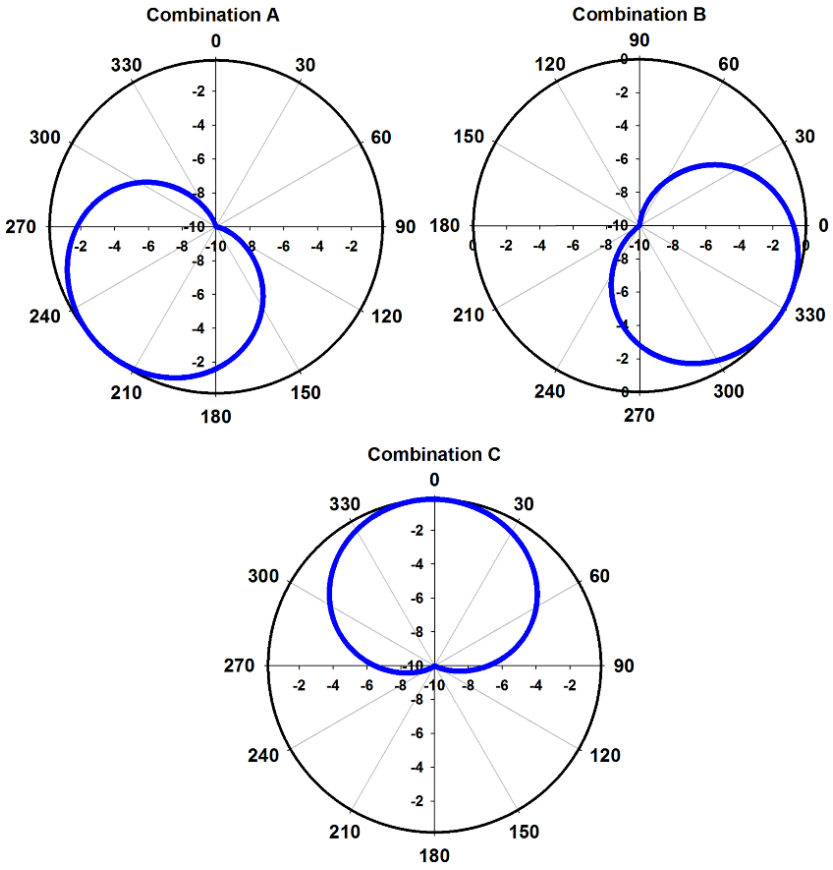

Figure 4. 18. Simulated radiation pattern of the proposed switched beamforming ATFSS antenna with dipole feed (in combination C).

4.5 Fabrication and measurement results

The proposed switched beamforming antenna is fabricated and measured. Figure 4. 19 shows multiple steps applied to assemble the fabricated antenna, and the measurement setup. In Step 1, an array of 2 x 6 passive FSS elements is fabricated. In Step 2, the unit cells are wrapped onto equilateral triangular foam to form AFSS. Due to the minimum dielectric thickness, the wrapping is done with ease but for an array designed on a material with larger substrate thickness can be arranged by cutting each side separately and binding their corner junctions using either glue or smallest diameter available plastic screws. While in Step 3, a high- frequency pin-diode is soldered in each passive FSS unit cell to form ATFSS element. To isolate the RF signal from DC biasing lines, RF chokes are used at top and bottom sides of each element. All the connections required a positive DC voltage supply are connected in parallel to make a single node, while all the GND connections are also unified making the second node (at the bottom). When the DC supply voltage of 1.2 V is applied, the diodes in AFSS operate in ON state, while 0V represents the OFF state. The antenna radiation pattern is measured in the anechoic chamber. The simulated and measured reflection coefficient gain and radiation patterns of the proposed antenna in the azimuth plane ($\theta = 90^{o}$) for different diode states are shown in Figure 4. 20 to Figure 4. 22. It is visible that the omnidirectional radiation pattern of the source antenna is converted into a directional pattern by using the proposed ATFSS switched beamforming screens. When the diodes in side 1 are OFF (combination A), the pattern is directed toward 240^{o}, when the diodes in side 2 are OFF (combination B), the pattern is directed towards 120^{o}, and when the diodes in side 3 are OFF (combination C), the pattern is oriented toward 0^{o}. Other beam steering directions can be achieved by choosing different sectors ON/OFF state combinations. With these features, the proposed antenna provides beam steering in the azimuth plane. The simulation and measurements show reasonably good agreement.

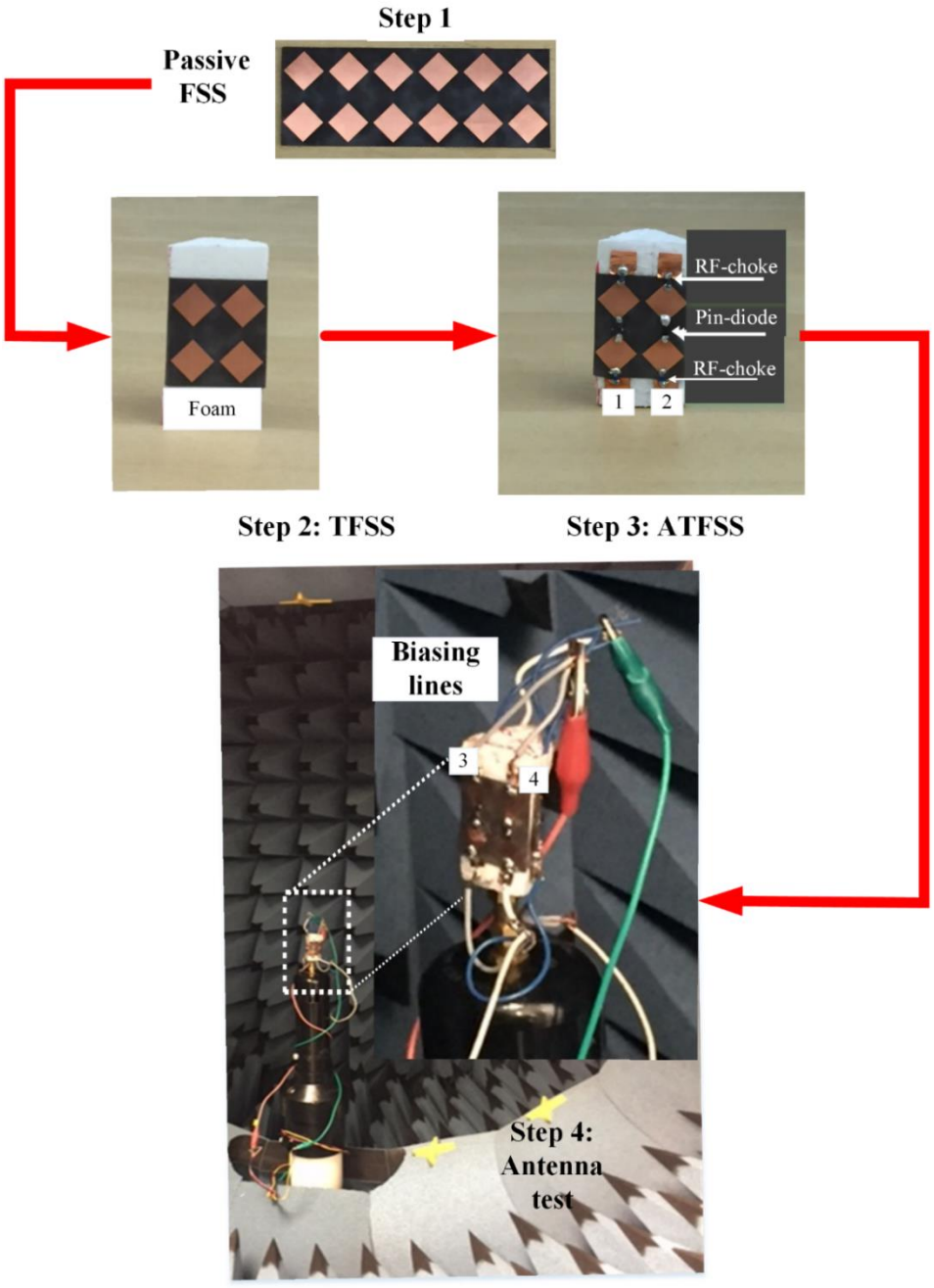

Figure 4. 19. Prototyping steps and measurement picture of the fabricated ATFSS antenna in an anechoic chamber.

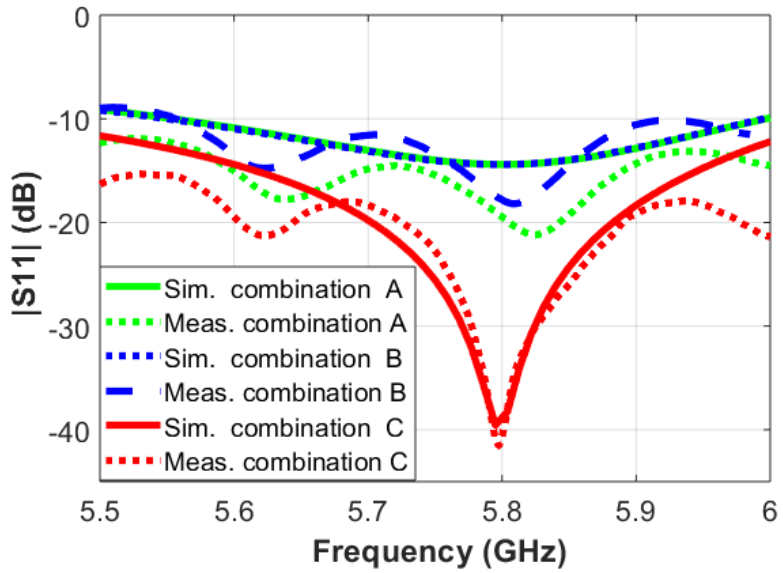

Figure 4. 20. Simulated and measured reflection coefficient of the proposed switched beamforming ATFSS antenna.

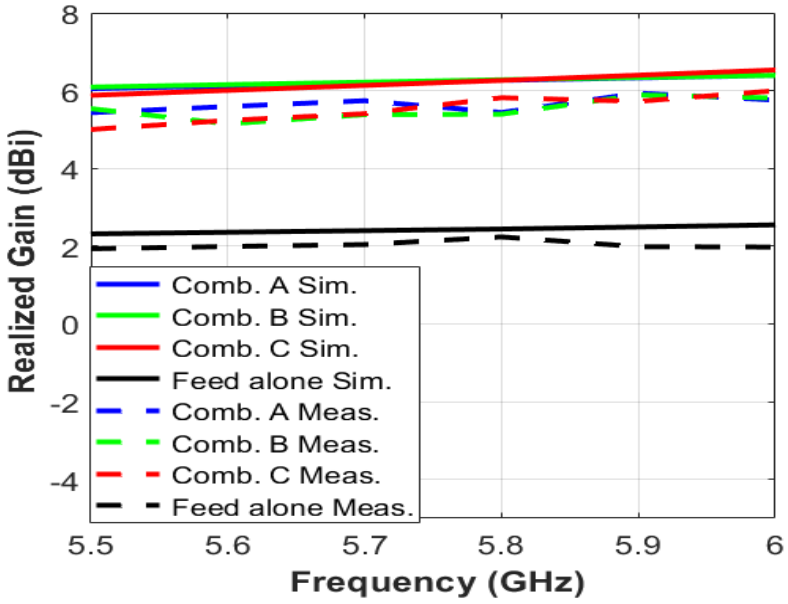

Figure 4. 21. Simulated and measured gain of the proposed switched beamforming ATFSS antenna.

Table (4. 4): Gain comparison in three used combinations along with the patch used as a source (at 5.8 GHz).

Combination	Gain (dBi)
Comb. A, sim.	6.264
Comb. A, meas.	*5.437*
Comb. B, sim.	6.280
Comb. B, meas.	*5.394*
Comb. C, sim.	6.289
Comb. C, meas.	*5.816*
Patch sim.	2.439
Patch meas.	*2.236*

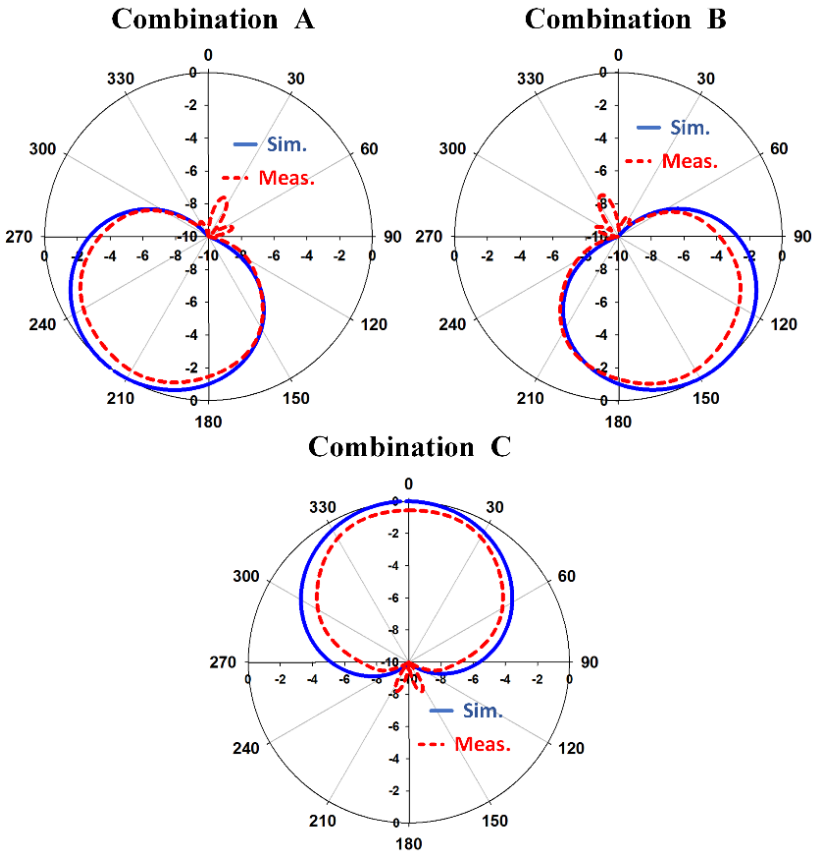

Figure 4. 22. Simulated and measured radiation patterns of the proposed switched beamforming ATFSS antenna (in combination C).

4.6 CONCLUSION

This paper has presented a new switched beamforming antenna using an active triangular frequency selective surface. The antenna consists of two parts: an FSS screen loaded with pin-diodes arranged in an equilateral triangle, and a radiating source with omnidirectional radiation pattern placed at the center of the structure. By applying multiple combinations of the diodes (in ON and OFF states) on each ATFSS screens, the switched beamforming has been achieved in various directions. The proposed switched beamforming antenna has shown the ability to sweep the radiations in the azimuth plane using three pin diode combinations on the ATFSS. The antenna has been fabricated and measured. Simulations and measurements have shown good agreement, in terms of reflection coefficient, beam directions, and realized gain.

4.7 REFERENCES

[1] J. Bernhard (2007). Reconfiguration Antennas. Lecture presented at Synthesis lectures on antenna in Urbana, Champaign.

[2] H. T. Friis, C. B. Feldman, and W. M. Sharpless, “The determination of the direction of arrival of short radio waves,” IEEE. Inst. Radio Eng., vol. 22, no. 1, pp. 47–78, 1934.

[3] E. Matthews, C. Cuccia, and M. Rubin, “Technology considerations for the use of multiple beam antenna systems in communications satellites,” IEEE Trans. Microw. Theory Techn., vol. 27, no.12, pp. 998–1004, 1979.

[4] A. Hakkarainen, J.Werner, N. Gulati. “Reconfiguration antenna based doa estimation and localization in cognitive radios: Low complexity algorithms and practical measurements,” CROWNCOM, Oulu, Finland, June 2014.

[5] A. Mozharovskiy, A. Artemenko, and A. Sevastyanov, “Beam steerable integrated lens antenna with waveguide feeding system for 71 76/81–86 GHz point-to-point applications,” EuCAP, Davos, Switzerland, 2016.

[6] A. Tamijani, L.Zhang, G. Pan et al., “Lens-enhanced phased array antenna system for high directivity beam-steering,” APSURSI, Spokane, WA., USA., July 2011.

[7] T.Ueda, S.Yamamoto, and Y. Kado, and T. Itoh, “Pseudo-traveling- wave resonator with magnetically tunable phase gradient of fields and its applications to beam-steering antennas,” IEEE Trans. Microw. Theory Techn., vol. 60, no.10, pp. 3043-3054, 2012.

[8] Y. Yokohama, T. Kodera, “Voltage Beam-Steerable Leaky-wave Antenna Using Magnet-less Non-Reciprocal Metamaterial (MNM),” ISAP, Hobart, TAS, Australia, 2015.

[9] T. A. Denidni, G.Y. Delisle, “A non linear algorithm for output power maximization of an indoor adaptive phased array,” IEEE Trans. Electromagn. Compat., Vol. 37, No. 2, pp. 201-209, May 1995.

[10] V. S. Rao, V.V. Srinivasan and S. Pal, “Generation of dual beams from spherical phased array antenna,” Electronics Lett., vol. 45, no. 3, pp. 441–442, 2009.

[11] G. Poilasne, P. Pouliquen, K. Mahdjoubi, L. Desclos, and C. Terret, “Active metallic photonic bandgap material MPBG: Experimental results on beam shaper,” IEEE Trans. Antennas Propag., vol. 48, no. 1, pp. 117–119, Jan. 2000.

[12] L. Zhang, Q. Wu, and T. A. Denidni, “Electronically Radiation Pattern Steerable Antennas Using Active Frequency Selective Surfaces,” IEEE Trans. Antennas Propag., vol. 61, no. 12, pp. 6000-6007, 2013.

[13] A. Edalati, and T. A. Denidni, “High-gain Reconfiguration sectoral antenna using an active cylindrical FSS structure,” IEEE Trans. Antennas Propag., vol. 59, no.7, 2011.

[14] J. Li, T. A. Denidni, and Q. Zeng, “Beam switching antenna based on active frequency selective surfaces,” IEEE NEMO, Ottawa, ON, Canada 2015.

[15] J. Li, T. A. Denidni, and Q. Zeng, “A dual-band Reconfiguration radiation pattern antenna based on active frequency selective surfaces,” Prop. APSURSI, Fajardo, Puerto Rico, July 2016.

CHAPTER 5 :(ARTICLE 2)

A New Corner-Reflector Antenna with Tunable Gain Based on Active Frequency Selective Surfaces

Ghada Hussain Elzwawi, Arun Kesavan, Rabeia Alwahishi, and Tayeb A. Denidni

IEEE Open Journal of Antennas and Propagation, vol. 1, pp. 88-94, 2020.

5.1 Abstract

A new corner-reflector antenna with a tunable gain based on active frequency selective surfaces (AFSSs) is presented. The proposed design comprises a dipole antenna as a source of the electromagnetic (EM) waves, and three reconfigurable AFSS layers of different size arranged at the same side of the dipole. Each screen consists of two AFSS panels that connected in series and rotated towards the feed to form a V-shaped corner reflector. These AFSS layers are mainly used to control the transmission/ reflection characteristics of the proposed antenna. By applying different combinations for ON/OFF states of diodes, the proposed antenna can adjust its gain value. The antenna performance in terms of reflection coefficient, radiation pattern in the H-plane and gain is analyzed at 5.8 GHz. To validate the concept of the proposed antenna, the prototype of this antenna is fabricated and measured. The measured results show a good agreement with the simulated ones.

5.2 Index terms

Active frequency selective surface, corner reflector antenna, directional radiation pattern, omnidirectional radiation pattern, tunable gain.

5.3 Introduction

Recently, wireless local area networks (WLANs) and point-to-point (PTP) systems have become widely used to connect two locations (stations), because of their low cost, simplicity, and flexibility compared with the hardwired networks such as fibre and copper. PTP wireless links are often used for telecommunications, security, and networking applications especially in rural areas where interference is not a significant issue. However, the quality of PTP wireless links is highly dependent on having a clear line of sight (LOS) between the two connected locations. Directional reconfigurable radiation antennas with high gain and beam steering capabilities have an important role in this aspect. This type of antennas can maximize the link performance, minimize the expected interference with other links, and extend the coverage range without the need of increasing the transmitting power [1]- [15]. In recent years, reconfigurable corner reflector antennas have received much attention from researchers as a promising solution for PTP wireless communications. By using this kind of antenna, a high level of directivity can be achieved [15]. The conventional corner reflector comprises a source of the electromagnetic (EM) waves and two metal reflecting sheets that are connected in series and rotated towards the feed to form a V shape [16]. This kind of reflector provides a wideband and high gain. However, the feeding space is determined as nearly 0.37λ, which is not always as convenient as expected [17]. By replacing the metal sheets of the corner reflector with artificial magnetic conductors (AMC), the overlap distance can be shortened, the structure will be lower profile and its gain will be improved [18]-[20]. For instance, in [22] C. Ma et al have presented a V antenna reflector based on (AMC) operating at 2.4GHz. By using this structure, the gain of the source (Monopole antenna) increases by about 5 dBi. Passive frequency selective surfaces have recently been used as another good alternative for the metal sheets in designing reflector antennas. In [23]- [24], authors have designed a corner reflector by using passive frequency selective surfaces. The existence of FSS behind the source antenna represses the backward radiation and enhances the directivity. However, these structures have no beam-steering ability. Active frequency selective surfaces have been used in [24] to add a reconfigurability feature and beam-steering capability to a corner reflector antenna.

This paper proposes a new corner reflector antenna with a tunable gain based on active frequency selective surfaces (AFSSs). The proposed antenna comprises a radiation source and three AFSS screens of different sizes. The radiation source is a dipole antenna with an omnidirectional radiation pattern. The AFSS screens are rotated toward the feed by an optimized angle of 60º and placed on the same side of the source. As we can figure, there is no work

published in the literature on corner-reflector antenna with a tunable and variable gain directional pattern.

With these features, the proposed antenna can be used in WLAN, long range PTP wireless links, cellular base stations, and other similar wireless communication systems.

This chapter is organized as follows. The design of the AFSS unit-cell is described in Section 5. 4. In Section 5. 5, the design and operational mechanism of the proposed antenna are discussed. Section 5. 6 presents the fabricated prototype and experimental results. The conclusion is presented in Section 5. 7.

5.4 Design of AFSS unit-cell

An array of AFSS is used to design an antenna with reconfigurable gain capability. The AFSS is suitable here because of its ability to realize the radiation pattern reconfigurability. The structure of the proposed AFSS unit-cell is shown in Figure. 5. 1. Each unit-cell consists of two diamond-shaped patches. The patches of the element are designed on Rogers RT 5880 substrate, which has a relative permittivity of 2.2, loss tangent of 0.0009, and thickness of h = 0.254 mm. These patches are electrically connected /disconnected by a pin-diode. When the diode is turned ON, the element provides a reflection characteristic. However, the transmission behaviour is achieved at the pin-diode OFF state. This element is simulated in a periodic environment of CST microwave studio considering an infinite number of elements along X- and Y-directions. In the simulation process, the high- frequency pin- diode (SMP1345-079LF) is modelled as a resistance of 1.5 Ω at pin-diode ON state. However, a parallel RC circuit with R_{OFF} =15 KΩ and C_{OFF} = 0.17 PF presents the diode at the OFF state. The values of the series resistor and parallel RC circuit are mentioned in the datasheet of the pin-diode [26]. To obtain more accurate simulation results, the element in [27] is re-simulated by considering both the RF chokes [28] and biasing circuits. The RF chokes are used at the top and bottom sides of the unit-cell to isolate the RF signal from biasing lines. The dimensions of the unit-cell improved model are listed in Table 5.1. The simulated transmission coefficients of the improved AFSS element are shown in Figure 5. 2. From this figure, it is noticeable that the unit-cell can reflect/ transmit the incident EM waves at the pin-diode ON and OFF states, respectively. These results were obtained under the normal wave incidence. However, as the AFSS reflectors should be arranged into V shape to form a new corner-reflector, the scattering parameters of the unit-cell were also tested under the oblique incidence of the waves ($\theta/2=30^{o}$). A match was found between the results of the normal and

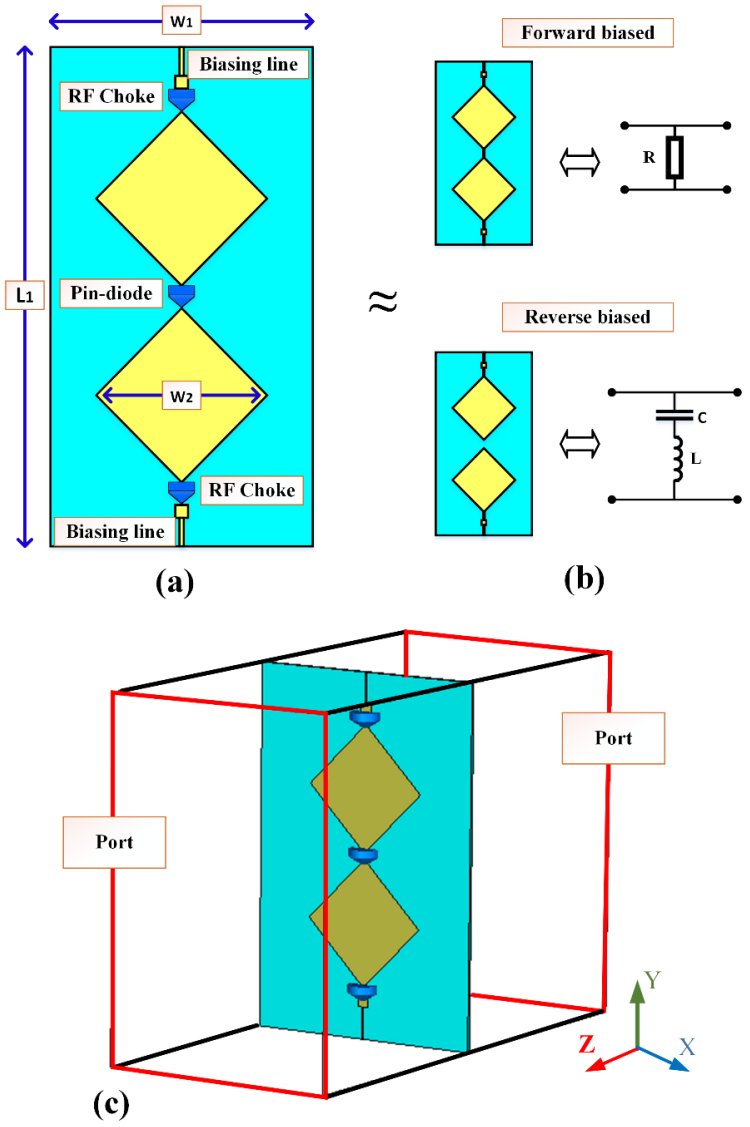

Figure 5. 1. (a) Structure of the proposed AFSS unit-cell, (b) equivalent circuit of the diode's ON/OFF states, (c) configuration of the AFSS element simulation.

oblique incidence as shown in Figure 5. 2. In the legend of this figure, (N) referred to normal incidence of waves, while the oblique incidence waves were expressed by (O). With these features, a new corner-reflector antenna with a tunable gain can be achieved by using this unit-cell.

Table (5. 1): Dimension of the improved AFSS unit- cell.

Parameters	L1	W1	W2
Values(mm)	30	20	10.5

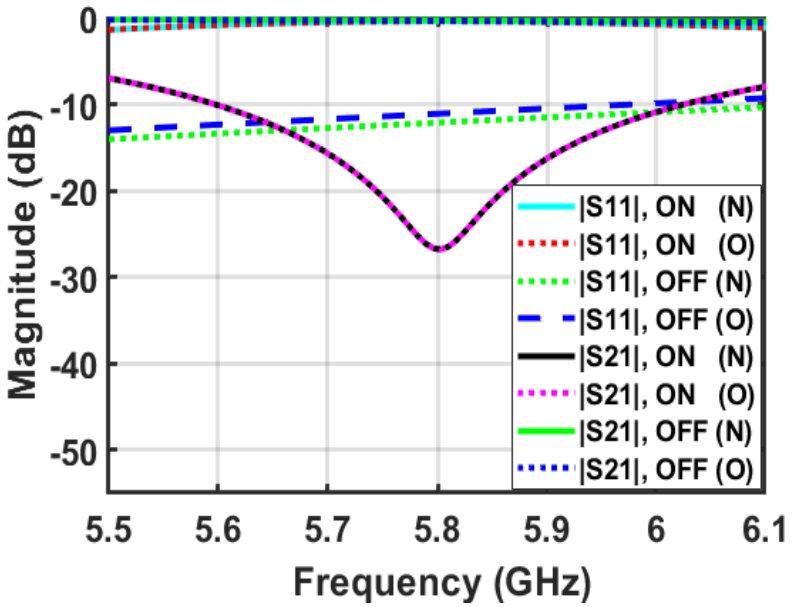

Figure 5. 2. Simulated scattering parameters of the proposed unit-cell under normal and oblique wave incidence (θ /2=30º).

5.5 Design and operational mechanism of the proposed antenna

5.5.1 Design of the proposed antenna

The configuration of the proposed antenna is shown in Figure 5.3. This antenna consists of a dipole as a source of the EM waves and three AFSS screens that are arranged on the same side of the dipole. The AFSS screens arranged in the order of Screen-3, Screen-2, Screen-1, where Screen 1 is the closest to the dipole. These screens are separated by an equal optimized space Sp=0.5λ. Each of Screen-2 and Screen-3 comprises two AFFS arrays that directed towards the feed by an angle θ=60º, (making V-shaped AFSS layer). However, two AFSS unit-cells rotated to each other by an angle of θ=60º formed Screen-1. The feed is placed away from Screen-1 by an optimized distance of Fs=0.3λ. Each AFSS array in Screen-2 has a size of 90 mm x 60 mm (1.74 λ ×1.16λ). These arrays consist of two sets of nine AFSS elements. 5x5 AFSS arrays forms Screen-3, each with a size of 150 mm x 100 mm (2.9 λ ×1.9λ).

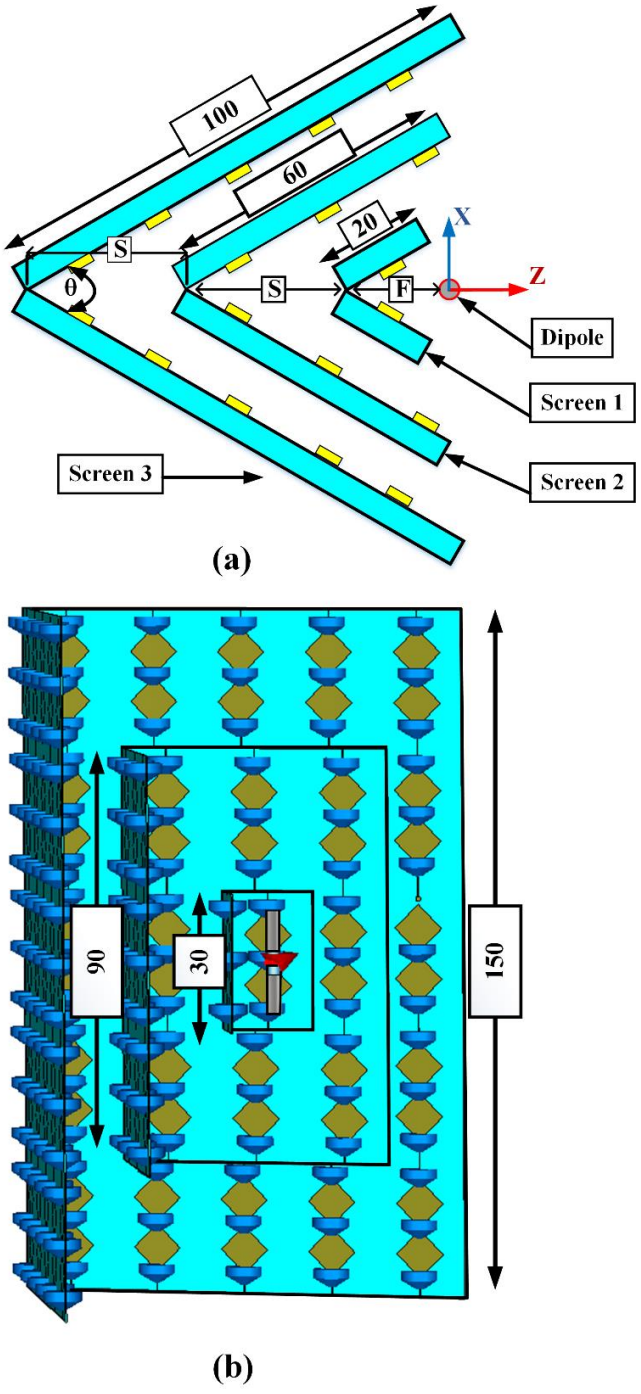

Figure 5. 3. Sketch of the proposed antenna. (a) top view, and (b) side 3-D view. (All dimensions are in mm).

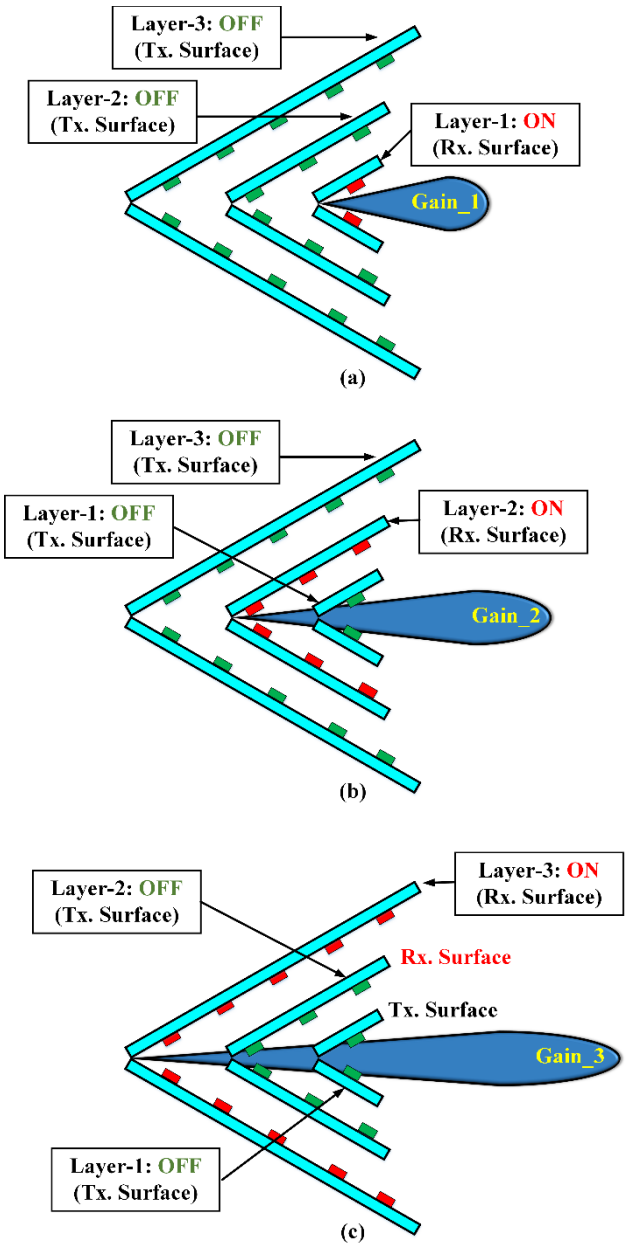

Figure 5. 4. Operational mechanism of the proposed antenna, (a) Case-I (ON-OFF-OFF State), (b) Case-II (OFF-ON-OFF State), (C) Case-III (OFF-OFF-ON State).

5.5.2 The operating mechanism of the proposed antenna

The operational mechanism of the proposed antenna is illustrated in Figure 5. 4. In this technique, the omnidirectional radiation pattern of the source is converted into a tunable gain directional

radiation pattern by using AFSS layers. The basic function of AFSS layers in this design is controlling the propagation of the incident waves in the resonance frequency band. When pin-diodes of these layers are switched OFF, the layers show transmitting behavior. However, in the ON state, the AFSS layers act as a reflecting surface. The performance of the proposed antenna is analyzed in three different cases. In these cases, different combinations of the AFSS diodes are applied into the proposed reflector antenna to alternate its gain between three different values. By adding more AFSS layers, more alternative values of gain can be achieved by the proposed design.

5.5.2.1 Case-I (ON-OFF-OFF State):

In this case, the diodes of layer-1 are switched ON, while other diodes are turned OFF. In another word, layer-1 represents a reflected surface, although layer-2 and layer-3 act as a transmitting surface. The effect of the feeding space (Fs) and the rotation angles of the AFSS layers (θ) are optimized for better antenna performance in terms of gain. During the optimizing process, different values of the rotating angles were tested. At each angle, the feeding space was moved into different positions ranging from 0.2 λ to 1.5λ. This range is selected to minimize the overall antenna size. The results of the parametric study process are shown in Figure 5. 5. This graph shows the relationship between the feeding space (Fs), the rotating angle of the AFSS layers (θ), and antenna gain. It is found that the maximum gain is obtained when Fs=0.3λ, and θ=60º. The proposed reflector antenna obtains a maximum gain of 7.11 dBi in Case-I.

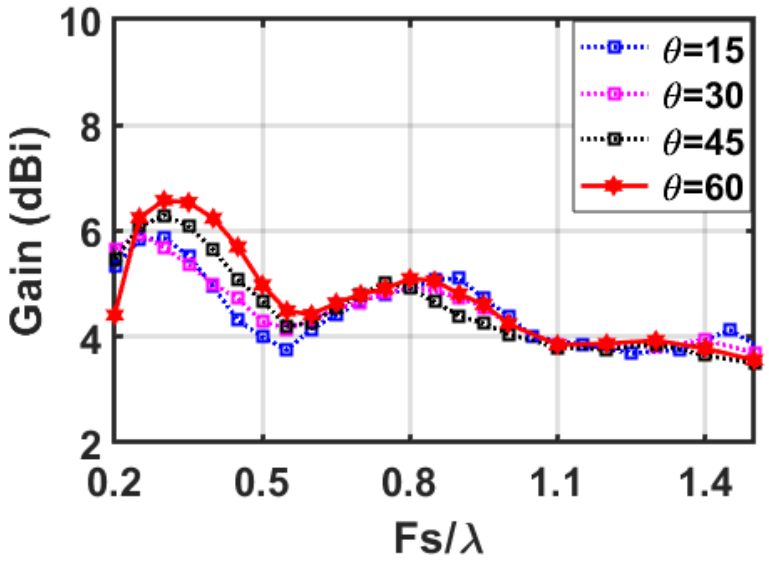

Figure 5. 5. Effect of feeding space (Fp), and rotating angle of the AFSS Screen (θ) on the simulated gain of the proposed antenna, when just one AFSS layer (Screen-1) is used.

5.5.2.2 Case-II (OFF-ON-OFF State):

The antenna performance in the OFF-ON-OFF state has also been investigated. Where, Screen-2 produces a reflection behaviour (ON state), while both of Screen-1 and Screen-3 act as a transmitting surface (OFF state). The feeding space (Fs), and rotation angles of the AFSS layers (θ) are used from the results presented in Case-I. However, the effect of the space between the AFSS layers (Sp) is optimized to achieve higher gain as shown in Figure 5. 6. In that the gain is plotted against various values of the space between the layers at different tested rotating angles of AFSS layers (θ). It is clearly seen that the proposed design produces a maximum gain at Sp=0.5λ which is about 11.1 dBi. In this case, the gain is increased by about 3.99 dBi compared with the obtained gain in Case-I (ON-OFF-OFF state).

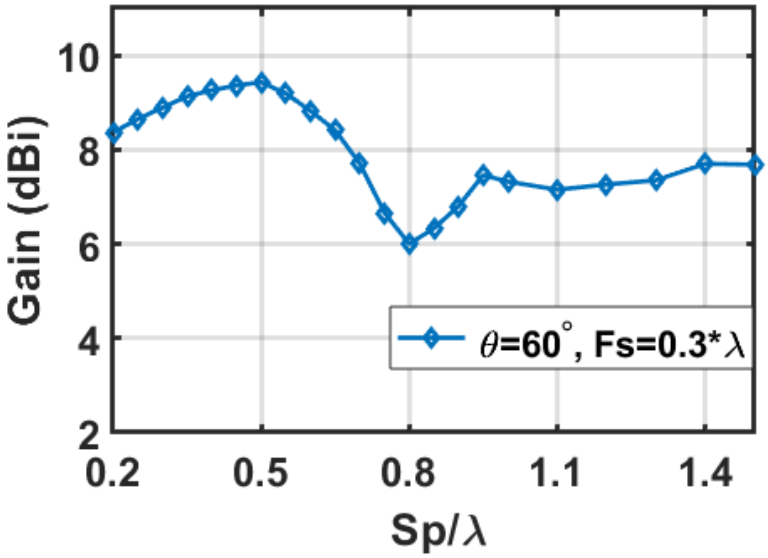

Figure 5. 6. Effect of space between layers (Sp) on the simulated gain of the proposed antenna, when two AFSS layers (Screen-1, Screen-2) are used. θ=60º, Fs=0.3λ.

5.5.2.3 Case-III (OFF-OFF-ON State):

In this case, the incident waves are passed through Screen-1 and Screen-2, while reflected by Screen-3. The feeding space (Fs), the space between the AFSS layers (Sp) and rotation angles of the AFSS layers (θ) are the same as used in Case-I and Case-II. The OFF-OFF-ON state produces the maximum gain of the proposed antenna, which is about 15 dBi. This value is higher than the value obtained in Case-I (ON-OFF-OFF state) by 7.89 dBi, and 3.9 dBi higher than that obtained in Case-II (OFF-ON-OFF state). The simulated reflection coefficient, realized gain, and

radiation patterns in the H plane of the proposed antenna are compared with the antenna source performance as shown in Figure 5. 7 – Figure 5. 9. From Case-I, Case-II, and Case-III, it is obvious that the proposed design can alternate its gain between three different values. It is important to mention here that the number of the reconfigurable AFSS layers controls the number of the alternating values of gain that can be produced by the proposed structure. Therefore, by adding more AFSS screens, the proposed design can provide more gain values.

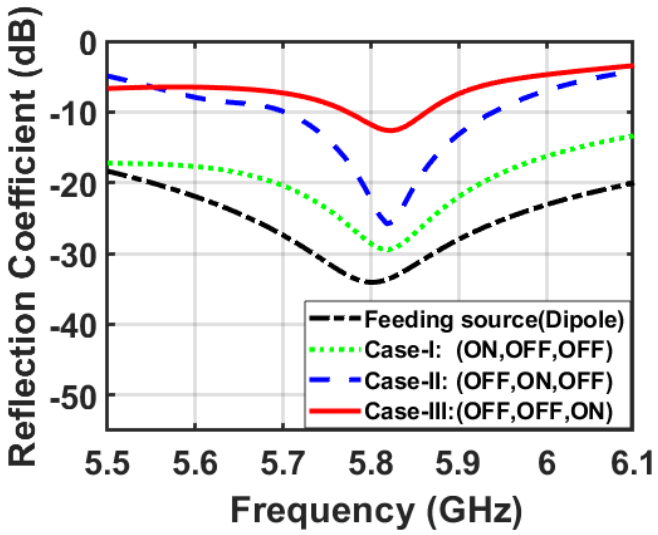

Figure 5.7. Simulated reflection coefficient of the proposed antenna, where θ=60º, Fs=0.3λ, and Sp=0.5λ.

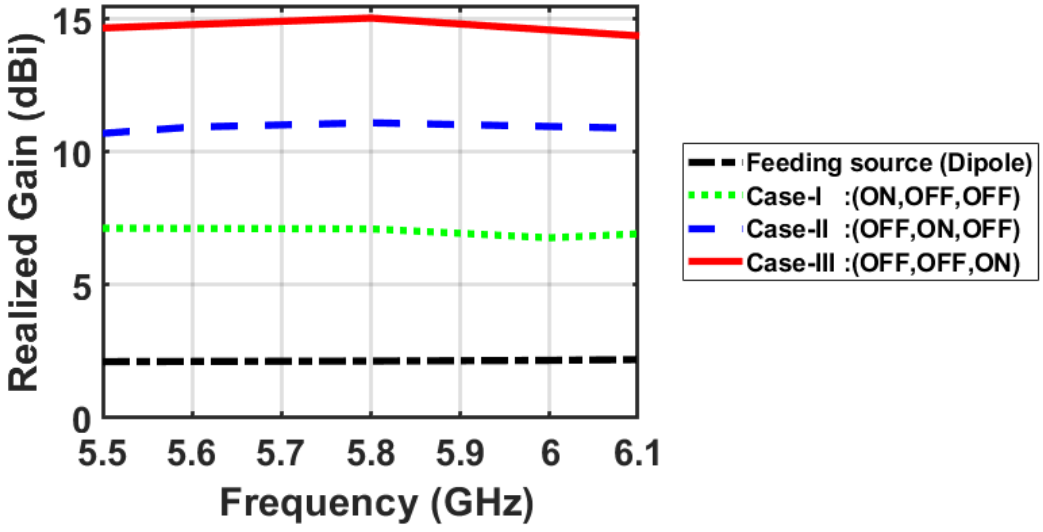

Figure 5. 8. Simulated gain of the proposed antenna, where θ=60º, Fs=0.3λ, and Sp=λ/2.

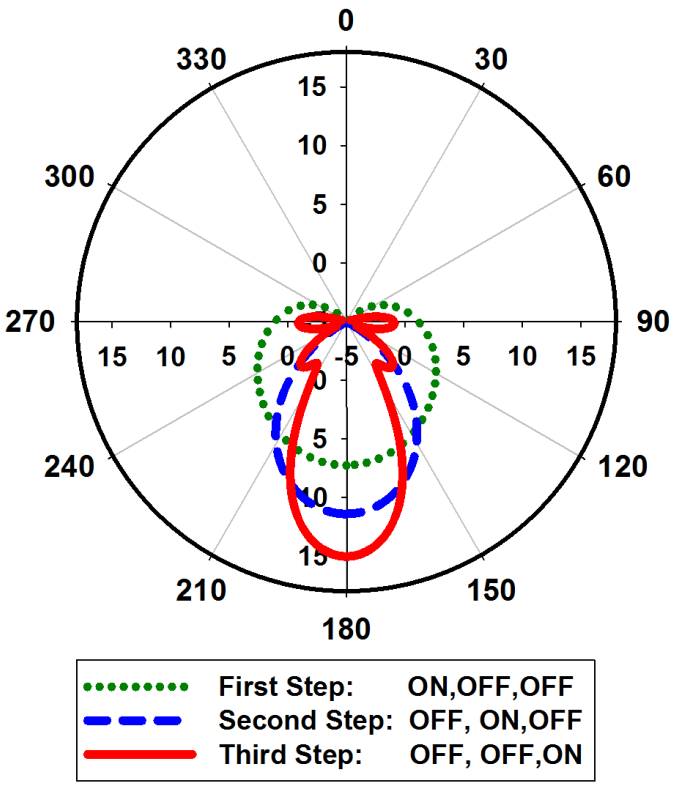

Figure 5. 9. Simulated radiation pattern of the proposed antenna in the H plane. Where θ=60º, Fs=0.3λ, and Sp=λ/2.

5.6 Fabrication and measurement results

The proposed antenna was fabricated, and its performance was measured. The fabrication and measurement process are done in different steps: In Step-1, a dipole antenna is fabricated. For simplicity, just two different AFSS screens (layers) are fabricated in Step-2. In Step-3, a Plexiglas-base is designed, to assemble and hold the multiple pieces of the proposed structure for the measurement process. The Plexiglas sheet has a size of 92 mm x131mm. Due to the minimum dielectric thickness of the AFSS layers, foam panels with the same size of these layers are used to support the AFSS screens by using glue. Moreover, some holes are drilled on the Plexiglas sheet to form V shape with an angle of 60º, and small plastic screws are used to fix the AFSS panels when inserted into the holes. The radiation patterns and realized antenna gain of the proposed design were measured in an anechoic chamber as shown in Figure 5. 10. However, the magnitude of the reflection coefficient (S11) was measured using a vector network analyzer. The measured and simulated reflection coefficients realized gain and radiation pattern in the H plane

of the proposed antenna in Case-I, and Case-II are shown in Figures 5. 11 to Figure 5. 13. The soldering of biasing lines and diodes in the fabricated prototype creates some amplitude losses. These losses observed in the marginal disagreement between the simulation and measurement results. From these figures, it is visible that the proposed design produces a directional radiation pattern with a maximum measured gain of 6.5 dBi in Case-I. However, a directional radiation pattern with a maximum measured gain of 10.5 dBi is obtained in Case-II. The results are also compared with the measured radiation pattern of the source (dipole antenna) which provides an omnidirectional with a maximum gain of 1.42 dBi. A comparison between the simulated and measured results is listed in Table 5. 2. Table 5. 3 lists a comparison between the performance of the proposed design and some previous designs exist in literature. It is clear that the proposed structure is the first corner-reflector antenna with a tunable and variable gain directional pattern.

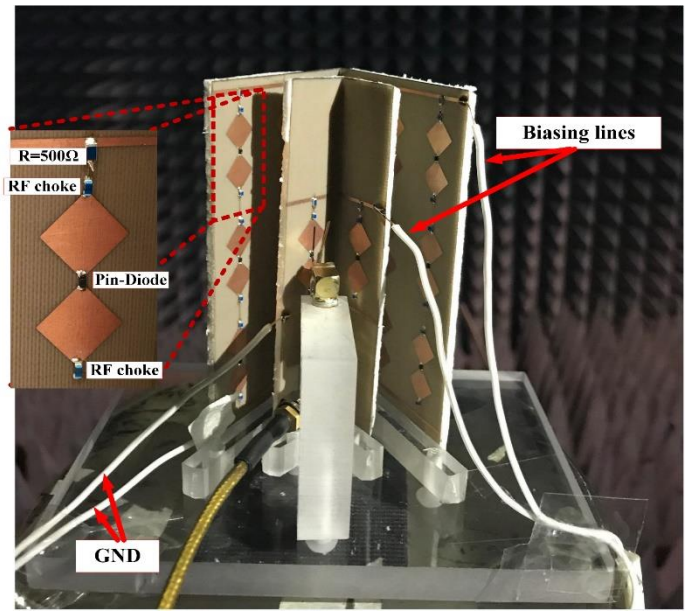

Figure 5. 10. A picture of the proposed prototype in an anechoic chamber.

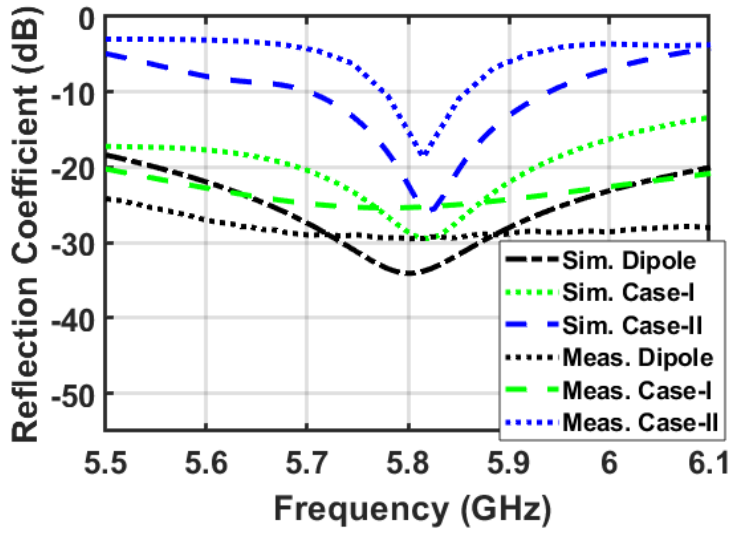

Figure 5. 11. Simulated and measured reflection coefficient of the proposed antenna, where θ=60º, Fs=0.3λ, and Sp=0.5λ.

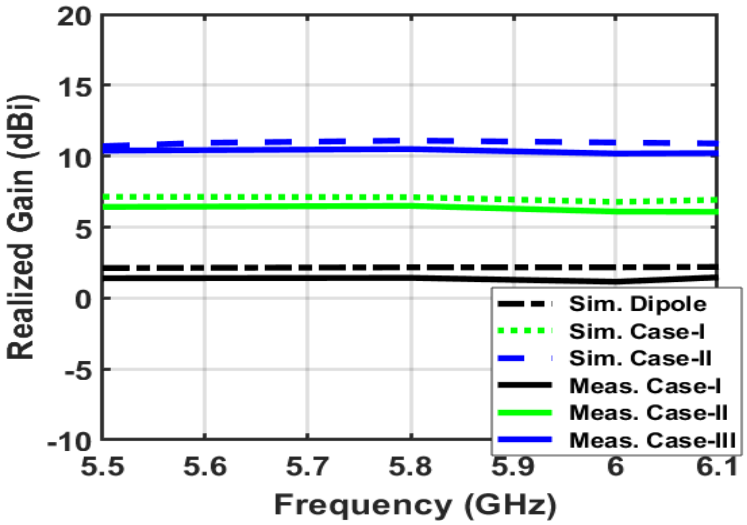

Figure 5. 12. Simulated and measured gain of the proposed antenna, where θ=60º, Fs=0.3λ, and Sp=λ/2.

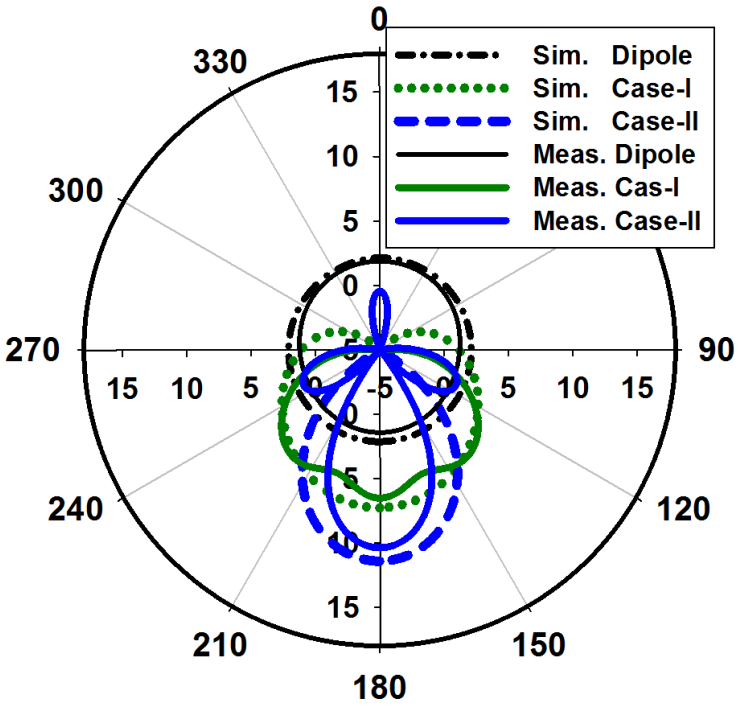

Figure 5. 13. Simulated and measured radiation pattern of Case-I and Case-II of the proposed antenna in the H plane. Where θ=60º, Fs=0.3λ, and Sp=λ/2.

Table (5. 2): The simulated and measured gain of the proposed antenna.

	Dipole	Case-I	Case-II
Simulated gain (dBi)	2.16	7.11	11.1
Measured gain (dBi)	1.42	6.5	10.4

Table (5. 3): Comparison of the proposed design with previous works.

Ref.	Freq. (GHz)	Size (λ)	Peak gain (dBi)	Tunable gain
[21]	2.4	0.96λ ×0.94λ	10 (sim.), 7.3(meas.)	-
[22]	4	1.5λ ×1.46λ	-	-
[24]	3	1.1λ ×1.1λ	Omnidirectional	-
	5.5	2.4 λ ×2.4λ	12.5(sim.), 14.5(meas.)	
proposed	5.8	0.58λ ×0.386λ	7.11(sim.), 6.5 (meas.)	Yes
		1.74 λ ×1.16λ	11.1(sim.), 10.4 (meas.)	
		2.9 λ ×1.9λ	15 (sim.)	

5.7 CONCLUSION

This paper has proposed a novel corner-reflector antenna with a tunable gain using active frequency selective surfaces (AFSSs). This new corner-reflector antenna contains two essential parts: an excitation source (a dipole antenna) and transmitting/reflecting sheets (reconfigurable AFSS layers). These layers have different sizes and formed in V shape at one side of the feed. By applying multiple combinations for diodes ON/OFF status on the AFSS screens, the omnidirectional radiation pattern of the source has been modified into a directional radiation

pattern with a tunable gain. The number of gain values that can be obtained by the proposed antenna depends on the number of the AFSS layers used in the proposed structure. Therefore, by adding more AFSS screens to the proposed structure, more values of gain can be achieved.

5.8 REFERENCES

[1] F. Yang, Y. Rahmat-Samii, (2008). Electromagnetic Band Gap Structures in Antenna Engineering. Cambridge, UK: Cambridge University Press. doi: https://doi.org/10.1017/CBO9780511754531.

[2] S. Akiba, M. Oishi, Y. Nishikawa, J. Hirokawa, M. Ando, “Photonic Approach to Beam Steering of Phased Array Antenna,” presented at the 2013 Int. Conf. URSI, Hiroshima, Japan.

[3] C. Ko, I. -. Tarn and S. Chung, "A Compact Dual-Band Pattern Diversity Antenna by Dual-Band Reconfigurable Frequency Selective Reflectors With a Minimum Number of Switches," IEEE Trans. Antennas Propag, vol. 61, no. 2, pp. 646-654, Feb. 2013.

[4] B. A. Decena, J. R. Luzon and M. C. L. Purisima, "2.4 GHz pattern reconfigurable corner reflector antennas using frequency selective conductor loops and strips,” presented at the 2017 Int. Conf. TENCON, Penang, pp. 2914-2919.

[5] Bai, Y., Xiao,S., Liu,C., et al.: “Design of pattern reconfigurable antennas based on a two-element dipole array model", IEEE Trans. Antennas Propag., vol.61, no.9, pp. 4867–4871, 2013.

[6] A. Edalati and T. A. Denidni, “High-gain reconfigurable sectoral antenna using an active cylindrical FSS structure," IEEE Trans. Antennas Propag., vol. 59, no. 7, pp. 2464_2472, Jul. 2011.

[7] A. Hakkarainen et al., “Reconfigurable antenna based doa estimation and localization in cognitive radios: Low complexity algorithms and prac-tical measurements," presented at the 2014 Int. Conf. CROWNCOM, Oulu, Finland, pp. 454_459.

[8] A. Mozharovskiy, A. Artemenko, A. Sevastyanov, V. Ssorin, and R. Maslennikov, “Beam-steerable integrated lens antenna with waveguide feeding system for 71_76/81_86 GHz point-to-point applications," presented at the 2016 Int. Conf. EuCAP, Davos, Switzerland, pp. 1_5.

[9] L. Zhang, Q. Wu, and T. A. Denidni, “Electronically radiation pattern steerable antennas using active frequency selective surfaces," IEEE Trans. Antennas Propag., vol. 61, no. 12, pp. 6000_6007, Dec. 2013.

[10] A. Dadgarpour, M. S. Sorkherizi, T. A. Denidni, and A. A. Kishk, “Passive beam switching and dual-beam radiation slot antenna loaded with ENZ medium and excited through ridge gap waveguide at millimeter-waves," IEEE Trans. Antennas Propag., vol. 65, no. 1, pp. 92_102, Jan. 2017.

[11] B. Liang, B. Sanz-Izquierdo, E. A. Parker, and J. C. Batchelor, “Cylindrical slot FSS con_guration for beam-switching applications,'' IEEE Trans. Antennas Propag., vol. 63, no. 1, pp. 166_173, Jan. 2015.

[12] J. Li, Q. Zeng, R. Liu, and T. A. Denidni, “A compact dual-band beamsweeping antenna based on active frequency selective surfaces,'' IEEE Trans. Antennas Propag., vol. 65, no. 4, pp. 1542_1549, Apr. 2017.

[13] M. Jusoh, T. Sabapathy, M. F. Jamlos and M. R. Kamarudin, "Reconfigurable Four-Parasitic-Elements Patch Antenna for HighGain Beam Switching Application," IEEE Antennas Wireless Propag. Lett., vol. 13, no., pp. 79-82, 2014.

[14] S. M. Mahmood and T. A. Denidni, "Pattern-Reconfigurable Antenna Using a Switchable Frequency Selective Surface With Improved Bandwidth," IEEE Antennas and Wireless Propagation Letters, vol. 15, pp. 1148-1151, 2016.

[15] Chih-Hsiang Ko, I-Young Tarn and Shyh-Jong Chung, “A Compact Dual-Band Pattern Diversity Antenna by Dual-Band Reconfigurable Frequency-Selective Reflectors With a Minimum Number of Switches,” IEEE Trans. Antennas Propag., vol. 61, no. 2, pp. 646-654, Feb. 2013.

[16] M. T. Jusoh, O. Lafond, F. Colombel and M. Himdi, "Performance and Radiation Patterns of a Reconfigurable Plasma Corner-Reflector Antenna," IEEE Antennas Wireless Propag. Lett., vol. 12, pp. 11371140, 2013.

[17] Thomas A. Milligan, Modern Antenna Design 2nd ed., John Wiley& Sons, Inc.,2005.

[18] J.D. Krraus, R. J. Marherfka, Antenna: For All Applications 3rd ed., McGraw-Hill Companies, Inc.,2003.

[19] M. Li, Q. L. Li, B. Wang, C. F. Zhou and S. W. Cheung, "A LowProfile Dual-Polarized Dipole Antenna Using Wideband AMC Reflector," IEEE Trans. Antennas Propag., vol. 66, no. 5, pp. 26102615, May 2018.

[20] K. N. Paracha et al., "A Low Profile, Dual-band, Dual Polarized Antenna for Indoor/Outdoor Wearable Application," IEEE Access, vol. 7, pp. 33277-33288, 2019.

[21] F. Mouhouche, A. Azrar, M. Dehmas and K. Djafri, "Gain improvement of CPW-Fed monopole antenna over dual-band AMC structure," presented at the 2017 Int. Conf. ICEE-B, Boumerdes, pp. 1-4.

[22] C. Ma et al., "Antenna reflector based on air loaded AMC structure," presented at the 2017 Int. Conf. ACES, Suzhou, China, pp. 1-2.

[23] Y. Tanizawa, K. Cho, H. So and A. Ando, "Radiation characteristics of corner reflector antenna employing frequency selective surface," presented at the 2016 Int. Conf. Asia-Pacific Radio Science Conference (URSI AP-RASC), Seoul, South Korea, pp. 1-3.

[24] A. Chatterjee and S. K. Parui, "Performance Enhancement of a DualBand Monopole Antenna by Using a Frequency-Selective SurfaceBased Corner Reflector," IEEE Trans. Antennas Propag., vol. 64, no. 6, pp. 2165-2171, June 2016.

[25] B. A. Decena, J. R. Luzon and M. C. L. Purisima, "2.4 GHz pattern reconfigurable corner reflector antennas using frequency selective conductor loops and strips," presented at the 2017 Int. Conf. TENCON, Penang, Malaysia, pp. 2914-2919.

[26] Skyworks Datasheet for SMP1345-079LF, Skyworks, Inc., Woburn, MA, USA, 2014. [Online]. Available: http://www.skyworksinc.com/uploads/documents/200046M.pdf

[27] G. Elzwawi, H. Elzwawi, M. M.Tahseen, and T.A. Denidni "Frequency Selective Surface Based Switched-Beamforming Antenna," IEEE Access, vol. 6, pp. 48042-48050, July 2018.

[28] CHIP COIL (CHIP INDUCTORS) LQW18AN00D REFERENCE SPECIFICATION. [Online]. Available: https://search.murata. co.jp/Ceramy/image/img/P02/JELF243A-0024.pdf

CHAPTER 6 :(ARTICLE 3)

Reconfigurable Reflector Antenna with Beam-Tilting Capability

Ghada Hussain Elzwawi, Muhammad M. Tahseen, and Tayeb A. Denidni

International Journal of Electronics and Communications, (submitted).

6.1 Abstract

A novel beam-tilting reconfigurable reflector antenna (RRA) based on active frequency selective surfaces (AFSS) is proposed. The AFSS-based RRA comprises of three smaller AFSS screens. These screens are arranged in a way resembling a parabolic reflector. The left and right AFSS screens are flexible to be able to rotate towards the feed. The AFSS is designed using periodic elements with dimensions of 0.13λ x 0.1λ, while the RRA holds a size of 235.5 mm x 169 mm (1.9 λ x1.37 λ). The transmission/ reflection characteristics of the proposed RRA are investigated in various combinations for diode ON/OFF states. The operating frequency of the antenna is 2.45 GHz. The performance of the RRA with a mechanical beam-tilting approach is also evaluated. To validate the concept of the proposed RRA, the prototype of the proposed antenna is fabricated and measured. A good agreement between simulations and measurements is observed. The maximum measured gain is 10.6 dBi. A measured mechanical beam-tilting range of ±30º (off broadside) has been obtained.

6.2 Keywords

Active frequency selective surface (AFSS), reconfigurable reflector antenna (RRA).

6.3 Introduction:

High-gain parabolic reflectors have widely been utilized for numerous applications, especially the ones that require high-data-rates and resolution [1]. The gain performance of a reflector is determined by the physical aperture area and its associated aperture efficiency [2]. The conventional parabolic reflector consists of two main parts: a feed, and a reflector surface. The excitation source is placed in the focal point of the parabolic reflector. A metal with a parabolic shape forms the reflector surface. This surface is used to reflect the electromagnetic (EM) waves that are generated by the feed. This antenna type can provide a beam with high directivity, low side-lobe level, high aperture efficiency, and wide bandwidth. However, the conventional parabolic reflector has a heavy structure and a limited beam-scanning capability.

For reducing the profile of the conventional reflector and controlling the incident waves' direction, various techniques have been used. For instance, reflectarray antennas (RA) incorporate the advantages of reflectors with the advantages of antenna arrays. Therefore, reflectarray can provide higher aperture efficiency, broad-beam scanning ability and wider bandwidth [3]-[5]. The split and displace panel method has been performed in [6] to develop the bandwidth of RA. In [7], two layers of passive frequency selective surfaces have been utilized to construct a reflector. This structure can support ultra-wideband (UWB) applications. However, incident waves cannot be transmitted by using this design. For this matter, an active planar metal surface has been presented in [8]. In [9], different curvatures of the conformal FSS have been incorporated in an omnidirectional antenna to achieve a wide beamwidth. By adding a corner reflector based on FSS operating at 5.8 GHz, the antenna exhibits a different beamwidth. This antenna introduces a maximum gain of 8.3 dBi and 6.8 dBi at 5.8 GHz and 3.5 GHz, respectively. M. M. Tahseen et al. have presented a new low-loss, and compact reconfigurable RA design [10]. This antenna produces electronically beam steering within ±40º. Due to the presence of ground plane at the back, lenses/ transmit array cannot be designed in such structure.

Beam-tilting can be achieved electronically or mechanically [11]-[20]. Electrical beam-tilting techniques are usually achieved by changing the characteristics of the signal phase using active elements, such as pin-diodes or varactors [12]– [16]. These techniques suffer from a noticeable gain drop when the beam is tilted. Mechanical beam-tilting techniques are accomplished by using mechanical setup increases the system size as well as the weight. However, these techniques introduce a better performance at higher tilt angles and conserve the gain of the system [17]. Conventionally, beam control can be accomplished by utilizing phased arrays. In this method,

phase controlling is achieved by phase shifters. Therefore, the phase shifter is one of the key elements in electronically beam-tilting array antenna systems. [18]- [19].

Recently, periodic structures have extensively been used for beam-tilting [20]-[22]. For example, beam-tilting from -21º to +24º at 9.4 GHz is performed in [22] by integrating five-layers of 3 × 3 FSS array in front of a planar Vivaldi antenna, which increases the overall antenna size.

This paper presents a novel beam-tilting reconfigurable reflector antenna (RRA) operating in WLAN band. The proposed structure is designed using an array of AFSS elements. This array is divided into three sections for an easy movability (central, right, and left sections). A WLAN-band patch antenna which is placed away from the array sections is used to excite the elements in the array. This model is optimized to introduce an RRA with high gain. A mechanical beam tilting technique is also employed, where the right and left sections of the AFSS array are rotated towards the feed to tilt the main beam off-broadside. This mechanical beam tilting mechanism is distinguished from the previous tilting techniques with its ability to tilt the main beam without adding any extra layers or setups to the main antenna structure. Therefore, the size and weight of the main structure of the RRA remains the same. The presented beam tilting method introduces a better performance at higher tilt angles and conserves almost the same gain of the system. By applying this beam-tilting technique, a maximum beam-tilting range of ±30° (off broadside) is achieved at 2.45 GHz. The proposed beam tilting RRA is fabricated and measured. A good agreement between the simulated and measured results is achieved in terms of reflection coefficient, beam direction, and realized gain. To our best knowledge, the proposed structure is the first design where active FSS is used to provide the beam reconfigurability when AFSS is arranged in a parabolic shape. As it is well known in literature that the main disadvantage in parabolic reflector designs is the minimum beam scanning ability, while using the proposed technique, a high gain antenna can be designed (when size of the antenna is increased based on any given specification). In the presented work, the antenna performance is investigated using pin-diode. The reflection/transmission behavior of AFSS is achieved when pin-diode states are switched using an external DC biasing voltage. In addition, a mechanical beam steering approach has also been presented when one of the side panels of the antenna are rotated either towards

or away from the central panel. It is also important to mention here that, if varactor diodes are attached in the FSS then electronically beam steering can be achieved instead of mechanical.

With these features, the proposed antenna can be used for various wireless applications, such as radiolocation findings, mobile satellite communication, amateur radio, and satellite communications.

The chapter is organized as follows. In Section 6. 4, the design of the AFSS unit-cell is presented. The proposed RRA and mechanical beam-tilting technique are discussed in Section 6.5 and Section 6. 6, respectively. Section 6. 7 presents the prototyping and measurement results. The conclusion is given in Section 6.7.

6.4 Design of an active FSS unit cell

To design an RRA, an AFSS (FSS surface embedded with pin-diodes) is used. This surface can control wave propagation when an external voltage is applied. The transmission/reflection characteristics of the AFSS are illustrated in [23]. When the diodes are switched ON, the reflection behavior from the surface is achieved. However, the OFF state provides a transmission characteristic. Fig. 6. 1 (a) shows the proposed AFSS element. This unit-cell contains two rectangular patches that are electrically connected /disconnected by a pin-diode. The high-frequency pin- diode (SMP1345-079LF) is used in this structure. This diode is modelled as a resistance of 1.5 Ω at ON state. However, a parallel RC circuit with Roff =15KΩ and Coff=0.17 pF represents the diode in the OFF state, as mentioned in the datasheet [24]. The unit cell patches are mounted on Rogers RT 5880 substrate. This substrate has a thickness of h = 1.575 mm, loss tangent of 0.0009, and relative permittivity of 2.2 [25]. The proposed element is simulated in a periodic environment of CST microwave studio considering an infinite number of elements along X- and Y- directions. To recognize the effect of the pin-diode on the scattering parameter of the unit-cell, the ideal case is also simulated. In this case, the ON state is obtained by connecting the unit cell patches by a copper strip. Whereas the OFF state is represented when patches are disconnected (open circuit). The equivalent circuits of the pin-diode in the ideal and non-ideal environment are shown in Fig. 6. 1 (b), while the scattering performance is presented in Fig. 6. 1 (c). It is visible that the magnitude of the reflection coefficient in the ideal ON state is higher compared to the non-ideal ON state. This difference in magnitude is due to the series resistance of the diode. Conversely, the capacitance that is used in OFF state in the non-ideal case increases the magnitude of the reflection coefficient compared to the ideal case. However, in both ideal and

non-ideal cases, the unit cell exhibits maximum transmission and reflection behavior in OFF and ON states, respectively. It is important to note that the non-ideal case is more practical than the ideal one. In this case, the switching between ON/OFF states can be achieved electrically by controlling the DC bias voltage. However, some drops in the antenna performance in the non-ideal case will be expected due to the embedded diodes. Whereas, in the ideal case, the proposed antenna will be exempted of the diode's loss. However, two different RR surfaces should be designed (ON state surface and OFF state surface). By alternating these surfaces, ON/OFF switching will be achieved. With these scattering features, the proposed element (in the non-ideal case) depicts suitability for designing beam tilting RRA.

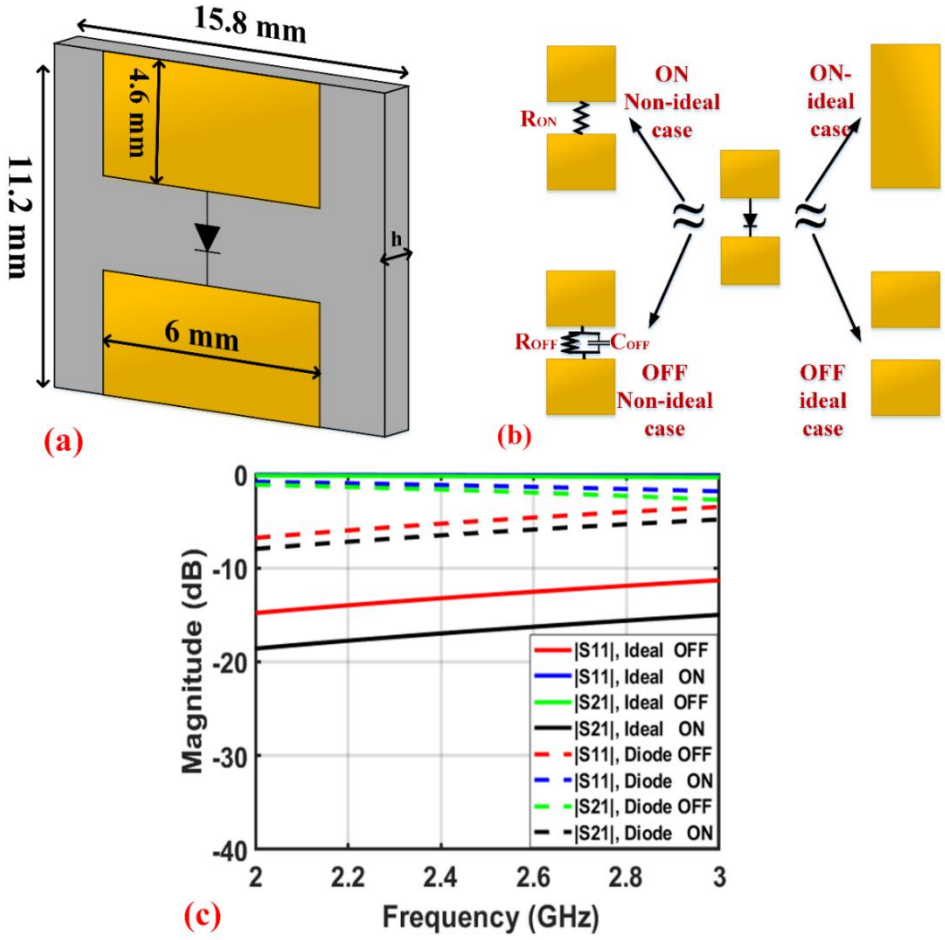

Figure 6. 1. AFSS unit cell: (a) front view, (b) equivalent circuit model of the ideal and non-ideal diode in ON/OFF states, and (c) transmission and reflection coefficients of the unit-cell for ideal and non-ideal diode ON/OFF states.

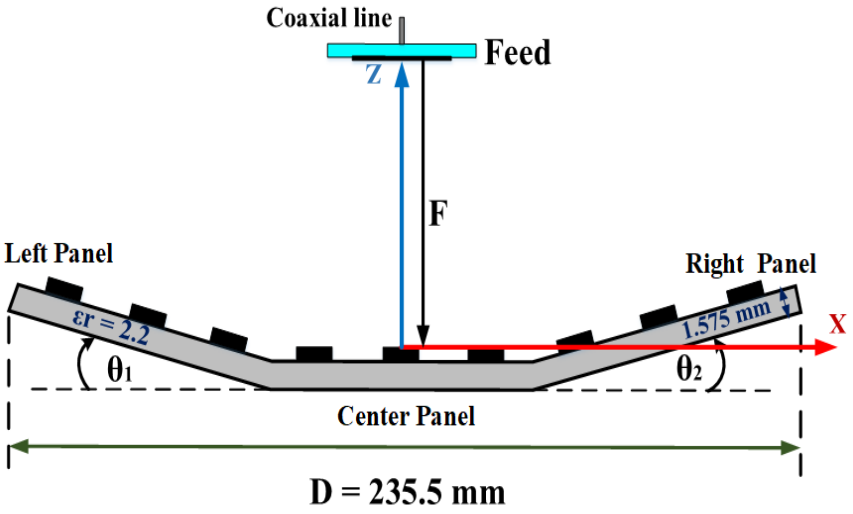

Figure 6. 2. Top view of the proposed RRA.

6.5 Reconfigurable reflector antenna design

The proposed antenna comprises of two main parts: a feed and a reconfigurable reflector (RR) surface as shown in Fig. 6. 2. The feed is placed away from the RR surface at the focal point.

6.5.1 Feed design

A patch antenna with a size of 57.6 mm x 46.8 mm (0.47λ x 0.38 λ) is used to excite the elements in the RR surface. A coaxial-fed method is employed, as shown in Fig. 6. 3. The feed antenna is designed using Rogers RT 5880, with a thickness of 1.575 mm, relative permittivity of 2.2, and loss tangent of 0.0009. The feed is placed away from the RR surface at the focal point with focal to diameter ratio (F/D) of 0.28. The feed antenna is fabricated and measured. The simulated and measured results in terms of reflection coefficient, realized gain, and radiation pattern in the H-plane are shown in Fig. 6. 4, which shows a good agreement

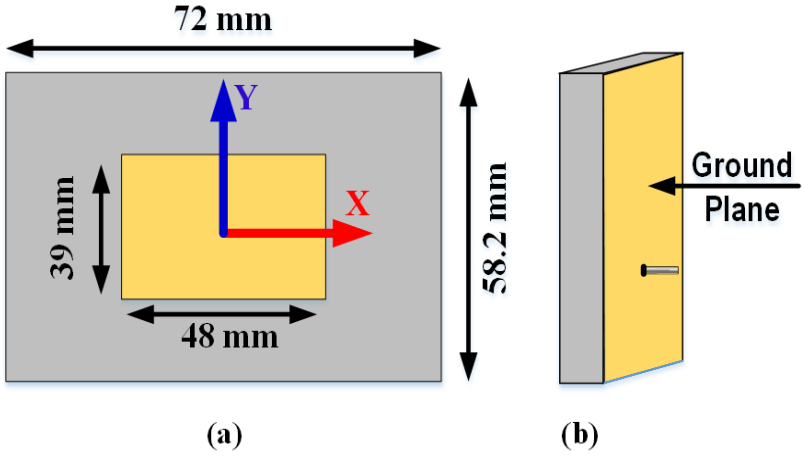

Figure 6. 3. Feed antenna structure, (a) Top view, (b) side view.

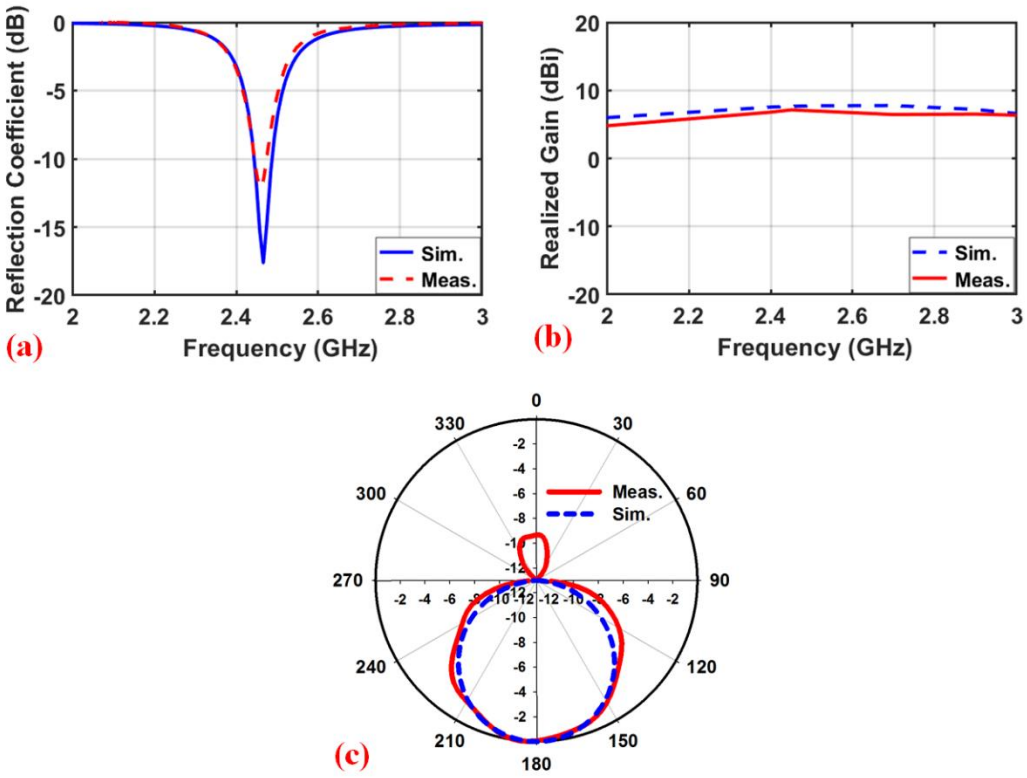

Figure 6. 4. Simulated and measured results of the patch antenna: (a) reflection coefficient, (b) gain, and (c) radiation pattern in the H plane.

6.5.2 RR surface design

The RR surface consists of three AFSS sub-screens that connected in series. The left and right sub-screens rotatable towards the feed to form a parabolic shape. The RR screen has a size of 235.5 mm x 169 mm (1.9 λ x 1. 37 λ). Each of AFSS sub-screens has a size of 78.5 mm x 169 mm (0.64 λ x 1.37 λ). The effect of the rotation angles of the side sub-screens (θ_1 and θ_2) is optimized for better antenna performance in terms of reflection coefficient and gain. It has been observed that the maximum gain is achieved when the rotating angles of the left and right screens are $\theta_1 = \theta_2 = 15^o$. As the diode ON state exhibits maximum reflection from the RRA, so the results obtained are compared with an equivalent antenna designed with metallic sheets. The performance of the proposed RRA in terms of reflection coefficient, gain, and radiation patterns are presented in Fig. 6. 5 (For brevity, the performance of the proposed RRA is not given in all tested angles). Preliminary results have recently been presented in [26]. The antenna performance is analyzed at 2.45 GHz. It is evident that the antenna experience with high reflection coefficient due to feed blockage. In the center fed RRA, due to the accumulation of the standing waves between the feed and RR surface, the feed matching level and bandwidth are reduced. The matching bandwidth can be increased by reducing feed blockage using a technique such as presented in [27]. In which, authors have presented a phase perturbation technique to improve the feed matching, and 5 dB matching improvement over 30% bandwidth has been achieved. The antenna produces a maximum gain of 11.9 dBi (ON state), and 7.8 dBi (OFF state), respectively.

6.6 Beam-tilting mechanism of the proposed RRA

A mechanical beam-tilting mechanism is presented using the proposed RRA. An off- broadside beam-tilting is achieved by mechanically rotating the left or right panel towards the feed, as shown in Fig. 6. 6. To tilt the main beam either towards positive or negative angles (Ψ) from the broadside, left/right panel of the RRA is mechanically rotated with θ_1 or θ_2, where $\theta_1 = +2\Psi_1$, and $\theta_2 = -2\Psi_2$. It is important to mention that this mechanical beam-tilting mechanism is analyzed in the diode ON state, while in the OFF state, the beam-tilting is not so effective due to the broad

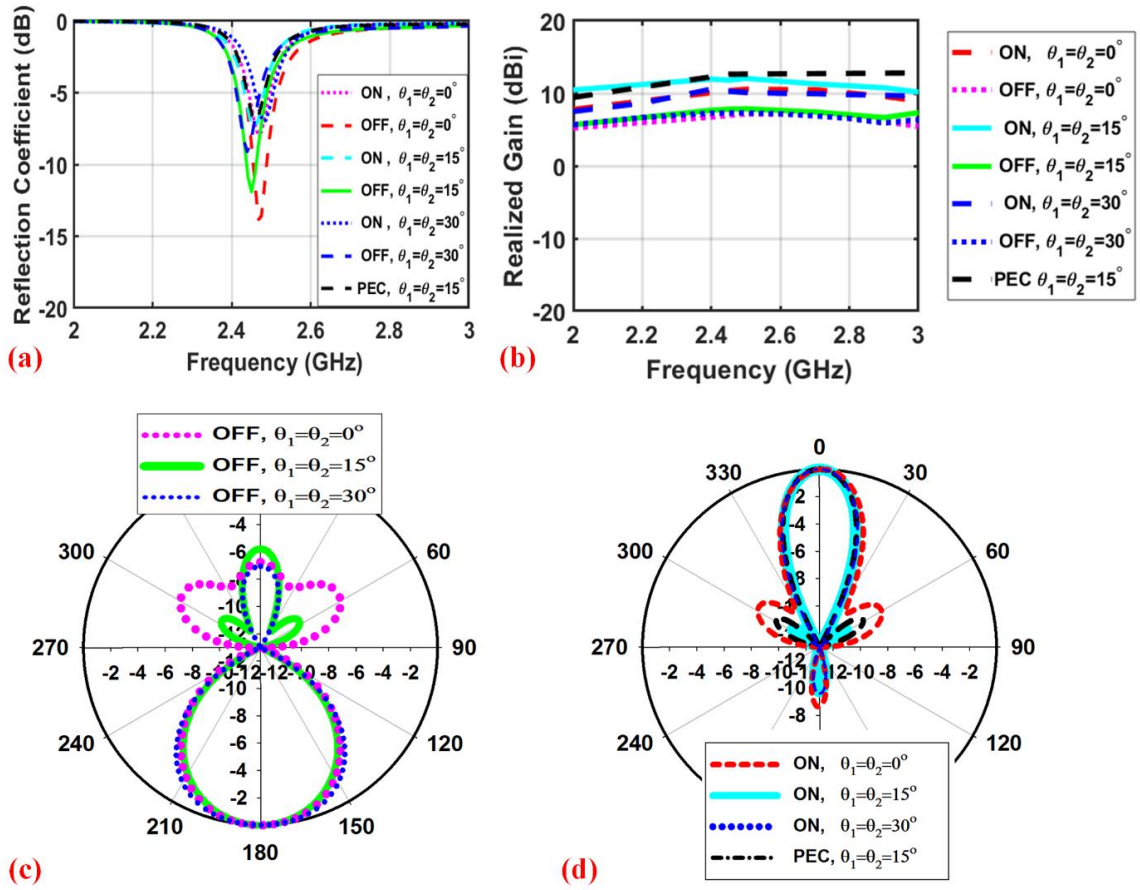

Figure 6. 5. Effect of (θ_1, and θ_2) on the proposed RRA performance: (a) reflection coefficient, (b) realized gain, (c) radiation patterns of the OFF state RRA in the H plane, (d) radiation patterns of the ON state RRA in the H plane.

half power beamwidth (HPBW) of the feed antenna. Fig. 6. 7 represents the beam-tilting performance of the RRA towards positive and negative angles off-broadside respectively, with variable rotation angles of the left and right panels. It is evident that the proposed antenna provides ±30° beam-tilting capabilities.

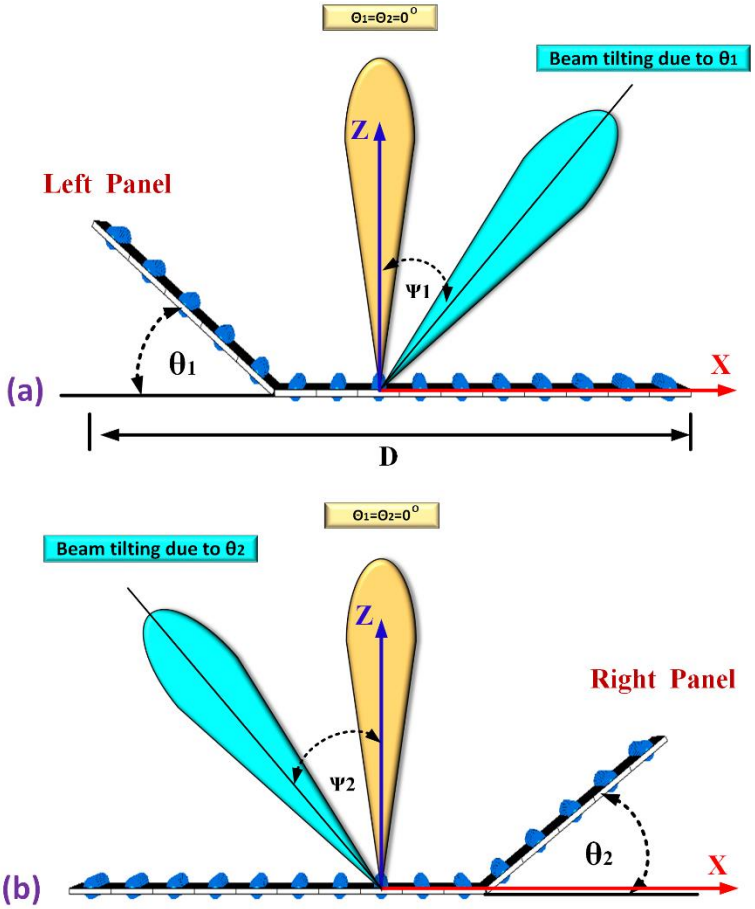

Figure 6. 6. Sketch of the proposed beam-tilting mechanism: (a) rotating the left sub-screen towards the feed by θ_1, (b) rotating the right sub-screen towards the feed by θ_2.

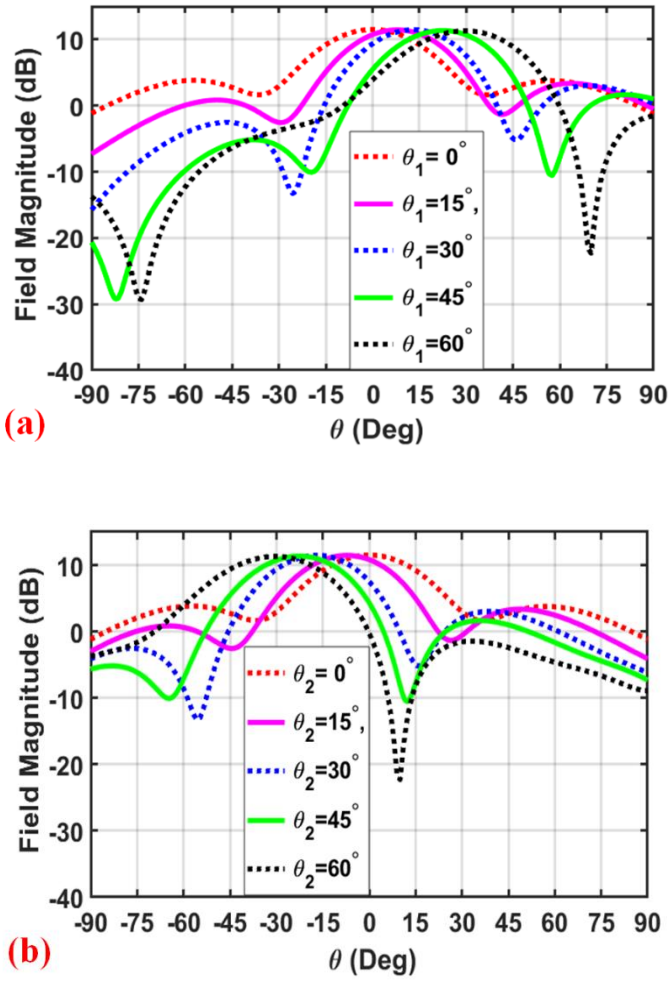

Figure 6. 7. Simulated radiation patterns of the proposed RRA in the H-plane: (a) with different values of θ_1, when $\theta_2=0^o$, (b) with different values of θ_2, when $\theta_1=0^o$.

6.7 Prototyping and measurement results

The proposed RRA structure was fabricated and measured. Fig. 6. 8 shows the fabrication and measurement steps. soldered in each unit cell. By applying a DC voltage of 5 V, the diodes in AFSS operate in ON state, while 0V represents the OFF state. A resistor of 500 Ω is used at the top of each column in the AFSS array. This resistance is used to protect diodes and to produce the same amount of current for all the diodes. The bottom of each column is connected with the ground plane. The proposed antenna is measured in an anechoic chamber. The simulated and measured performances of the proposed RRA at $\theta_1=\theta_2=15^o$ (in OFF-ON state) in terms of

reflection coefficient, beam direction, and realized gain are presented in Fig.6. 9. It is visible that the proposed RRA provides a maximum measured gain of 6 dBi in the diode OFF state, and 10.6 dBi in the diode ON state. The beam- tilting features of the proposed RRA structure are also measured for variable rotation angles. The results in terms of radiation patterns are presented in Fig. 6. 10. (To avoid crowding of figures, results are not given in all tested angles). These results show that the proposed antenna provides a maximum beam-tilting range of ±30º (off broadside). All the measured results are evaluated at the operating frequency of 2.45 GHz. The simulation and measured results show a good agreement. The performance of the proposed RRA structure is compared with some previous designs exist in literature. The obtained results are presented in Table 1. It is evident that the model exhibits better measured performance in terms of higher gain, and wider beam scanning ability.

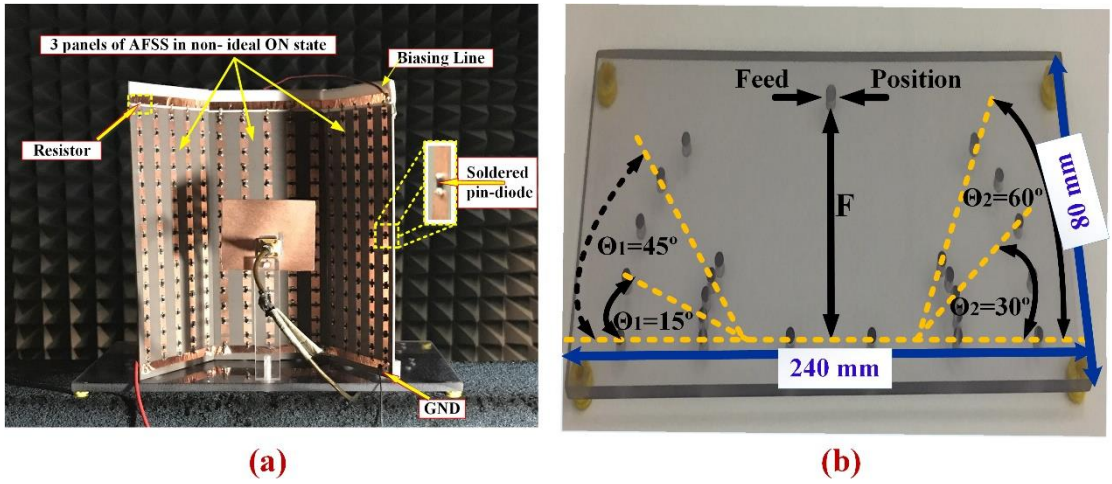

Figure 6. 8. Prototyping and measurement steps: (a) A picture of the proposed RRA prototype in an anechoic chamber, (b) Plexiglas base.

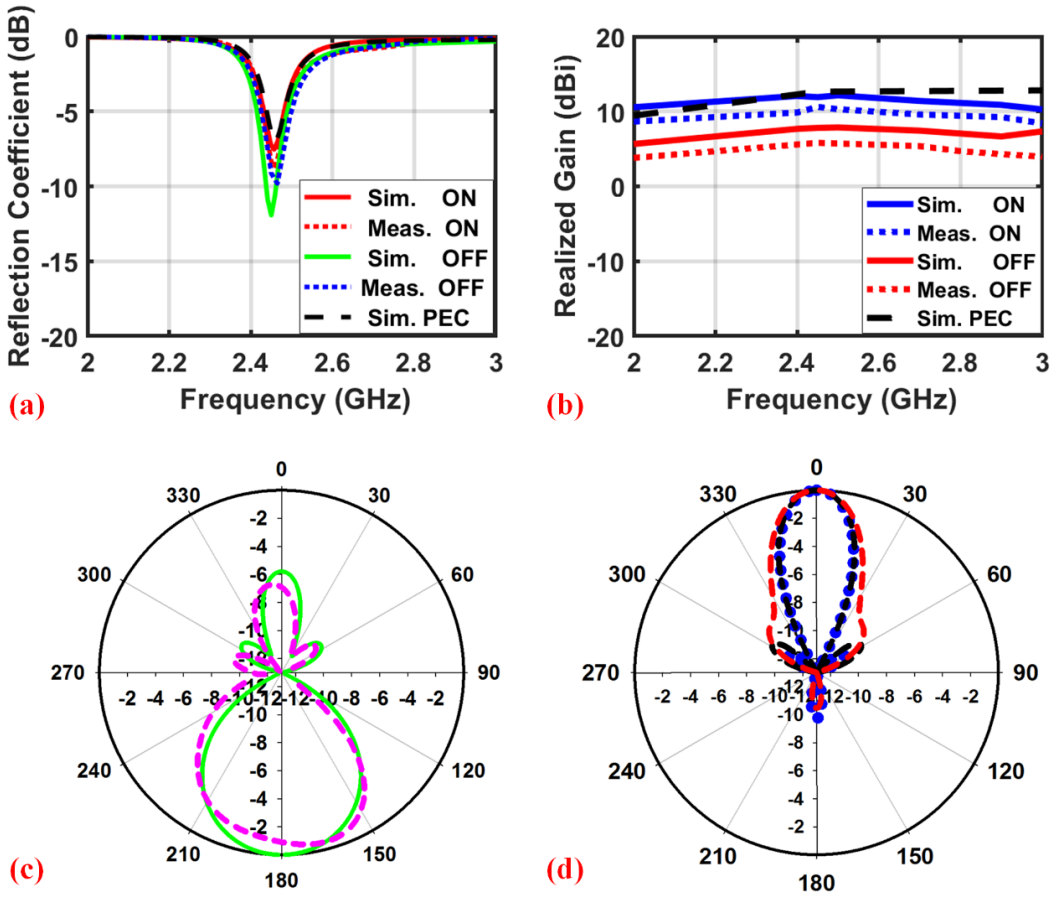

Figure 6. 9. Simulated and measured results of the proposed RRA, where $\theta_1=\theta_2=15^o$: (a) reflection coefficient of (b) gain, (c) radiation pattern in the H plane.

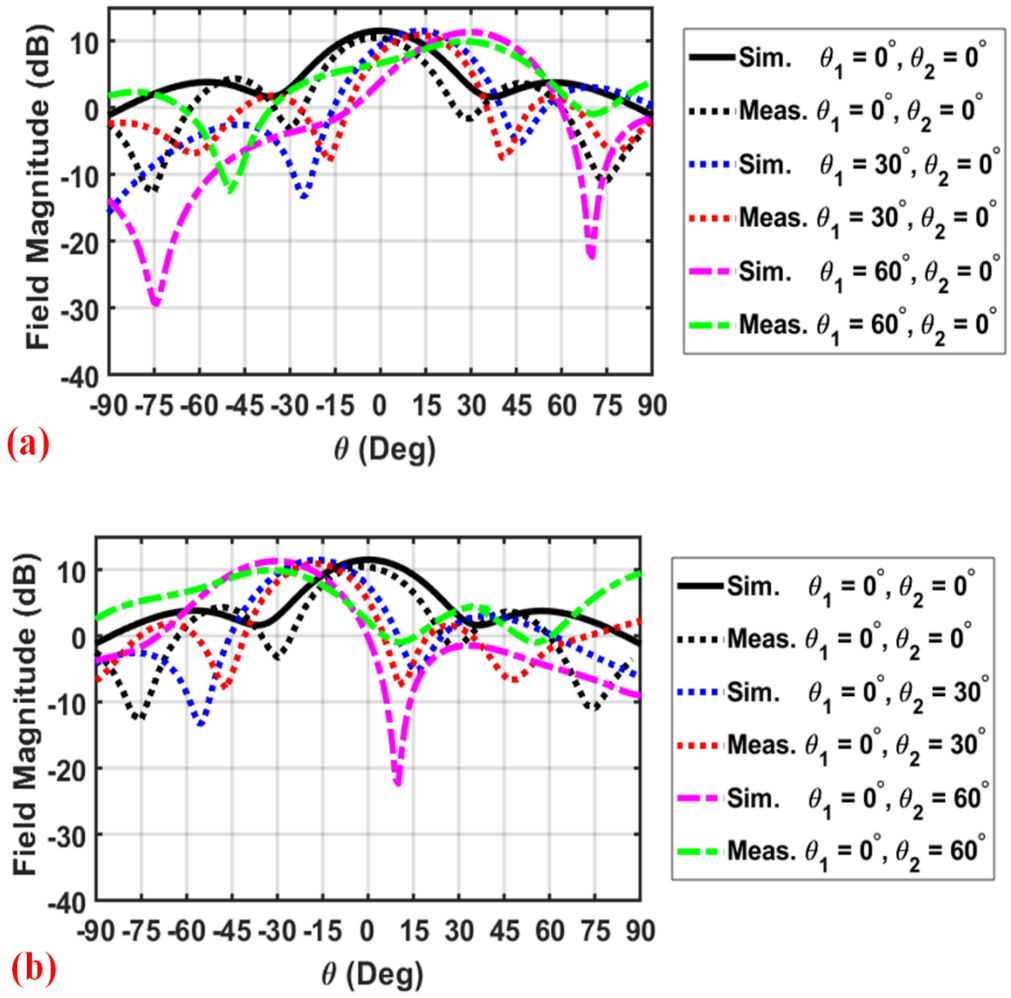

Figure 6. 10. Simulated and measured radiation patterns of the proposed non-ideal beam-tilting RRA in H-plane: (a) with different values of θ_1, when $\theta_2=0^o$, (b) with different values of θ_2, when $\theta_1=0^o$.

Table (6. 1): Comparison of the proposed antenna performance with recent publications

	Ref.	Freq. (GHz)	Feed	Size(λ)	Max. measured gain (dBi) before applying beam-tilting technique	Max. beam-tilting angle	Max. measured gain (dBi) after applying beam-tilting technique
Proposed RRA	Single-layer RRA	2.45	Patch	1.9 λ_0 X 1.37λ_0	10.6	±30°	11.25
[9]	Antenna with convex shaped FSS	3.5 & 5.8	Monopole	1.9 λ_0 X 1.33λ_0	6.4 @ 3.5GHz	No beam-tilting characteristics	
	Antenna with concave shaped FSS				8.5 @ 3.5GHz		
	Antenna with FSS-based corner reflector			1.9 λ_0 X 2 λ_0	8.3 @ 5.8GHz		
[14]	Antenna alone	28-31	Yagi–Uda	13 λ_0 X 9 λ_0	9.6	+23° & –29°	8.71
	Antenna with FSS				8.71		
	Antenna with rotated FSS				8.65		

6.8 Conclusion

A novel reconfigurable reflector antenna RRA has been designed using AFSS in the WLAN band. The AFSS based RRA comprises of multiple panels arranged like a parabolic reflector. The AFSS element has a size of 0.13λ x 0.1λ. An array of AFSS has been designed to investigate the transmittive and reflective behavior. A patch antenna has been used to excite the AFSS. The RRA holds a size of 235.5 mm x 169 mm (1.9 λ x 1.37 λ). The antenna performance has been analyzed at 2.45 GHz. The performance of the proposed antennas with mechanical beam-tilting feature has also been analyzed. The antenna has been fabricated and measured. A good agreement between simulation and measurements has been observed. The RRA shows a maximum measured gain of 10.6 dBi. A maximum measured beam-tilting range of ±30º (off broadside) has also been achieved.

6.9 References

[1] Rahmat-Samii, Y., Haupt, R.: 'Reflector antenna developments: A perspective on the past, present and future'. IEEE Antennas Propag. Mag., 2015, 57, (2), pp. 85–95.

[2] Manohar, V., Kovitz,J., Samii, Y.: 'Synthesis and Analysis of Low Profile, Metal-only Stepped Parabolic Reflector Antenna', IEEE Trans. Antennas Propag., 2018, 66, (6), pp. 2788-2798.

[3] Tahseen, M. M., Kishk, A. A.: 'Broadband Performance of Novel Closely Spaced Elements in Designing Ka-Band Circularly Polarized Reflectarray Antennas', IEEE Antennas Wireless Propag. Lett., 2017, 16, pp. 1184-1187

[4] Ahmad, G., Brown, T., Underwood, C., et al.: 'Millimetre Wave Reflectarray Antenna Unit Cell Measurements', LAPC, Loughborough, UK., 2017, pp. 1-5.

[5] Edalati, A., Sarabandi, K.: 'Wideband reflectarray antenna based on miniaturized element frequency selective surfaces', EUCAP, Prague, 2012, pp. 362-364.

[6] Tahseen, M., Kishk, A.: 'Paneled Center-fed Reflectarray for Bandwidth Enhancement' URSI GASS, Montreal, QC, Canada, 2017, pp. 1-4.

[7] Singsura, P., Hongnara, T., Thaiwirot, W.,' Design of antenna reflector using two-layer frequency selective surfacs for gain enhancement in UWB application', ISAP., Phuket, Thailand, 2017, pp. 1-2.

[8] Ratni, B., de Lustrac, A., Piau, G., et al.: 'Planar Metasurface for Parabolic Reflector Antenna: Frequency Agility and Beam Steering', USNC/URSI., San Diego, CA, USA., 2017, pp. 2073-2074.

[9] Chatterjee, A., Parui,S.:' Beamwidth Control of Omnidirectional Antenna Using Conformal Frequency Selective Surface of Different Curvatures', IEEE Trans. Antennas Propag., 2018, 66, (6), pp. 3225 – 3230.

[10] Tahseen, M., Denidni, T., Kishk, A.: 'Proof of Concept Low-Loss Reconfigurable Reflectarray for Beam Steering', 18th ANTEM, Waterloo, ON, 2018, pp. 1-2.

[11] Dadgarpour, A., Zarghooni,B., Virdee, B. S., et al.: 'Enhancement of tilted-beam in elevation plane for planar end-fire antennas using artificial dielectric medium', IEEE Trans. Antennas Propag., 2015, 63,(10), pp. 4540–4545.

[12] Bai, Y., Xiao,S., Liu,C., et al.: 'Design of pattern reconfigurable antennas based on a two-element dipole array model', IEEE Trans. Antennas Propag.,2013, 61, (9), pp. 4867–4871.

[13] Bai, Y.Y., Xiao, S., Tang, M.-C., et al.: ‘Wide angle scanning phased array with pattern reconfigurable elements’, IEEE Trans. Antennas Propag.,2011, 59, (11), pp. 4071–4076.

[14] Mantash, M., Kesavan, A., Denidni, T. A.: ’Beam-Tilting Endfire Antenna Using a Single-Layer FSS for 5G Communication Networks’, IEEE Antennas Wireless Propag. Lett., 2018, 17, (1), pp. 29-33.

[15] Shi, S. J., Ding, W. P.: ‘Radiation pattern reconfigurable microstrip antenna for WiMAX applications’, Electron. Lett., 2015, 51, (9), pp. 662–664.

[16] Ren, J., Yang, X., Yin, J.-Y., et al.: ‘A novel antenna with reconfigurable patterns using H-shaped structures’, IEEE Antennas Wireless Propag. Lett.,2015, 14, pp. 915–918.

[17] Niemelä, J. Isotalo, T. Lempiäinen, J.: ‘Optimum Antenna Downtilt Angles for Macrocellular WCDMA Network’, in EURASIP Journal on Wireless Communications and Networking,20015, 5, (5), PP. 816–827,

[18] Lee, Y., Moon, J., Ha, J., et al.: ‘Phase shifter using an artificial magneto-dielectric for beam-tilting of base station array antenna’, APMC, Melbourne, VIC, Australia, 2011, pp. 1334-1337.

[19] Ibrahim, S. A., Wang, Z., Farrell, R.: ‘An MEMS Phase Shifter with High Power Handling for Electronic Beam Tilt in Base Station Antennas’, IEEE Microwave and Wireless Components Letters, 2017, 27, (3), pp. 269-271.

[20] Li, J. Zeng, Q. Liu, R., et al.:’Beam-Tilting Antenna with Negative Refractive Index Metamaterial Loading’, IEEE Antennas Wireless Propag. Lett., 2017, 16, pp. 2030-2033.

[21] Tanizawa, Y., Cho, K., So, H., et al.: ‘Radiation characteristics of corner reflector antenna employing frequency selective surface’, URSI AP-RASC, Seoul, 2016, pp. 1-3.

[22] Kesavan, A., Chacko, B. P., Denidni, T. A.: ‘Beam tilting Vivaldi antenna using cantilever based-frequency selective surfaces’, APSURSI, Fajardo, PR, USA, 2016, pp. 961–962.

[23] Elzwawi, G., Elzwawi, H., Tahseen, M. M. et al.: ‘Frequency Selective Surface Based Switched-Beamforming Antenna’, IEEE Access, 2018, 6, pp. 48042-48050.

[24] Skyworks Datasheet for SMP1345-079LF, Skyworks, Inc., Woburn, MA, USA, 2014. [Online]. Available: http://www.skyworksinc.com/uploads/documents/200046M.pdf.

[25] Edalati, A., Denidni, T.: ’Beam-switching Antenna Based on Active Frequency’, APSURSI., Spokane, WA, USA.,2011, PP. 2254-2257.

[26] Elzwawi, G. H., Tahseen M. M., Denidni, T. A.: ‘Reflecto-Transmittive Antenna using Active Frequency Selective Surfaces’, 18th ANTEM, Waterloo, ON, 2018, pp. 1-2.

[27] Tahseen, M., Kishk, A.: ‘Feed Matching Improvement for Center Fed Reflectarray’, Progress in Electromagnetics Research, 2017, 54, pp. 67-74

CHAPTER 7

Conclusion and Future Work

7.1 Conclusion

In this thesis, the frequency selective surfaces and its application in designing pattern reconfigurable antennas have been studied. Novel frequency selective surface unit- cells for the beam-steering applications have been designed. Moreover, various new beam-steering antennas based on frequency selective surfaces have been proposed. The following paragraphs present the methodology steps that taken to achieve the thesis goal:

First step: a comprehensive research of frequency selective surfaces and its applications in the modern antennas has been performed. This study showed the vital role of the frequency selective surfaces in designing the radiation pattern reconfigurable antenna. Different AFSS unit-cells have been proposed. Some of these elements operates at 2.45 GHz and other at 5.8 GHz.

Second step: a novel frequency selective surface-based switched-beamforming antenna has been proposed. This design consists of a novel active triangular frequency selective surface (ATFSS) surrounding an excitation source. The proposed design succeeded in converting the omnidirectional radiation pattern of the source into a directional one. The main beam has effectively steered in different directions in the azimuth plane with 120º radiation beamwidth at 5.8 GHz. The proposed technique enhanced the maximum gain of the source by 4 dBi. A minimum number of active elements has been used in this design. This leads to upgrade gain of the antenna and reduce the cost.

Third step: The authors propose a new corner-reflector antenna with a tunable gain based on active frequency selective surfaces (AFSSs). In this structure, three reconfiguration AFSS layers with different sizes are arranged in one side of a dipole antenna to form a V-shaped corner

reflector. By using this technique, the omnidirectional radiation pattern of the source is successfully modified into a directional radiation pattern with a tunable gain. We figure out, this design is the first corner-reflector antenna with a tunable and variable gain directional pattern.

Final step: a new reconfigurable reflector antenna (RRA) with beam-tilting capability operating in WLAN band has been designed and fabricated. The proposed design consists of an array of AFSS unit-cells and a WLAN-band patch antenna as an excitation source. A mechanical beam tilting technique has been applied on the proposed design. By using this technique, the main beam has effectively tilted without adding any extra layers or setups to the main antenna structure. (the size and weight of the main structure remain the same). To our knowledge, this design provides the beam reconfigurability when AFSS is arranged in a parabolic shape for the first time.

7.2 Future Work

This thesis introduced research works in reconfigurable active frequency selective surface (AFSS) and reconfigurable radiation pattern antennas. Several new beam-switching antennas based on frequency selective surfaces (AFSSs) have been proposed. Nevertheless, many other investigations need to be explored in this field which will lead to future works as indicated in the following paragraphs.

First: Developing the switching mechanism and Dc voltage controlling circuit will be an important issue. This will enhance the performance of the reconfigurable prototypes. Plasma, MEMS, and ferroelectric are some new suggested reconfiguration mechanism.

Second: This thesis proposes a beam scanning radiation patterns of antennas in the azimuth plane. Proposing new antennas able to scan the radiation patterns in both elevation and azimuth planes will be an interesting work.

Third: The proposed antennas in this thesis can be developed to work at double and three bands. This can be achieved by using multi AFSS layers, each layer operates at a specific band.

Forth: In this thesis, we propose a new corner-reflector antenna with a tunable gain based on active frequency selective surfaces (AFSSs). It is worthy to improve this structure to be a beam steering corner-reflector antenna with a tunable gain. This can be easily done by adding more AFSS layers around the excitation source. By switching the pin-diodes of the AFSS layers between ON and OFF, the tunable gain radiation pattern will be steered in the whole azimuth plane.

Finally: This thesis presented a novel beam-tilting reconfigurable reflector antenna operating in WLAN band. This structure is the first design where AFSS is used to provide the beam reconfigurability when AFSS is arranged in a parabolic shape. However, this design is suffering from high reflection coefficient due to feed blockage. It is worthy to produce a technique that can reduce the feed blockage and enhance the matching bandwidth of the proposed antenna.

CHAPTER 8

RÉSUMÉ

8.1 Introduction

Le résumé de cette thèse de doctorat est présenté dans ce chapitre. La motivation de mon projet de recherche, l'identification du problème et les objectifs de ce travail sont présentés. De plus, le concept des antennes reconfigurables proposées est illustré. Enfin, la conclusion et les travaux futurs sont également présentés.

8.2 Motivation

Les systèmes de communication sans fil sont récemment devenus l'un des domaines technologiques les plus vitaux ainsi que les plus rapides en développement. Dans cette technique, l'information est transmise de l'émetteur au récepteur de manière souple, facile et peu coûteuse. « Wireless Fidelity » (Wi-Fi), la nouvelle génération de communications mobiles, les récepteurs GPS, les radars militaires et civils sont quelques exemples des systèmes de communication sans fil largement utilisés dans notre vie quotidienne. Ces dernières années, la miniaturisation, la multifonctionnalité, la réduction des coûts et la robustesse sont devenues les exigences les plus importantes des systèmes de communication modernes. En conséquence, il est nécessaire de concevoir une antenne aux fonctionnalités variées en intégrant quelques fonctions dans un seul élément. Afin de surmonter les problèmes des interférences et du phénomène de propagation multivoix, cet élément doit avoir la capacité de diriger le faisceau vers la direction souhaitée, tout en supprimant les signaux non désirés dans les autres directions. Pour cette raison, les antennes à commutation de faisceau (qui est l'application la plus étendue de l'antenne à reconfiguration de diagramme de rayonnement) ont obtenu une attention significative dans les systèmes de communication sans fil. Ces antennes peuvent réduire considérablement

les signaux parasites et améliorer la capacité du système. Des propriétés plus flexibles et des fonctionnalités supplémentaires peuvent être obtenues en utilisant ces antennes. En outre, ce type d'antenne occupe un volume physique identique ou inférieur à celui des réseaux d'antennes intelligentes traditionnels [1].

Les applications intéressantes et les caractéristiques remarquables des surfaces sélectives en fréquence pour des antennes à commutation de faisceau destinées aux systèmes de communication modernes nous ont motivés à mettre en place une recherche approfondie dans ce domaine. Ce projet vise donc à concevoir et à fabriquer plusieurs nouvelles antennes à commutation de faisceaux basées sur des surfaces sélectives en fréquence (AFSSs).

8.3 Identification des problèmes

Diverses techniques ont été utilisées pour orienter le faisceau de rayonnement, telles que les antennes à lentille intégrée (ILAs) [2-4], les antennes à ondes progressives [5-6], les réseaux adaptatifs [7], les réseaux à déphasage [8] et les structures électromagnétiques à bande interdite (EBG) [9]. Chacune de ces technologies présente des avantages et des inconvénients. Par exemple, les antennes à ondes progressives utilisées pour la direction du faisceau sont de grande taille. Pour les réseaux d'antennes à déphasage, l'amplitude et la phase de chaque élément doivent être contrôlées pour orienter le faisceau dans une direction spécifique, ce qui complique la structure et augmente le coût de fabrication. L'AMPBG est une structure encombrante et souffre d'un niveau de lobes latéraux (SLL) et d'une polarisation croisée plus élevés. Pour surmonter la complexité de la conception, la taille plus importante et l'ampleur des techniques susmentionnées, les AFSSs ont récemment été utilisées pour obtenir une performance de guidage du faisceau élevée. En raison du comportement de réflexion/transmission partielle de la surface sélective en fréquence (FSS), le modèle de rayonnement peut être soit transmis, soit réfléchi dans une direction spécifique souhaitée.

8.4 Objectifs de la recherche

Dans cette thèse, une nouvelle surface active sélective en fréquence (AFSS) à cellules unitaires avec des structures simples sont proposées. Ces éléments sont utilisés pour convertir le diagramme de rayonnement omnidirectionnel de la source d'antenne en un diagramme directionnel formant une nouvelle classe d'antennes à commutation de faisceau. Une nouvelle antenne à commutation de faisceaux utilisant une nouvelle surface active triangulaire sélective en fréquence (ATFSSs) est introduite. Cette antenne peut orienter le faisceau dans différentes

directions dans le plan azimutal avec une largeur de faisceau de rayonnement de 120º. De plus, les tableaux AFSS sont utilisées pour concevoir une nouvelle antenne à réflecteur en coin avec un gain accordable pour la première fois. Cette thèse présente également une antenne à réflecteur reconfigurable (RRA) à inclinaison de faisceau fonctionnant dans la bande WLAN. À notre connaissance, la structure proposée est la première conception où l'AFSS est utilisée pour fournir la reconfigurabilité du faisceau lorsque l'AFSS est disposée en forme parabolique.

8.5 Antenne à formation de faisceaux commutée basée sur des surfaces sélectives en fréquence

Cette partie présente une nouvelle antenne de formation de faisceaux commutée utilisant une nouvelle surface ATFSS. L'antenne comprend plusieurs surfaces AFSS, disposées dans un triangle équilatéral à trois panneaux, et une alimentation placée au milieu de la structure utilisée pour exciter l'ATFSS. En appliquant de multiples combinaisons de diodes (ON et OFF) sur chaque panneau de l'ATFSS, le guidage du faisceau est réalisé dans différentes directions. L'antenne de guidage de faisceau proposée peut orienter le faisceau dans différentes directions dans le plan azimutal avec une largeur de faisceau de rayonnement de 120º. L'antenne de formation de faisceaux commutée proposée offre un gain maximum de 7 dBi, ce qui est presque 4 dBi de plus que le gain d'alimentation. L'antenne est fabriquée et mesurée. Les résultats obtenus montrent un bon accord entre les simulations et les mesures en termes de coefficient de réflexion, de direction du faisceau et de gain réalisé à 5,8 GHz.

L'antenne proposée peut être utilisée dans la bande WLAN WI-FI supérieure (à 5,8 GHz), les satellites fixes, la radiolocalisation, la vue à la première personne (FPV) et d'autres applications similaires.

8.5.1 Conception d’élements ATFSS

Chaque panneau de l'AFSS proposée est constitué de deux cellules unitaires, comme le montre la Figure 8.1. Chaque cellule unitaire est soumise soit à l'émission soit à la réflexion des ondes incidentes dans l'état ON ou OFF de la diode. Pour atteindre cet objectif, un élément de l'ATFSS a été conçu à l'aide du logiciel Microwave CST, compte tenu du fait qu'il existe un nombre infini d'éléments dans les directions X et Y. Chaque élément est constitué de deux plaques en forme

de diamant, qui sont électriquement connectées/déconnectées l'une de l'autre par une diode PIN. La diode PIN haute fréquence (GMP4202-GM1) est modélisée comme un circuit RLC en série. Une petite résistance de Rs = 1,8 Ω représente la polarisation directe de la diode (état ON), tandis qu'une capacité série de Cp = 0,09 pF et une inductance de Lp = 0,5 nH présentent l'état OFF, comme l'illustrent les circuits équivalents présentés à la Figure 8. 1 [14]. Une onde incidence plane polarisée dans la direction Y est utilisée pour obtenir les caractéristiques de diffusion de l'élément. L'élément est conçu sur le substrat RT/Duroid 5880 de Roger avec une épaisseur de 0,127 mm, une permittivité de 2,2, et une tangente de perte de 0,0009. Le Tableau 8. 1 montre les diamètres de la cellule unitaire AFSS. Le coefficient de réflexion de la cellule unitaire AFSS proposée est indiqué dans la Figure 8. 2.

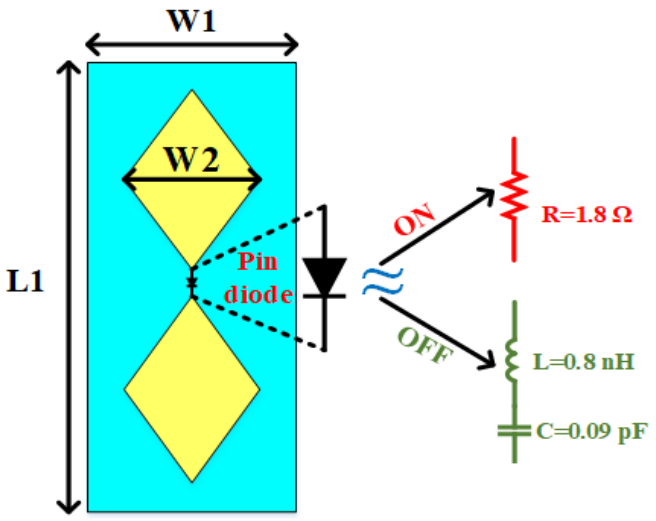

Figure 8.1. L'élément AFSS proposé avec un modèle de circuit équivalent des états ON/OFF de la diode.

Tableau (8.1) : Les dimensions de l'élément ATFSS proposé.

Parameter	L1	W1	W2
Value (mm)	**24**	**11**	**10**

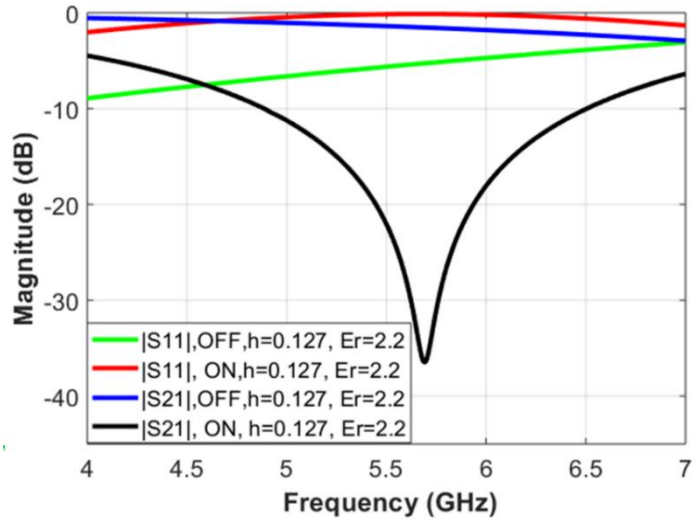

Figure 8.2. Coefficient de réflexion de la cellule unitaire AFSS proposée.

8.5.2 Conception d'une antenne à formation de faisceau commutée

La Figure 8. 3 montre la structure de l'antenne proposée. Cette antenne se compose de deux parties principales : la première partie comprend trois panneaux ATFSS disposés selon une configuration triangulaire équilatérale, tandis que la seconde partie est un patch avec un diagramme de rayonnement unipolaire, comme le montre la Figure 8. 4. Ce patch est utilisé comme alimentation et placé au milieu de la structure.

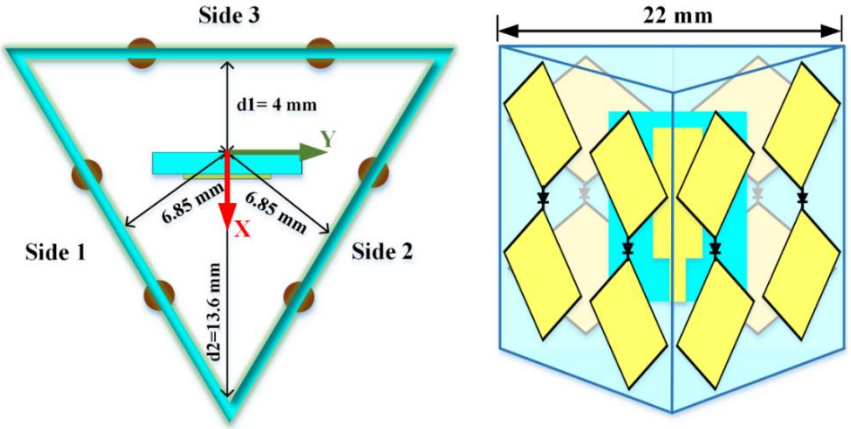

Figure 8. 3. Modèle simulé de l'antenne ATFSS proposée en vue 3D, supérieure et latérale.

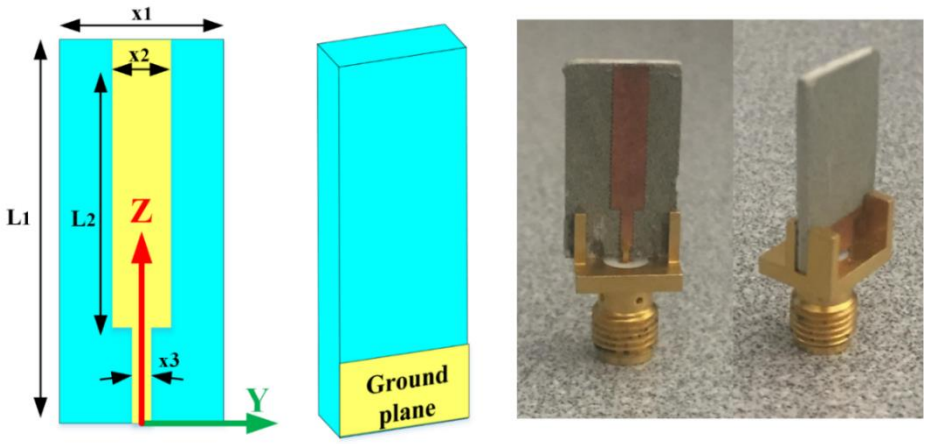

Figure 8. 4. Modèle d'antenne d'alimentation simulé et fabriqué pour exciter les éléments ATFSS.

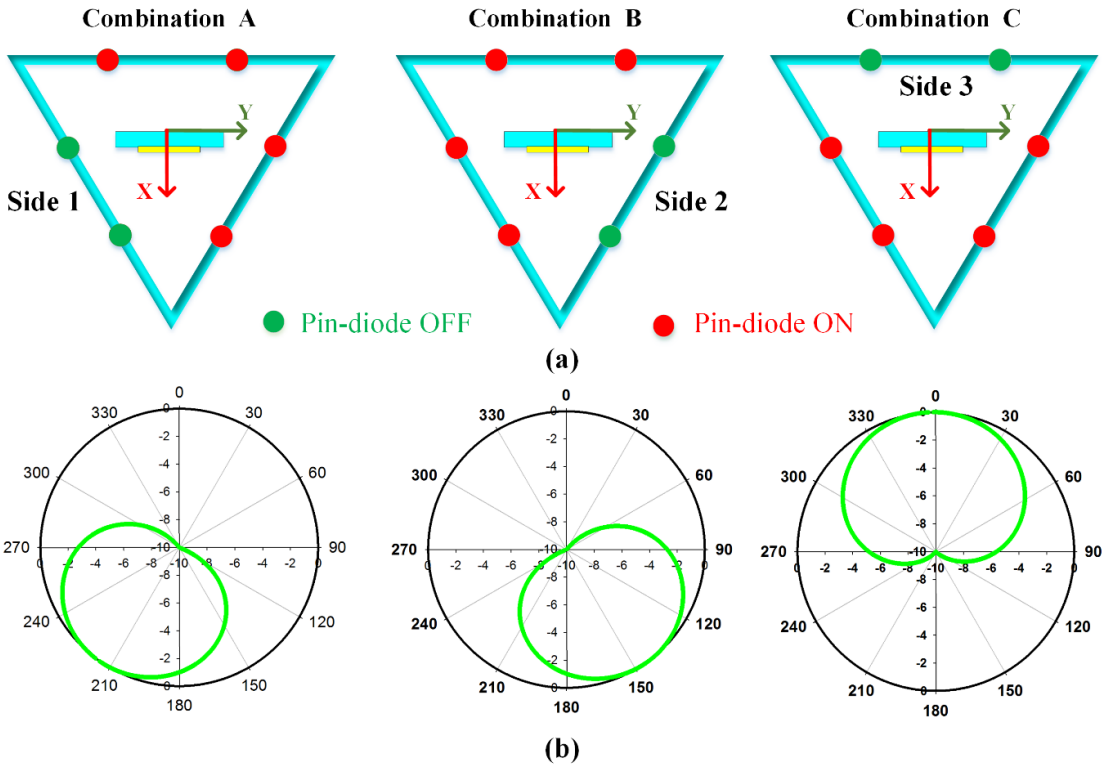

Figure 8. 5. Croquis de l'antenne ATFSS proposée, (a) avec de multiples combinaisons de diodes pour orienter le faisceau dans différentes directions, et (b) les résultats de la simulation pour chaque combinaison.

8.5.3 Le mécanisme opérationnel de l'antenne à formation de faisceaux commutée

Le mécanisme opérationnel de l'antenne proposée est basé sur la conversion du diagramme de rayonnement omnidirectionnel de la source en diagramme directionnel en utilisant l'ATFSS proposée. Lorsque les diodes PIN de l'ATFSS sont éteintes, l'ATFSS se comporte comme une surface d'émission, tandis qu'à l'état allumé, elle agit comme une surface réfléchissante. Les écrans ATFSS sont disposés en triangle équilatéral pour commuter le faisceau dans plusieurs directions en utilisant différentes combinaisons de diodes. Les schémas de principe illustrant le mécanisme de fonctionnement de l'antenne proposée et les résultats simulés de trois étapes de direction du faisceau (différentes combinaisons) sont présentés dans la Figure 8. 5 (a), (b).

8.5.4 Résultats de la fabrication et des mesures

L'antenne à formation de faisceau commutée proposée est fabriquée et mesurée. La Figure 8.6 montre les différentes étapes de l'assemblage de l'antenne fabriquée et le dispositif de mesure. Dans la première étape, un réseau de 2 x 6 éléments passifs du FSS est fabriqué. Dans la deuxième étape, les cellules unitaires sont enroulées sur une mousse triangulaire équilatérale pour former l'AFSS. En raison de l'épaisseur minimale du diélectrique, l'enrobage se fait facilement, mais pour un réseau conçu sur un matériau ayant une plus grande épaisseur de substrat, il est possible d'agencer les cellules en coupant chaque côté séparément et en liant leurs jonctions d'angle à l'aide de colle ou de vis en plastique de plus petit diamètre disponible. Lors de la troisième étape, une diode PIN à haute fréquence est soudée dans chaque cellule passive de l'unité FSS pour former un élément ATFSS. Pour isoler le signal RF des lignes de polarisation en courant continu, des bobines de réactance RF sont utilisées sur les côtés supérieur et inférieur de chaque élément. Toutes les connexions nécessaires à une alimentation en tension continue positive sont connectées en parallèle pour former un seul nœud, tandis que toutes les connexions GND sont également unifiées pour former le deuxième nœud (en bas). Lorsque la tension d'alimentation continue de 1,2 V est appliquée, les diodes de l'AFSS fonctionnent à l'état ON, tandis que 0 V représente l'état OFF. Le diagramme de rayonnement de l'antenne est mesuré dans la chambre anéchoïque. Les Figures 8. 7 à 8. 11 montrent le gain du coefficient de réflexion simulé et mesuré et les diagrammes de rayonnement de la source d'antenne et de l'antenne proposée dans le plan azimutal ($\theta = 90^{o}$) pour différents états de diode. Il est visible que le diagramme de rayonnement omnidirectionnel de l'antenne source est converti

en un diagramme directionnel en utilisant les écrans de formation de faisceau commutés ATFSS proposés. Lorsque les diodes du côté 1 sont éteintes (combinaison A), le diagramme est dirigé vers 240º, lorsque les diodes du côté 2 sont éteintes (combinaison B), le diagramme est dirigé vers 120º, et lorsque les diodes du côté 3 sont éteintes (combinaison C), le diagramme est orienté vers 0º. D'autres directions du faisceau peuvent être obtenues en choisissant différentes combinaisons d'états ON/OFF des secteurs. Grâce à cette caractéristique, l'antenne proposée permet de diriger le faisceau dans le plan azimutal. La simulation et les mesures montrent un accord raisonnablement bon.

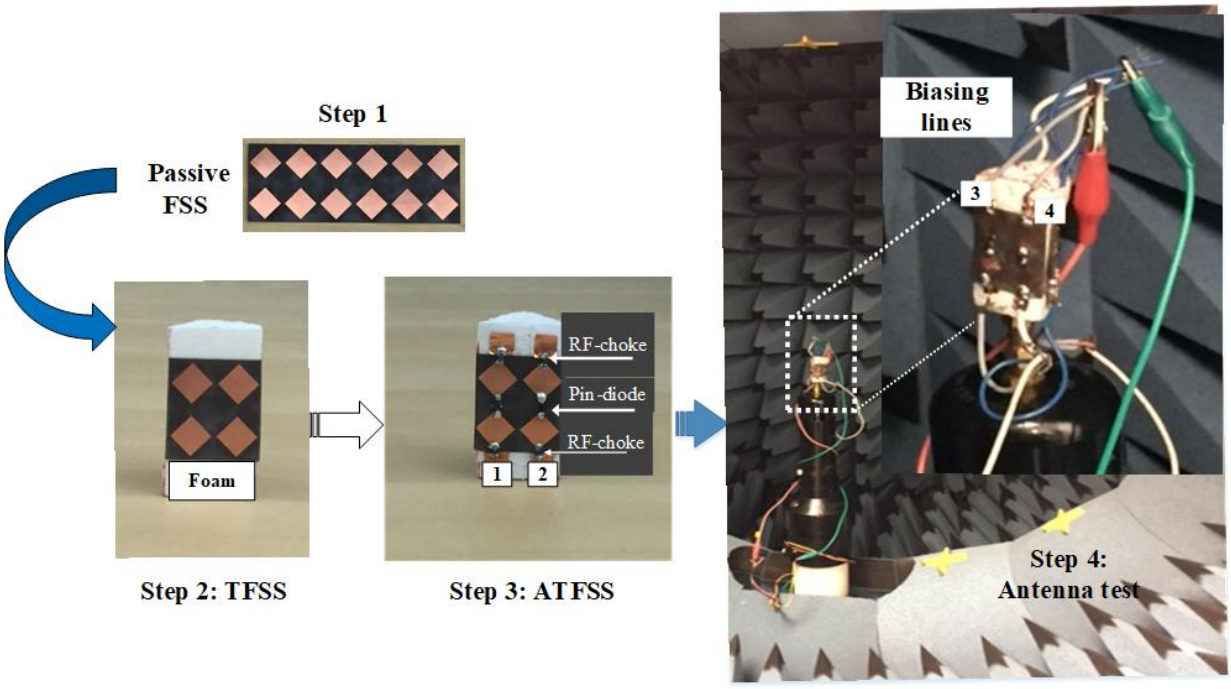

Figure 8. 6. Étapes de prototypage et image de mesure de l'antenne ATFSS fabriquée dans une chambre anéchoïque.

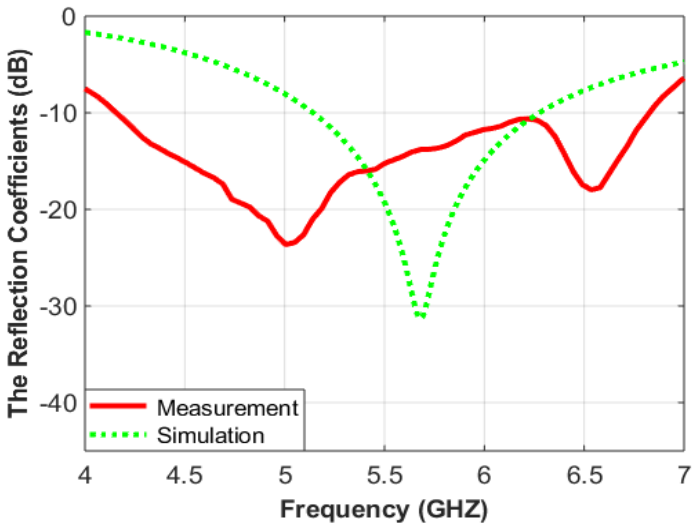

Figure 8. 7. Simulation et mesure du coefficient de réflexion de l'alimentation.

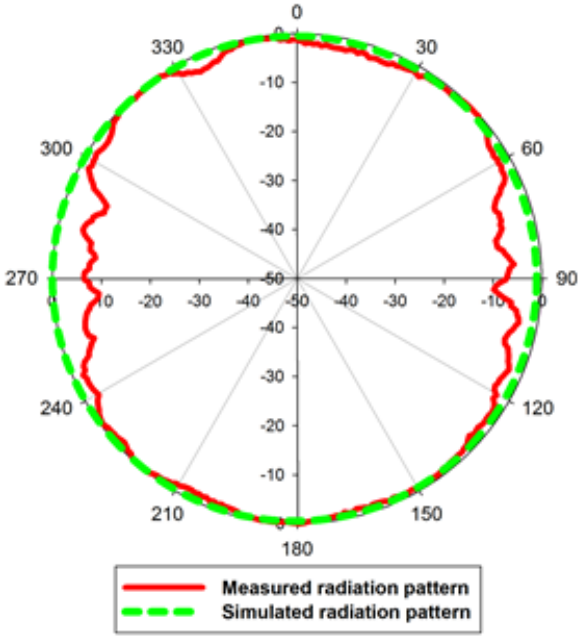

Figure 8. 8. Simulation et mesure des diagrammes de rayonnement dans le plan H de l'antenne planaire unipolaire.

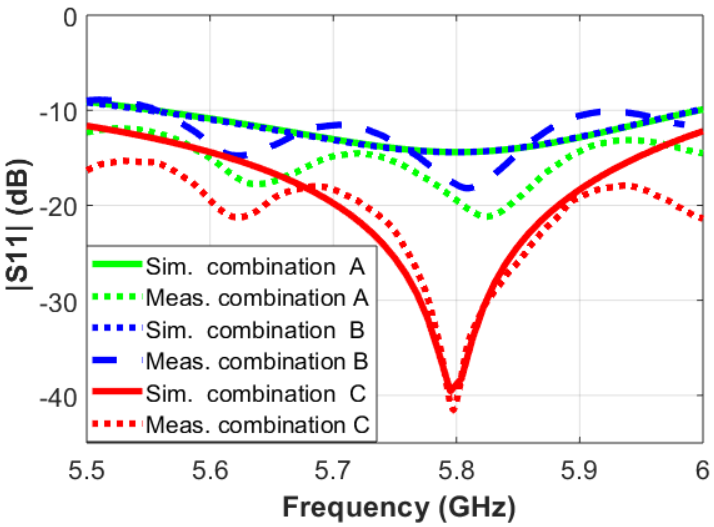

Figure 8. 9. Simulation et mesure du coefficient de réflexion de l'antenne ATFSS à formation de faisceau commutée proposée.

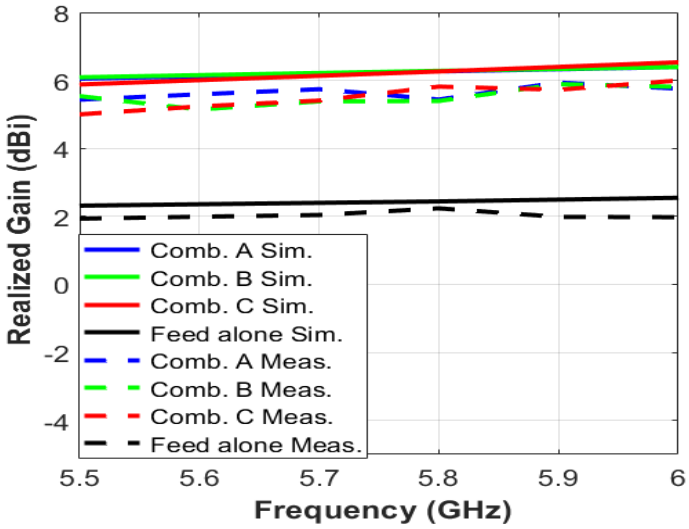

Figure 8. 10. Simulation et mesure du gain de l'antenne ATFSS à formation de faisceau commutée proposée.

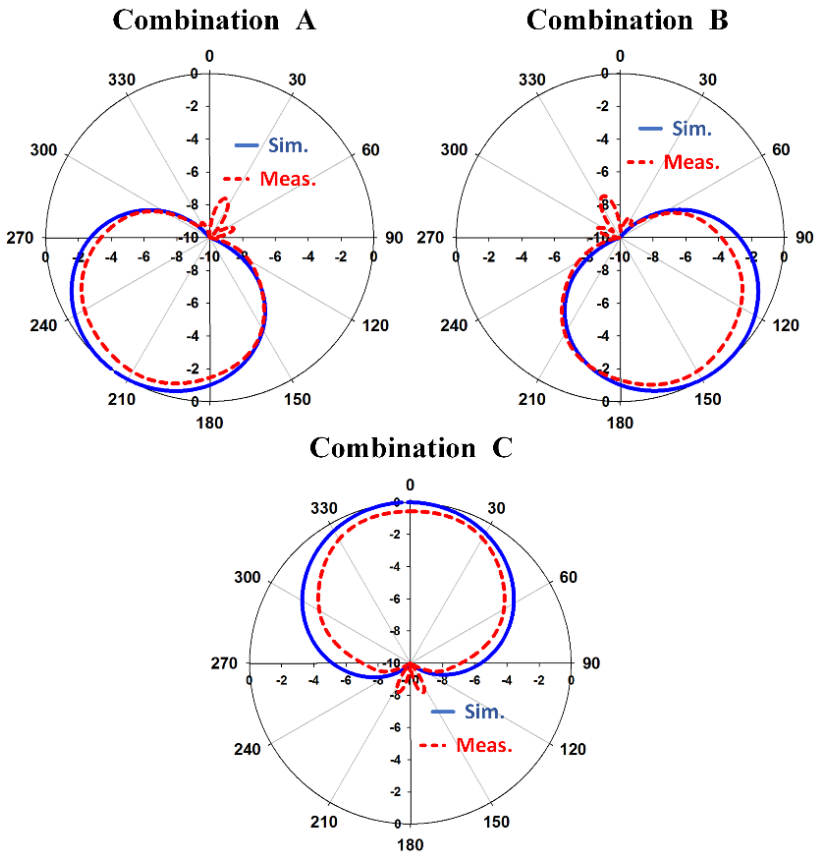

Figure 8. 11. Simulation et mesure des diagrammes de rayonnement de l'antenne ATFSS à formation de faisceaux commutée proposée (en combinaison C).

8.6 Une nouvelle antenne à réflecteur en coin avec un gain accordable basée sur des surfaces actives sélectives en fréquence

Cette partie propose une nouvelle antenne à réflecteur en coin avec un gain accordable basé sur les surfaces actives sélectives en fréquence (AFSSs). L'antenne proposée comprend une source de rayonnement et trois écrans AFSS de tailles différentes. La source de rayonnement est une antenne dipôle avec un diagramme de rayonnement omnidirectionnel. Les écrans AFSS sont tournés vers l'alimentation d'un angle optimisé de 60º et placés du même côté de la source. Selon le meilleur de nos connaissances, il n'existe pas de travaux publiés dans la littérature sur les antennes à réflecteur en coin avec un gain accordable et variable de diagramme directionnel.

Grâce à ces caractéristiques, l'antenne proposée peut être utilisée dans les réseaux locaux sans fil (WLAN), les liaisons sans fil PTP à longue distance, les stations de base cellulaires et d'autres systèmes de communication sans fil similaires.

8.6.1 Conception de la cellule unitaire AFSS

Un réseau d'AFSS est utilisé pour concevoir une antenne avec une capacité de gain reconfigurable. L'AFSS convient ici en raison de sa capacité à réaliser la reconfigurabilité du diagramme de rayonnement. La structure de la cellule unitaire AFSS proposée est illustrée sur la Figure. 8.12. Chaque cellule unitaire est constituée de deux plaques en forme de diamant. Les plaques de l'élément sont conçues sur le substrat Rogers RT 5880, qui a une permittivité relative de 2,2, une tangente de perte de 0,0009 et une épaisseur de h = 0,254 mm. Ces patchs sont connectés/déconnectés électriquement par une diode PIN. Lorsque la diode est allumée, l'élément fournit une caractéristique de réflexion. Cependant, le comportement de transmission est obtenu lorsque la diode est éteinte (état OFF). Cet élément est simulé dans un environnement périodique du studio micro-ondes de la CST en considérant un nombre infini d'éléments le long des directions X et Y. Dans le processus de simulation, la diode PIN à haute fréquence (SMP1345-079LF) est modélisée comme une résistance de 1,5 Ω à l'état ON de la diode PIN. Cependant, un circuit RC parallèle avec Roff =15 KΩ et Coff = 0,17 PF présente la diode à l'état OFF. Les valeurs de la résistance en série et du circuit RC parallèle sont mentionnées dans la fiche technique de la diode PIN [25]. Pour obtenir des résultats de simulation plus précis, l'élément dans [26] est resimulé en considérant à la fois les bobines de réactance RF [28] et les circuits de polarisation. Les bobines de réactance RF sont utilisées sur les côtés supérieur et inférieur de la cellule pour isoler le signal RF des lignes de polarisation. Les dimensions du modèle amélioré de cellule unitaire sont indiquées dans le Tableau 8. 2. Les coefficients de transmission simulés de l'élément AFSS amélioré sont indiqués dans la Figure 8. 13. Sur cette figure, on remarque que la cellule peut réfléchir/transmettre les ondes EM incidentes aux états ON et OFF de la diode PIN, respectivement. Ces résultats ont été obtenus sous l'incidence normale des ondes. Cependant, comme les réflecteurs AFSS doivent être disposés en V pour former un nouveau réflecteur en coin, les paramètres de diffusion de la cellule unitaire ont également été testés sous l'incidence oblique des ondes ($\Psi/2=30^{o}$). Une correspondance a été trouvée entre les résultats de l'incidence normale et de l'incidence oblique, comme le montre la Figure 8. 13. Dans la légende de cette figure, (N) se réfère à l'incidence normale des ondes, tandis que les ondes à incidence oblique sont exprimées par (O). Grâce à ces caractéristiques, une nouvelle antenne à réflecteur en coin avec un gain accordable peut être réalisée en utilisant cette cellule unitaire.

Tableau (8.2): Dimension de la cellule unitaire AFSS améliorée.

Parameters	L1	W1	W2
Values(mm)	30	20	10.5

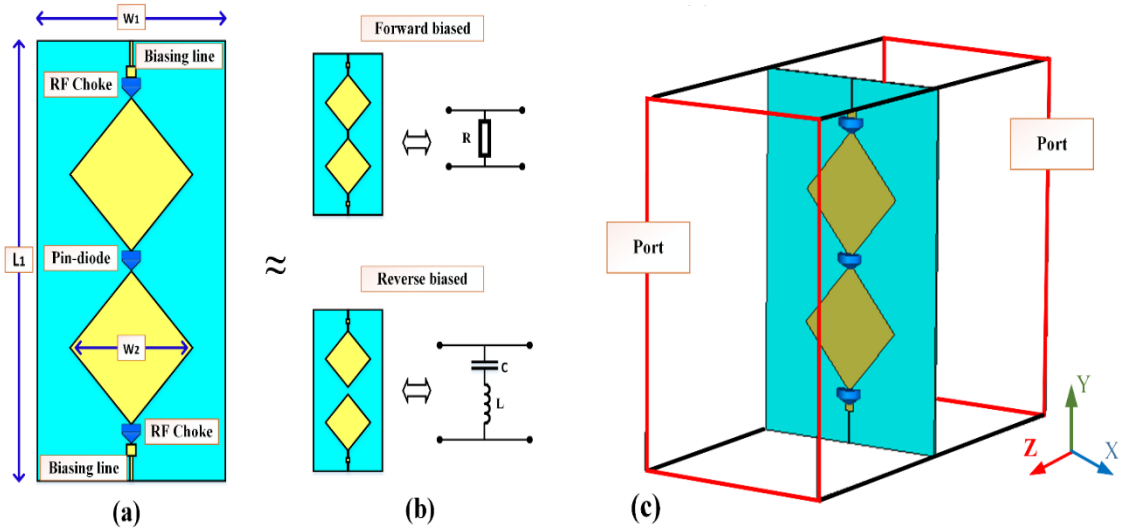

Figure 8. 12. (a) Structure de la cellule unitaire AFSS proposée, (b) circuit équivalent des états ON/OFF de la diode, (c) configuration de la simulation de l'élément AFSS.

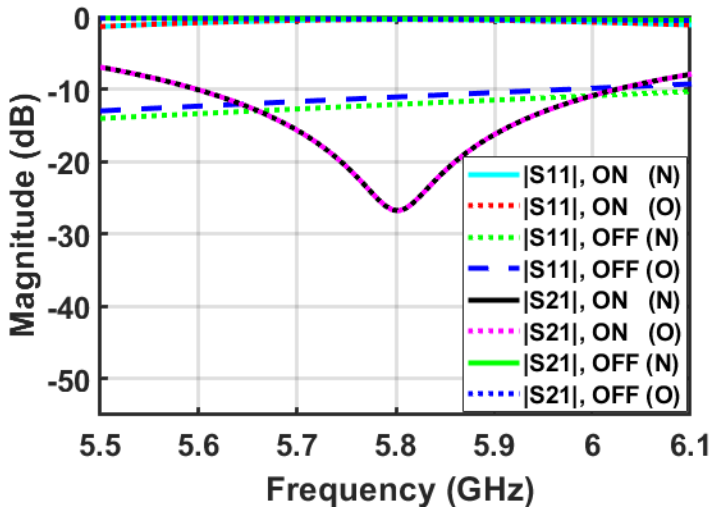

Figure 8. 13. Paramètres de diffusion simulés de la cellule unitaire proposée sous une onde incidente normale et oblique (Ψ/2=30º).

8.6.2 Conception de l'antenne

La configuration de l'antenne proposée est illustrée dans la Figure 8.14. Cette antenne se compose d'un dipôle comme source des ondes EM et de trois écrans AFSS qui sont disposés du même côté du dipôle. Les écrans AFSS sont disposés dans l'ordre suivant : écran-3, écran-2, écran-1, l'écran-1 étant le plus proche du dipôle. Ces écrans sont séparés par un espace optimisé égal Sp=0.5λ. Chacun des écrans 2 et 3 comprend deux réseaux AFFS qui sont dirigés vers l'alimentation selon un angle θ=60º, (ce qui donne une couche AFSS en forme de V). Cependant, deux cellules unitaires AFSS pivotées l'une par rapport à l'autre d'un angle de θ=60º forment l'écran-1. L'alimentation est placée loin de l'écran-1 par une distance optimisée de Fs=0.3λ. Chaque réseau AFSS de l'écran-2 a une taille de 90 mm x 60 mm (1.74 λ × 1.16λ). Ces réseaux sont constitués de deux ensembles de neuf éléments AFSS. Un réseau de 5x5 AFSS forme l'écran-3, chacun ayant une taille de 150 mm x 100 mm (2.9 λ × 1.9λ).

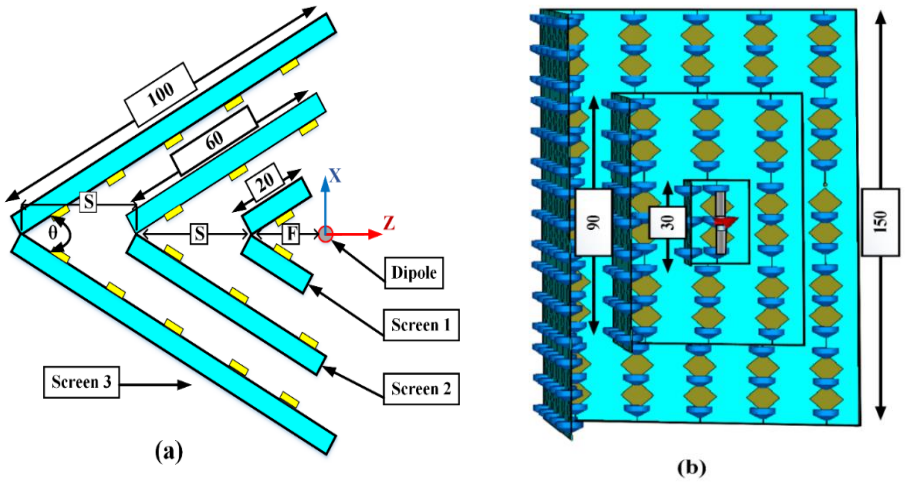

Figure 8. 14. Croquis de l'antenne proposée. (a) vue de dessus, et (b) vue latérale en 3-D. (Toutes les dimensions sont en mm).

8.7 Mécanisme de fonctionnement de l'antenne

Le mécanisme opérationnel de l'antenne proposée est illustré dans la Figure 8. 15. Dans cette technique, le diagramme de rayonnement omnidirectionnel de la source est converti en un diagramme de rayonnement directionnel à gain accordable en utilisant des couches AFSS. La fonction de base des couches AFSS dans cette conception est de contrôler la propagation des ondes incidentes dans la bande de fréquence de résonance. Lorsque les diodes PIN de ces

couches sont désactivées, les couches présentent un comportement de transmission. Cependant, à l'état ON, les couches AFSS agissent comme une surface réfléchissante. La performance de l'antenne proposée est analysée dans trois cas différents. Dans ces cas, différentes combinaisons de diodes AFSS sont appliquées dans l'antenne à réflecteur proposée pour alterner son gain entre trois valeurs différentes. En ajoutant d'autres couches AFSS, la conception proposée permet d'obtenir d'autres valeurs de gain.

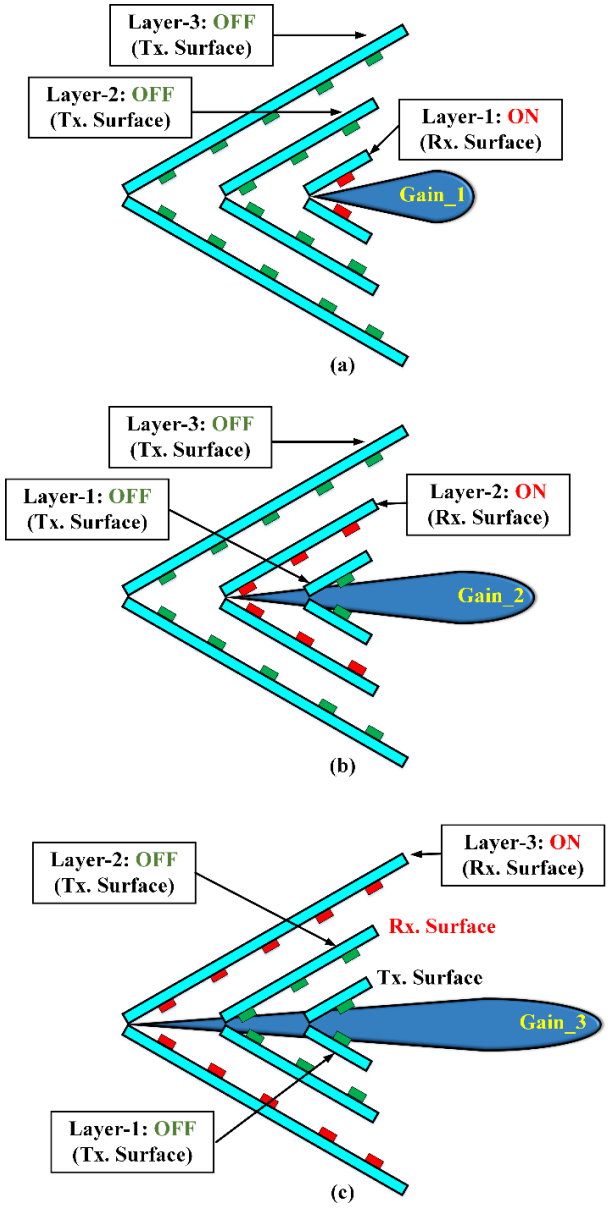

Figure 8.15. Mécanisme opérationnel de l'antenne proposée, (a) Cas I (État ON-OFF-OFF), (b) Cas II (État OFF-ON-OFF), (C) Cas III (État OFF-OFF-ON).

8.7.1 Résultats de la fabrication et des mesures

L'antenne proposée a été fabriquée, et sa performance a été mesurée. Le processus de fabrication et de mesure se fait en plusieurs étapes : Dans la première étape, une antenne dipôle est fabriquée. Pour plus de simplicité, seuls deux écrans (couches) AFSS différents sont fabriqués lors de la deuxième étape. Dans la troisième étape, une base en plexiglas est conçue pour assembler et maintenir les multiples pièces de la structure proposée pour le processus de mesure. La feuille de plexiglas a une taille de 92 mm x 131 mm. En raison de l'épaisseur diélectrique minimale des couches de l'AFSS, des panneaux de mousse de la même taille que ces couches sont utilisés pour soutenir les écrans de l'AFSS à l'aide de colle. De plus, certains trous sont percés sur la feuille de plexiglas pour former un V avec un angle de 60º, et de petites vis en plastique sont utilisées pour fixer les panneaux AFSS lorsqu'ils sont insérés dans les trous. Les diagrammes de rayonnement et le gain d'antenne réalisé de la conception proposée ont été mesurés dans une chambre anéchoïque, comme le montre la Figure 8. 16. De plus, l'amplitude du coefficient de réflexion (S11) a été mesurée à l'aide d'un analyseur de réseau vectoriel. Les coefficients de réflexion mesurés et simulés, le gain réalisé et le diagramme de rayonnement dans le plan H de l'antenne proposée dans le cas I et le cas II sont présentés dans les Figures 5. 17 à 5. 19. Le soudage des lignes de polarisation et des diodes dans le prototype fabriqué crée certaines pertes d'amplitude. Ces pertes ont été observées dans le désaccord marginal entre les résultats de la simulation et de la mesure. Il ressort de ces figures que la conception proposée produit un diagramme de rayonnement directionnel avec un gain maximal mesuré de 6,5 dBi dans le cas I. Cependant, un diagramme de rayonnement directionnel avec un gain maximal mesuré de 10,5 dBi est obtenu dans le cas II. Les résultats sont également comparés avec le diagramme de rayonnement mesuré de la source (antenne dipôle) qui fournit un diagramme de rayonnement omnidirectionnel avec un gain maximum de 1,42 dBi. À notre connaissance, la structure proposée est la première antenne à réflecteur en coin avec un diagramme directionnel accordable et à gain variable.

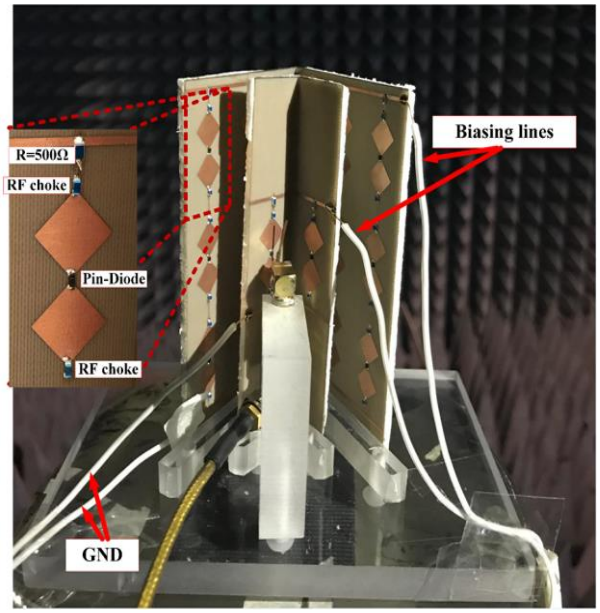

Figure 8. 16. Une photo du prototype offerte dans une chambre anéchoïque.

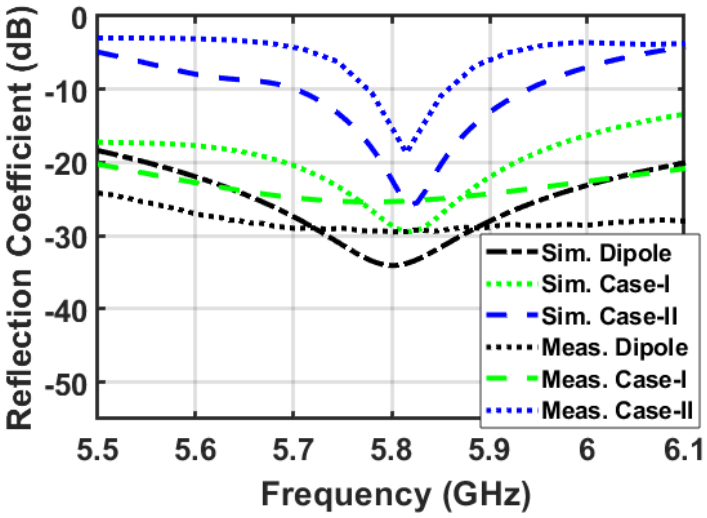

Figure 8. 17. Coefficient de réflexion simulé et mesuré de l'antenne proposée (θ=60º, Fs=0.3λ, and Sp=0.5λ).

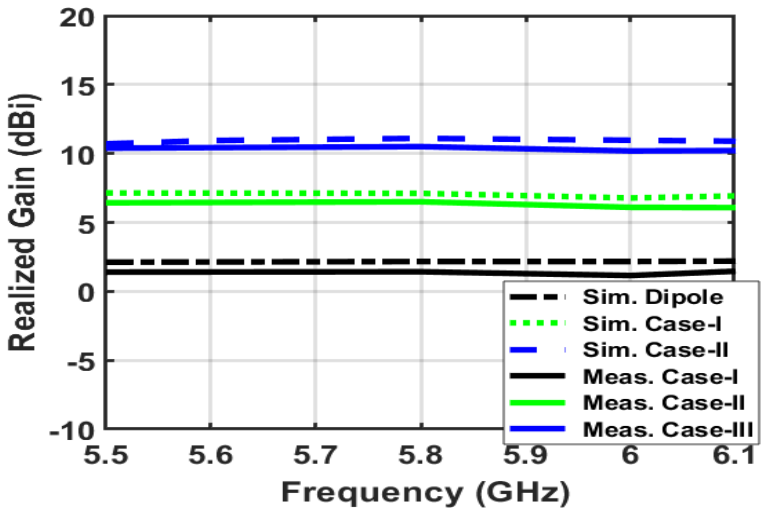

Figure 8. 18. Gain simulé et mesuré de l'antenne proposée (θ=60º, Fs=0.3λ, and Sp=λ/2).

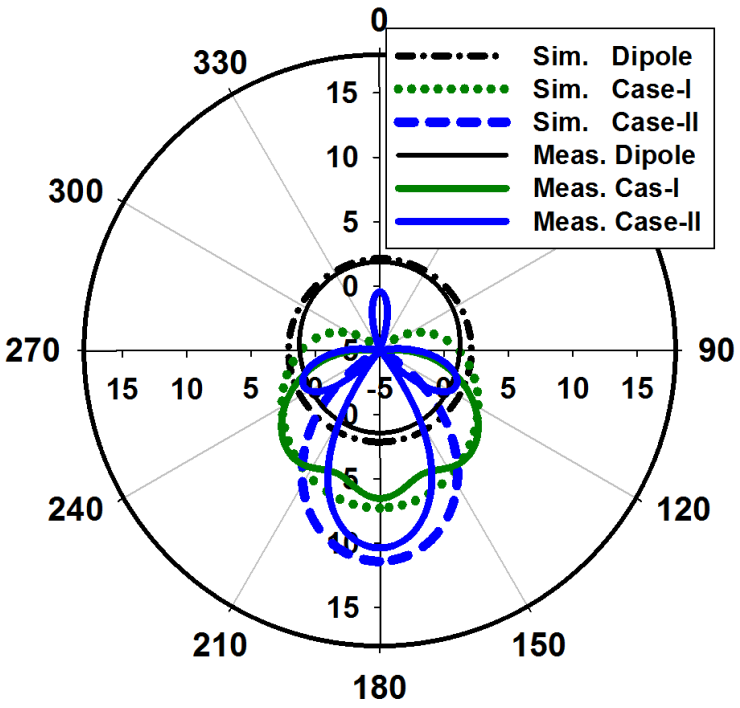

Figure 8. 19. Simulation et mesure du diagramme de rayonnement de l'antenne proposée dans le plan H (θ = 60 °, Fs = 0,3λ et Sp = λ / 2).

8.8 Antenne réflecteur reconfigurable avec capacité d'inclinaison du faisceau

Cette section présente une nouvelle antenne à réflecteur reconfigurable (RRA) à inclinaison de faisceau fonctionnant dans la bande WLAN. La structure proposée est conçue à l'aide d'un réseau d'éléments AFSS. Ce réseau est divisé en trois sections pour faciliter le déplacement (sections centrale, droite et gauche). Une antenne planaire en bande WLAN, placée à l'écart des sections du réseau, est utilisée pour exciter les éléments du réseau. Ce modèle est optimisé pour introduire une RRA à haut gain. Une technique mécanique d'inclinaison du faisceau est également utilisée, où les sections droite et gauche du réseau AFSS sont tournées vers l'alimentation pour incliner le faisceau principal hors de la bande large. Ce mécanisme d'inclinaison mécanique du faisceau se distingue des techniques d'inclinaison précédentes par sa capacité à incliner le faisceau principal sans ajouter des couches ou des configurations supplémentaires à la structure de l'antenne principale. Par conséquent, la taille et le poids de la structure principale de l'RRA restent les mêmes. La méthode d'inclinaison présentée du faisceau introduit une meilleure performance à des angles d'inclinaison plus élevés et conserve presque le même gain du système. En appliquant cette technique d'inclinaison du faisceau, une plage d'inclinaison maximale de ±30° (hors bord) est obtenue à 2,45 GHz. Le système RRA d'inclinaison de faisceau proposé est fabriqué et mesuré. Un bon accord entre les résultats simulés et mesurés est obtenu en termes de coefficient de réflexion, de direction du faisceau et de gain réalisé. À notre connaissance, la structure proposée est la première conception où la FSS active est utilisée pour assurer la reconfigurabilité du faisceau lorsque la FSS est disposée en forme parabolique. Comme il est bien connu dans la littérature que le principal inconvénient des conceptions à réflecteur parabolique est la capacité de balayage minimal du faisceau, alors qu'en utilisant la technique proposée, une antenne à gain élevé peut être conçue (lorsque la taille de l'antenne est augmentée en fonction d'une spécification donnée). Dans le travail présenté, la performance de l'antenne est étudiée à l'aide d'une diode PIN. Le comportement en réflexion/transmission de l'AFSS est obtenu lorsque les états de la diode PIN sont commutés à l'aide d'une tension de polarisation continue externe. En outre, une approche mécanique de la direction du faisceau a également été présentée lorsque l'un des panneaux latéraux de l'antenne est tourné vers ou à l'écart du panneau central. Il est également important de mentionner ici que si des diodes varicap sont fixées dans la FSS, il est possible d'obtenir une orientation électronique du faisceau au lieu d'une orientation mécanique.

Grâce à ces caractéristiques, l'antenne proposée peut être utilisée pour diverses applications

sans fil, telles que la radiolocalisation, les communications mobiles par satellite, les liaisons radioamateur et les communications par satellite.

8.8.1 Conception d'une cellule unitaire FSS active

Pour concevoir une RRA, on utilise une AFSS (surface FSS encastrée avec des diodes PIN). Cette surface peut contrôler la propagation des ondes lorsqu'une tension externe est appliquée. Les caractéristiques de transmission/réflexion de l'AFSS sont illustrées dans [23]. Lorsque les diodes sont allumées, le comportement de réflexion de la surface est réalisé. Cependant, l'état OFF fournit une caractéristique de transmission. La figure 8. 20 (a) montre l'élément AFSS proposé. Cet élément contient deux patchs rectangulaires qui sont électriquement connectés/déconnectés par une diode PIN (dans le cas non idéal). La diode PIN à haute fréquence (SMP1345-079LF) est utilisée dans cette structure. Cette diode est modélisée comme une résistance de 1,5 Ω à l'état ON. Cependant, un circuit RC parallèle avec Roff =15KΩ et Coff = 0,17 PF représente la diode à l'état OFF, comme mentionné dans la fiche technique [24]. Les patchs des cellules unitaires sont montés sur le substrat Rogers RT 5880. Ce substrat a une épaisseur de h = 1,575 mm, une tangente de perte de 0.0009 et une permittivité relative de 2,2 [25]. Cet élément est simulé dans un environnement périodique du studio Microwave CST en considérant un nombre infini d'éléments le long des directions X et Y. Les circuits équivalents de la diode PIN dans l'environnement idéal et non idéal sont représentés sur la figure 8. 20 (b), tandis que les performances de diffusion sont présentées sur la figure 8. 20 (c). Il est visible que l'amplitude du coefficient de réflexion dans l'état ON idéal est plus élevée par rapport à l'état ON non idéal. Cette différence d'amplitude est due à la résistance en série de la diode. Inversement, la capacité utilisée à l'état OFF dans le cas non idéal augmente l'amplitude du coefficient de réflexion par rapport au cas idéal. Cependant, dans les deux cas, idéal et non idéal, la cellule unitaire présente un comportement de transmission et de réflexion maximal dans les états OFF et ON, respectivement. Grâce à ces caractéristiques de diffusion, l'élément proposé illustre l'aptitude à concevoir une RRA à inclinaison de faisceau. Il est important de noter que le cas non idéal est plus pratique que le cas idéal. Dans ce cas, la commutation entre les états ON/OFF peut être réalisée électriquement en contrôlant la tension de polarisation continue. Cependant, on peut s'attendre à une baisse de la performance de l'antenne dans le cas non idéal en raison des diodes intégrées. Alors que, dans le cas idéal, l'antenne proposée sera exempte de la perte due aux

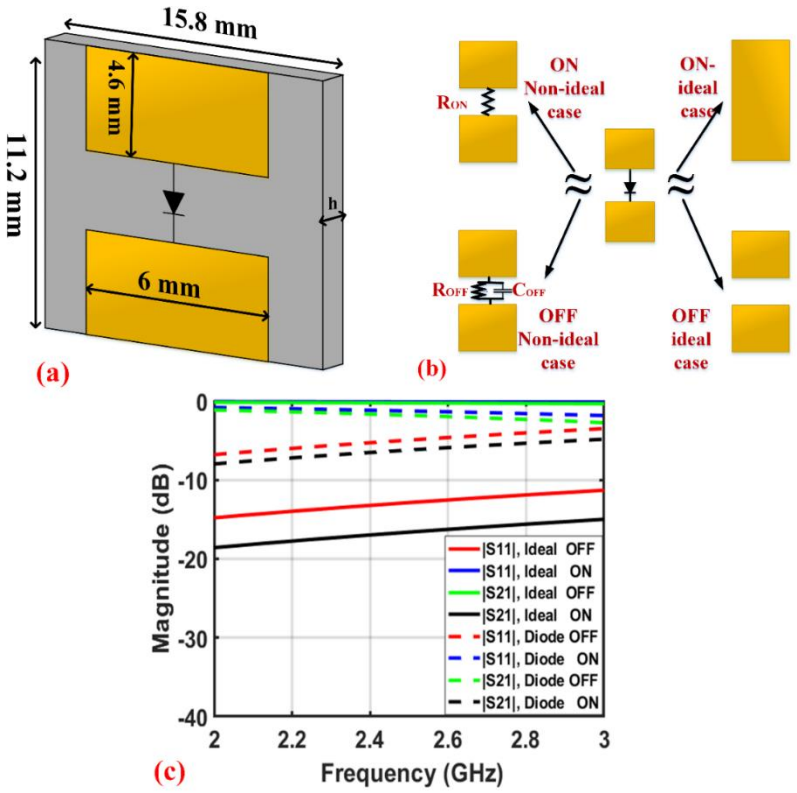

Figure 8. 20. Cellule unitaire AFSS : (a) vue de face, (b) modèle de circuit équivalent de la diode idéale et non idéale dans les états ON/OFF, et (c) coefficients de transmission et de réflexion de la cellule unitaire pour les états ON/OFF de la diode idéale et non idéale.

diodes. Cependant, deux surfaces RR différentes devraient être conçues (surface RR à l'état ON et surface RR à l'état OFF).

8.8.2 Conception d'une antenne à réflecteur reconfigurable

L'antenne proposée se compose de deux parties principales : une alimentation et une surface de réflecteur reconfigurable (RR), comme le montre la Figure 8. 21. L'alimentation est placée à l'écart de la surface RR au point focal.

8.8.3 Conception de l'alimentation

Une antenne planaire de 57,6 mm x 46,8 mm (0.47λ x 0.38 λ) est utilisée pour exciter les éléments de la surface de la RR. Une méthode d'alimentation coaxiale est utilisée, comme le montre la Figure 8. 22. L'antenne d'alimentation est conçue à l'aide de Rogers RT 5880, avec une épaisseur

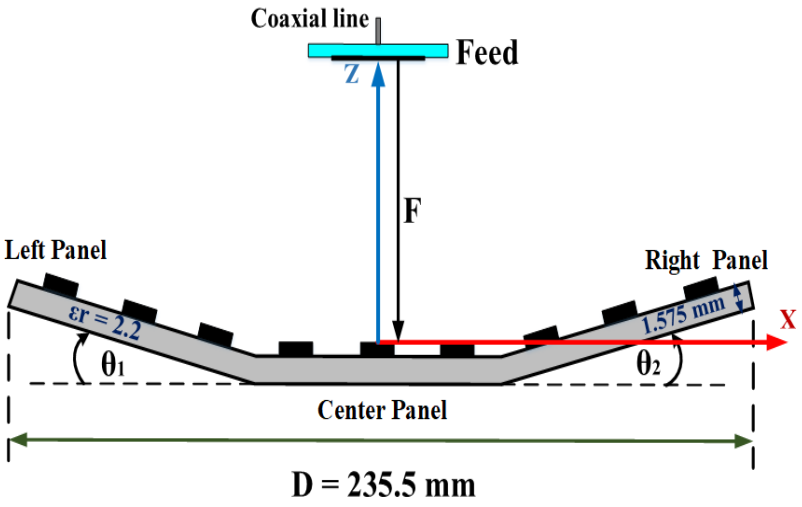

Figure 8. 21. Vue de dessus de la RRA proposée.

de 1,575 mm, une permittivité relative de 2,2, et une tangente de perte de 0,0009. L'alimentation est placée loin de la surface RR au point focal avec un rapport foyer/diamètre (F/D) de 0,28. L'antenne d'alimentation est fabriquée et mesurée. Les résultats simulés et mesurés en termes de coefficient de réflexion, de gain réalisé et de diagramme de rayonnement dans le plan H sont présentés sur la Figure 8. 23, qui montre un bon accord.

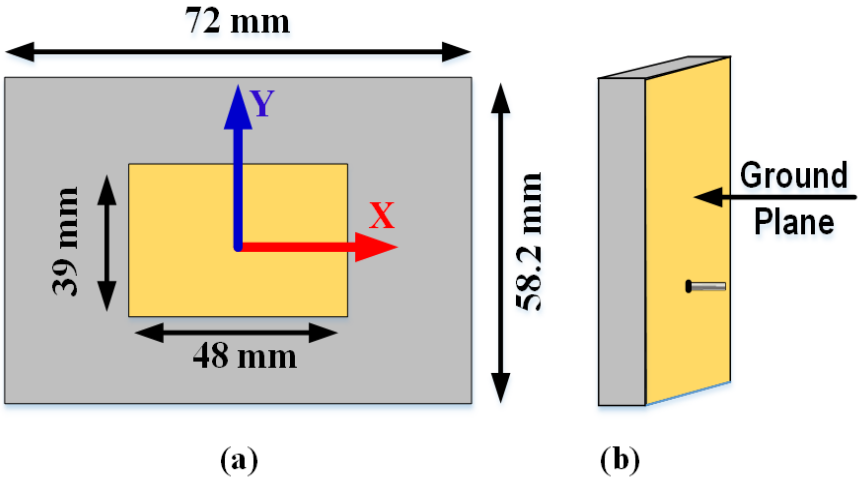

Figure 8. 22. Structure de l'antenne d'alimentation, (a) vue de dessus, (b) vue de côté.

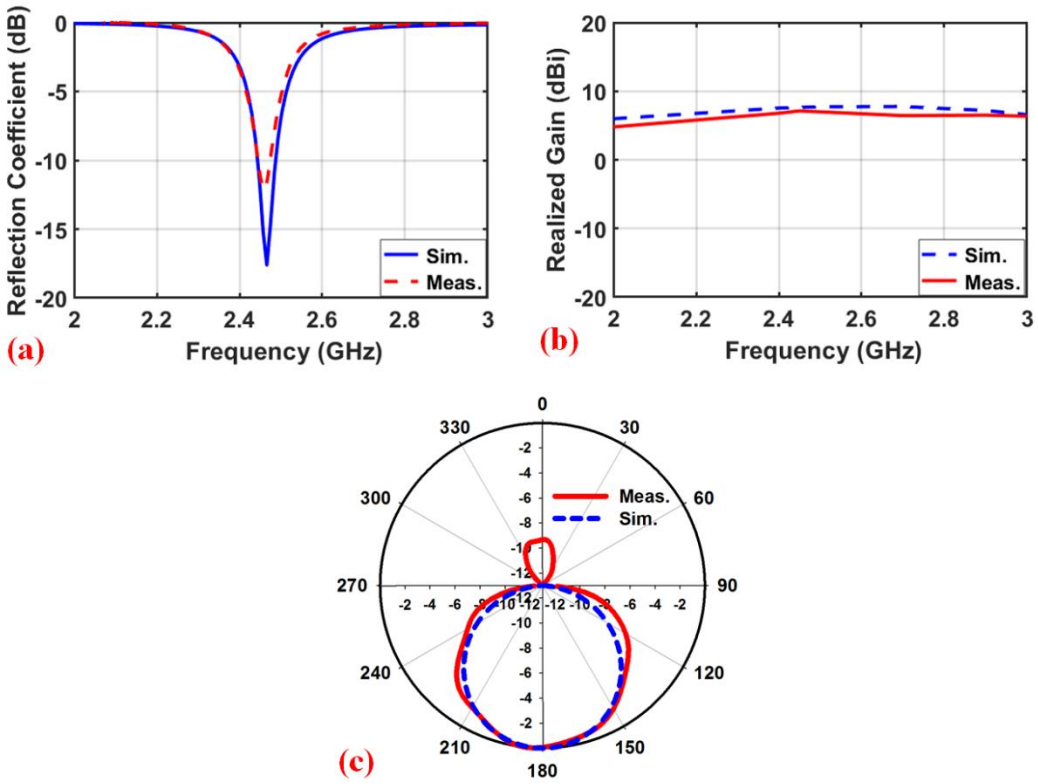

Figure 8. 23. Simulation et mesure des résultats de l'antenne planaire : (a) coefficient de réflexion, (b) gain, et (c) diagramme de rayonnement dans le plan H.

8.8.4 Conception de la surface RR

La surface RR est composée de trois sous-écrans AFSS qui sont connectés en série. Les sous-écrans gauche et droit peuvent se transformer en nourriture pour prendre une forme parabolique. L'écran RR a une taille de 235,5 mm x 169 mm (1,9 λ x 1,37 λ). Chacun des sous-écrans AFSS mesure 78,5 mm x 169 mm (0,64 λ x 1,37 λ). L'effet des angles de rotation des sous-écrans latéraux (θ_1 et θ_2) est optimisé pour de meilleures performances d'antenne en termes de coefficient de réflexion et de gain. Les performances de l'antenne proposée sont analysées pour les états ON / OFF des diodes PIN. Il a été observé que le gain maximum est atteint lorsque les angles de rotation des écrans gauche et droit sont $\theta_1 = \theta_2 = 15^o$. Comme l'état ON de la diode présente une réflexion maximale du RRA, les résultats obtenus sont comparés à une antenne équivalente conçue avec des feuilles métalliques. La performance de l'antenne est analysée à 2,45 GHz. Il est évident que l'antenne présente un coefficient de réflexion élevé en raison du

blocage de l'alimentation. Dans le RRA à alimentation centrale, en raison de l'accumulation des ondes stationnaires entre l'alimentation et la surface du RR, le niveau d'adaptation de l'alimentation et la largeur de bande sont réduits. La largeur de bande d'adaptation peut être augmentée en réduisant le blocage de l'alimentation en utilisant une technique telle que celle présentée dans [27]. Les auteurs ont présenté une technique de perturbation de phase pour améliorer l'adaptation de l'alimentation, et une amélioration de l'adaptation de 5 dB sur 30% de la largeur de bande a été obtenue. L'antenne produit un gain maximum de 11,9 dBi (à l'état passant) et 7,8 dBi (à l'état éteint).

8.9 Mécanisme d'inclinaison du faisceau de l'RRA

Un mécanisme mécanique d'inclinaison du faisceau est présenté en utilisant la RRA proposée. Une inclinaison du faisceau hors-bord est obtenue en faisant tourner mécaniquement le panneau gauche ou droit vers l'alimentation, comme le montre la Figure 8. 24. Pour incliner le faisceau principal vers des angles positifs ou négatifs (Ψ) à partir du bord, on fait tourner mécaniquement le panneau gauche/droit du RRA avec θ_1 ou θ_2. Il est important de mentionner que ce mécanisme mécanique d'inclinaison du faisceau est analysé dans l'état ON de la diode, alors que dans l'état OFF, l'inclinaison du faisceau n'est pas aussi efficace en raison de la grande largeur du faisceau à mi-puissance (HPBW) de l'antenne d'alimentation. Pour incliner le faisceau à un angle (±Ψ du bord), les panneaux doivent être tournés mécaniquement à des angles $\theta_1 = +2\Psi_1$ ou $\theta_2 = -2\Psi_2$. Pour incliner le faisceau dans une direction spécifique, il faut faire pivoter les panneaux de gauche ou de droite. Les deux panneaux ne sont pas tournés en même temps.

8.10 Prototype et résultats de mesures

La structure de l'RRA proposée a été fabriquée et mesurée. La Figure 8. 25 montrent les étapes de fabrication et de mesure. L'antenne proposée est encadrée en plusieurs pièces (étiquetées comme des panneaux), chacune de taille 78,5 mm x 169 mm (0.64λ x 1.37λ). Un support de montage à base de plexiglas est conçu pour placer la surface RR et l'alimentation, comme le montre la Figure 8. 25 (b). Plusieurs trous sont percés sur la feuille de Plexiglas (alors que des vis en plastique sont utilisées), pour maintenir les panneaux RRA, pour le processus de mesure.

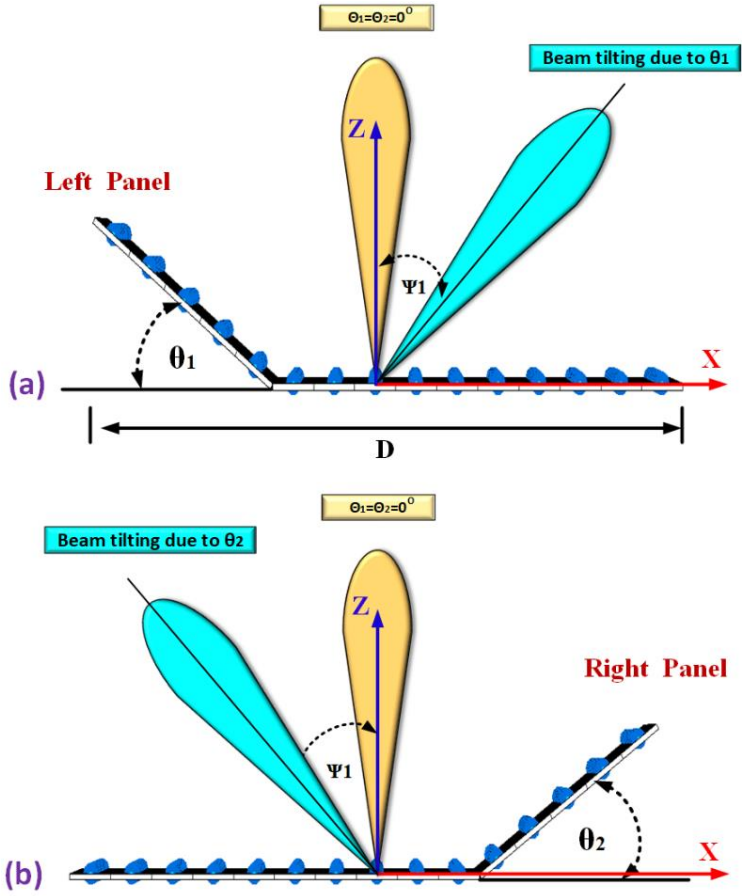

Figure 8. 24. Croquis du mécanisme d'inclinaison du faisceau proposé : (a) rotation du sous-écran de gauche vers l'alimentation par θ1, (b) rotation du sous-écran de droite vers l'alimentation par θ2.

Pour faire pivoter les panneaux latéraux droit et gauche, les trous séparés sont percés de 0º à 60º. Chaque trou adjacent est à 15º de l'autre. La feuille de plexiglas a une taille de 240 mm x 120 mm. Une diode à broches est soudée dans chaque cellule unitaire. La tension CC a été utilisée pour vérifier l'état des diodes PIN. En appliquant une tension continue de 5 V, les diodes AFSS fonctionnent à l'état ON, tandis que 0 V représente l'état OFF. Une résistance de 500 Ω est utilisée en haut de chaque colonne du réseau AFSS. Cette résistance est utilisée pour protéger les diodes et pour produire la même quantité de courant pour toutes les diodes. Le bas de chaque colonne est relié au plan de masse. Les résultats de simulation et de mesure des performances des antennes sont présentés dans Figure 8. 26- Figure 8. 29.

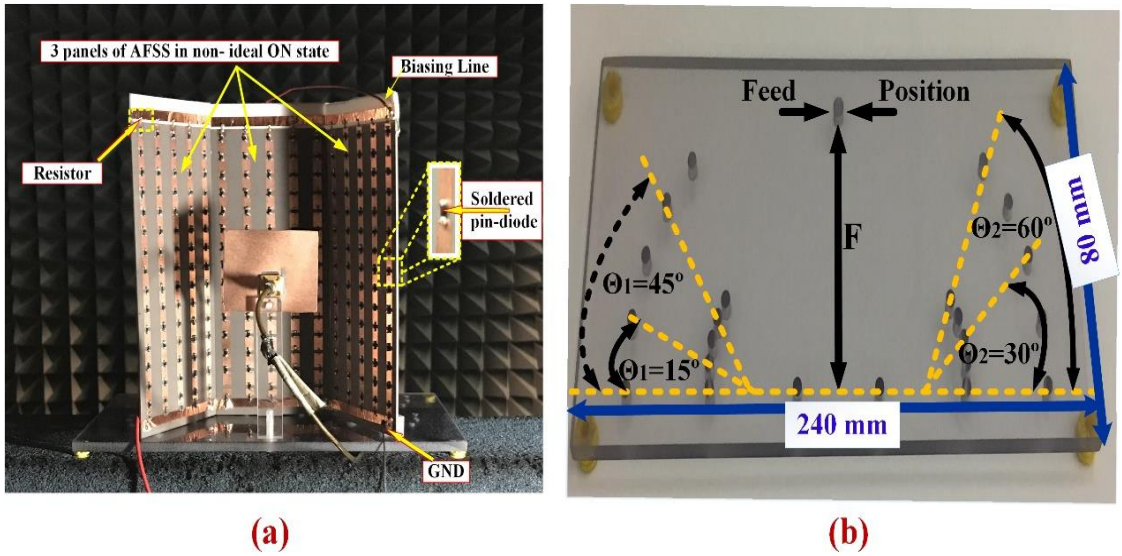

Figure 8. 25. Étapes de prototypage et de mesure : (a) photos des prototypes du RRA proposé dans une chambre, (b) base en plexiglas.

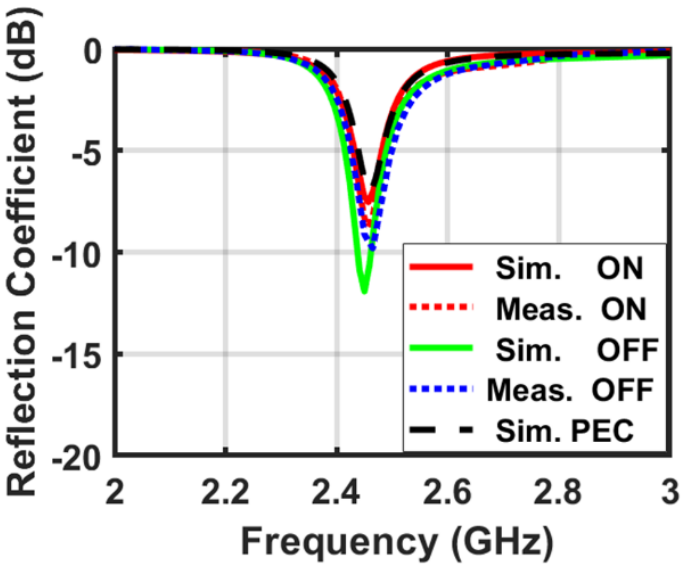

Figure 8. 26. Coefficient de réflexion simulé et mesuré de la RRA idéale proposée, où $\theta_1=\theta_2=15^o$

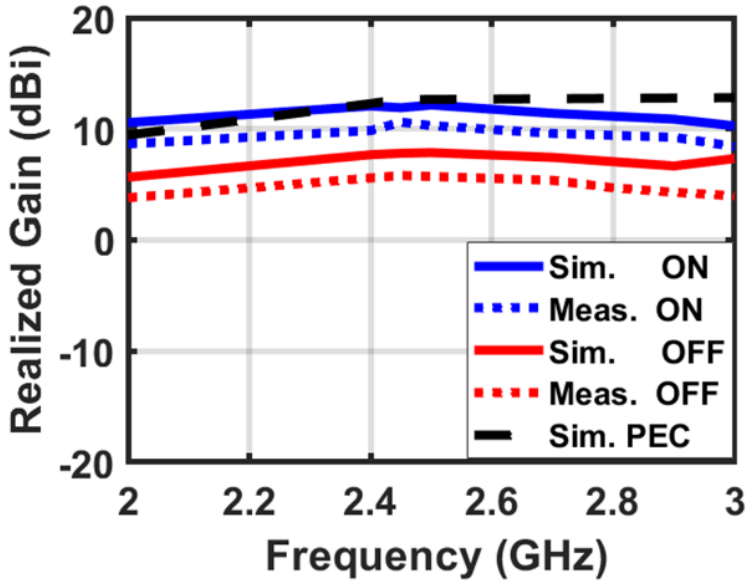

Figure 8. 27. Gain simulé et mesuré de la RRA proposée, où θ1=θ2=15º

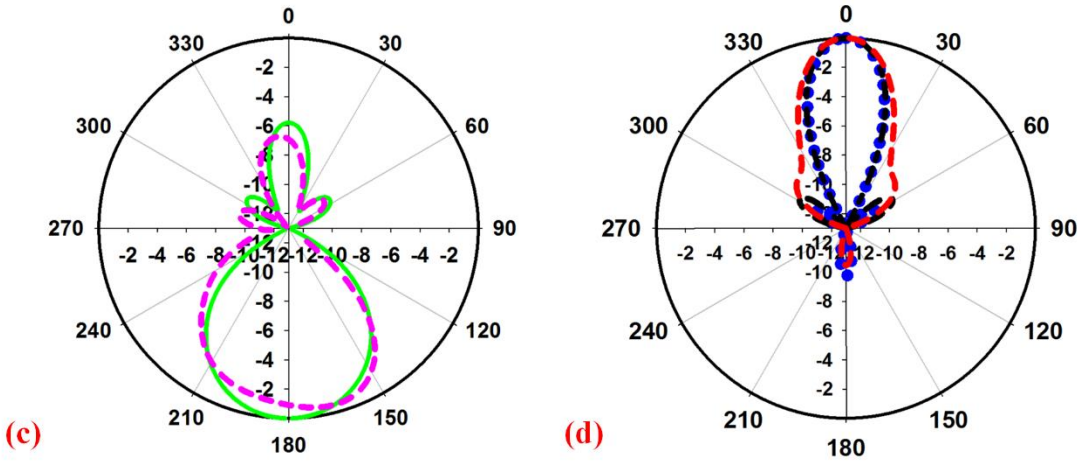

Figure 8. 28. Simulation et mesure du diagramme de rayonnement de la RRA proposée dans le plan H, où $\theta_1=\theta_2=15º$: (a) ON, (b) OFF.

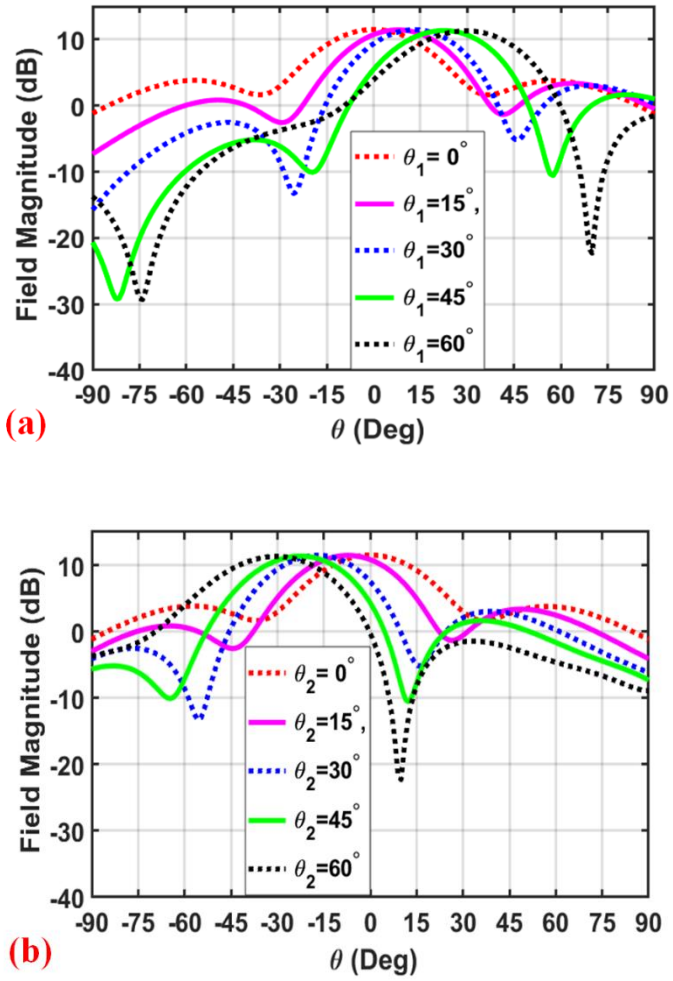

Figure 8. 29. Diagrammes de rayonnement simulés et mesurés du RRA à inclinaison de faisceau non idéal proposé dans le plan H: (a) avec différentes valeurs de θ_1, lorsque $\theta_2=0^o$, (b) avec différentes valeurs de θ_2, lorsque $\theta_1=0^o$.

8.11 Conclusion

Dans cette thèse, les surfaces sélectives en fréquence et leurs applications dans la conception des antennes réconfigurables ont été étudiées. De nouvelles cellules unitaires de surface sélectives en fréquence ont été conçues pour les applications de formation de faisceaux. De plus, diverses nouvelles antennes à formation de faisceaux basées sur des surfaces sélectives en fréquence ont été proposées. Les paragraphes suivants présentent les étapes méthodologiques qui ont été prises pour atteindre les objectifs de la thèse :

Première étape: une recherche approfondie sur les surfaces sélectives en fréquence et ses applications dans les antennes modernes a été effectuée. Cette étude a montré le rôle essentiel des surfaces sélectives en fréquence dans la conception de l'antenne reconfigurable du diagramme de rayonnement. Différentes cellules unitaires AFSS ont été proposées. Certains de ces éléments fonctionnent à 2,45 GHz et d'autres à 5,8 GHz.

Deuxième étape: une nouvelle antenne de surface sélective en fréquence, basée sur la formation de faisceaux commutés, a été proposée. Cette conception consiste en une nouvelle surface active triangulaire sélective en fréquence (ATFSS) entourant une source d'excitation. La conception proposée a réussi à convertir le diagramme de rayonnement omnidirectionnel de la source en un diagramme directionnel. Le faisceau principal a effectivement été orienté dans différentes directions dans le plan azimutal avec une largeur de faisceau de rayonnement de 120º à 5,8 GHz. La technique proposée a amélioré le gain maximal de la source de 4dBi. Un nombre minimum d'éléments actifs a été utilisé dans cette conception. Cela permet d'améliorer le gain de l'antenne et de réduire son coût.

Troisième étape : une nouvelle antenne à réflecteur en coin avec un gain accordable basé sur les surfaces actives sélectives en fréquence (AFSS), a été proposée et conçue. Dans cette structure, trois couches AFSS de reconfiguration de tailles différentes sont disposées autour d'une antenne dipôle pour former un réflecteur en coin en forme de V. En utilisant cette technique, le diagramme de rayonnement omnidirectionnel de la source est modifié avec succès en un diagramme de rayonnement directionnel avec un gain accordable. À notre connaissance, cette conception est la première antenne à réflecteur en coin avec un diagramme de rayonnement directionnel à gain variable et accordable.

Dernière étape : une nouvelle antenne à réflecteur reconfigurable (RRA) à inclinaison de faisceau fonctionnant dans la bande WLAN a été conçue et fabriquée. La conception proposée consiste en un réseau de cellules unitaires AFSS et une antenne planaire en bande WLAN comme source d'excitation. Une technique d'inclinaison mécanique du faisceau a été appliquée à la conception proposée. Grâce à cette technique, le faisceau principal s'est effectivement incliné sans ajouter des couches ou des configurations supplémentaires à la structure de l'antenne principale (la taille et le poids de la structure principale restent les mêmes). À notre connaissance, cette conception permet pour la première fois de reconfigurer le faisceau lorsque l'AFSS est disposé en forme parabolique.

8.12 Travaux futurs

Cette thèse a présenté des travaux de recherche sur les surfaces actives sélectives en fréquence (AFSS) reconfigurables et les antennes à diagramme de rayonnement reconfigurable. Plusieurs nouvelles antennes à commutation de faisceau basées sur des surfaces sélectives en fréquence (AFSS) ont été proposées. Néanmoins, de nombreuses autres recherches doivent être explorées dans ce domaine, qui donneront lieu à des travaux futurs, comme indiqué dans les paragraphes suivants :

Premièrement : Le développement du mécanisme de commutation et du circuit de contrôle de la tension continue sera une question importante. Cela permettra d'améliorer les performances des prototypes reconfigurables. Le plasma, les MEMS et les dispositifs ferroélectrique sont quelques-uns des nouveaux mécanismes de reconfiguration proposés.

Deuxièmement : Cette thèse propose des antennes à balayage du diagramme de rayonnement dans le plan azimutal. Proposer de nouvelles antennes capables de balayer le diagramme de rayonnement à la fois dans les plans d'élévation et d'azimut sera un travail intéressant.

Troisièmement : les antennes proposées dans cette thèse peuvent être développées pour fonctionner à deux et trois bandes. Cela peut être réalisé en utilisant plusieurs couches AFSS, chaque couche fonctionnant à une bande spécifique. L'utilisation d'une couche AFSS multi-bandes est une autre façon de réaliser des antennes reconfigurables à double et trois bandes.

Quatrièmement : Dans cette thèse, nous proposons une nouvelle antenne à réflecteur en coin avec un gain accordable basé sur les surfaces actives sélectives en fréquence (AFSS). Il sera intéressant d'améliorer cette structure pour en faire une antenne à réflecteur en coin à direction de faisceau avec un gain accordable. Cela peut être facilement réalisé en ajoutant des couches AFSS supplémentaires autour de la source d'excitation. En commutant les diodes PIN des couches AFSS entre ON et OFF, le diagramme de rayonnement à gain accordable sera dirigé dans tout le plan azimutal.

Finalement : Cette thèse a présenté une nouvelle antenne à réflecteur reconfigurable à inclinaison de faisceau fonctionnant dans la bande WLAN. Cette structure est la première conception où l'AFSS est utilisée pour fournir la reconfigurabilité du faisceau lorsque l'AFSS est disposé en forme parabolique. Cependant, cette conception souffre d'un coefficient de réflexion élevé en raison du blocage de l'alimentation. Il est donc intéressant de mettre au point une technique permettant de réduire le blocage de l'alimentation et d'améliorer la largeur de bande d'adaptation de l'antenne proposée.

REFERENCES

1. A. Edalati, and T. A. Denidni, “Frequency selective surfaces for beamswitching applications," IEEE Transactions on Antennas and Propagation, vol. 61, no. 1, pp.195–200, Jan. 2013.

2. A. Hakkarainen, J.Werner, and N. Gulati. “Reconfiguration antenna based doa estimation and localization in cognitive radios: Low complexity algorithms and practical measurements,” CROWNCOM, Oulu, Finland, June 2014.

3. A. Mozharovskiy, A. Artemenko, and A. Sevastyanov, “Beam steerable integrated lens antenna with waveguide feeding system for 71 76/81–86 GHz point-to-point applications,” EuCAP, Davos, Switzerland, 2016.

4. A. Tamijani, L. Zhang, G. Pan et al., “Lens-enhanced phased array antenna system for high directivity beam-steering,” APSURSI, Spokane, WA., USA., July 2011.

5. T. Ueda, S. Yamamoto, and Y. Kado, and T. Itoh, “Pseudo-traveling- wave resonator with magnetically tunable phase gradient of fields and its applications to beam-steering antennas,” IEEE Trans. Microw. Theory Techn., vol. 60, no.10, pp. 3043-3054, 2012.

6. Y. Yokohama, and T. Kodera, “Voltage Beam-Steerable Leaky-wave Antenna Using Magnet-less Non-Reciprocal Metamaterial (MNM),” ISAP, Hobart, TAS, Australia, 2015.

7. T. A. Denidni, and G.Y. Delisle, “A nonlinear algorithm for output power maximization of an indoor adaptive phased array,” IEEE Trans. Electromagn. Compat., Vol. 37, No. 2, pp. 201-209, May 1995.

8. V. S. Rao, V.V. Srinivasan and S. Pal, “Generation of dual beams from spherical phased array antenna,” Electronics Lett., vol. 45, no. 3, pp. 441–442, 2009.

9. G. Poilasne, P. Pouliquen, K. Mahdjoubi, L. Desclos, and C. Terret, “Active metallic photonic bandgap material MPBG: Experimental results on beam shaper,” IEEE Trans. Antennas Propag., vol. 48, no. 1, pp. 117–119, Jan. 2000.

10. B. A. Munk, Frequency Selective Surfaces Theory and Design John Wiley & Sons, 2000.

11. P. Callaghan and E. A. Parker. Tuning interactions of cascaded-frequency selective-slot arrays. IEE Proc. on Mic., Ant. and Propag., 141(4):290–294, 1994.

12. K. Karkkainen and M. Stuchly, “Frequency Selective Surface as a Polarisation Transformer,” IEE Proc. on Mic. Ant. and Propag., Vol. 149 (No. 56), p. p. 248- 252, 2002.

13. P. Callaghan, E. A. Parker and R. J. Langley, “Influence of Supporting Dielectric Layers on The Transmission Properties of Frequency Selective Surfaces,” IEE Proc. on Mic. Ant. and Propag., Vol. 138 (No. 5), p. p. 448-454, 1991.

14. L. Zhang, Q. Wu and T. A. Denidni, "Electronically Radiation Pattern Steerable Antennas Using Active Frequency Selective Surfaces," IEEE Transactions on Antennas and Propagation, vol. 61, no. 12, pp. 6000-6007, Dec. 2013.

15. Jennifer T. Bernhard, Reconfiguration Antennas, Morgan & Claypool Publishers, 2007.

16. C. Sulakshana and L. Anjaneyulu, “Reconfiguration antennas with frequency, polarization, and pattern diversities for multi-radio wireless applications,” International Journal of Microwave and Wireless Technologies, vol. 9, no. 1, pp. 121–132, 2017.
17. Mahmoud Niroo-Jazi, Nimble Radiation-Pattern Antennas Using Agile Frequency Selective Surfaces, Thesis, 2012.

18. T. Li, H. Zhai, X. Wang, L. Li and C. Liang, "Frequency-Reconfiguration Bow-Tie Antenna for Bluetooth, WiMAX, and WLAN Applications," in IEEE Antennas and Wireless Propagation Letters, vol. 14, pp. 171-174, 2015.

19. A. Raveendran, P. Mathur and S. Raman, "Mechanically Frequency Reconfiguration Antenna and its Application as a Fluid Level Detector for Wireless Sensor Networks," 2019 URSI Asia-Pacific Radio Science Conference (AP-RASC), New Delhi, India, 2019, pp. 1-4.

20. F. Wu and K. M. Luk, "A wideband high-efficiency polarization Reconfiguration antenna for wireless communication," 2017 IEEE International Symposium on Antennas and Propagation & USNC/URSI National Radio Science Meeting, San Diego, CA, 2017, pp. 1371-1372.

21. J. R. Costa, E. B. Lima, and C. A. Fernandes, “Compact beam-steerable lens antenna for 60-GHz wireless communications,” IEEE Trans. Antennas Propag., vol. 57, no. 10, pp. 2926–2933, Oct. 2009

22. G. Washington, Hwan-Sik Yoon, M. Angelino and W. H. Theunissen, "Design, modeling, and optimization of mechanically Reconfiguration aperture antennas," IEEE Transactions on Antennas and Propagation, vol. 50, no. 5, pp. 628-637, May 2002.

23. H. L. Zhu, S. W. Cheung and T. I. Yuk, "Mechanically pattern Reconfiguration antenna using metasurface," IET Microwaves, Antennas & Propagation, vol. 9, no. 12, pp. 1331-1336, 9 17, 2015.

24. M. S. Alam and A. M. Abbosh, "Beam-Steerable Planar Antenna Using Circular Disc and Four PIN-Controlled Tapered Stubs for WiMAX and WLAN Applications," IEEE Antennas and Wireless Propagation Letters, vol. 15, pp. 980-983, 2016.

25. T. Aboufoul, C. Parini, X. Chen and A. Alomainy, "Pattern-Reconfiguration Planar Circular Ultra Wideband Monopole Antenna," IEEE Transactions on Antennas and Propagation, vol. 61, no. 10, pp. 4973-4980, Oct. 2013

26. P. K. Li, Z. H. Shao, Q. Wang and Y. J. Cheng, "Frequency- and Pattern-Reconfiguration Antenna for Multistandard Wireless Applications," IEEE Antennas and Wireless Propagation Letters, vol. 14, pp. 333-336, 2015.

27. G. H. Huff and J. T. Bernhard, “Integration of Packaged RF MEMS Switches with Radiation Pattern Reconfiguration Square Spiral Microstrip Antennas,” IEEE Trasn. on Ant. and Propag., Vol. 54 (No. 2), p. p. 464-469, 2006.

28. A. G. Besoli and F. D. Flaviis, “A Multifunctional Reconfiguration Pixeled Antenna Using MEMS Technology on Printed Circuit Board,” ," IEEE Transactions on Antennas and Propagation, Vol. 59 ,No. 12, p. p. 4413-4424, 2011.

29. G. Lovat, P. Burghignoli, and S. Celozzi, A tunable ferroelectric antenna for fixed-frequency scanning applications. IEEE Antennas and Wireless Propagation Letters, vol. 5, 2006, pp.353-356

30. J. Taeksoo, H. Yoon, J. K. Abraham and V. K. Varadan, “Ku-Band Antenna Array Feed Distribution Network with Ferroelectric Phase Shifters on Silicon,” IEEE Transactions on Microwave Theory and Techniques, Vol. 54 ,No.3, p. p. 1131-1138, 2006.

31. M. F. Iskander, Z. Q. Yun, Z. J. Zhang, R. Jensen, and S. Redd, Design of a low-cost 2-D beamsteering antenna using ferroelectric material and the CTS technology. IEEE Transactions on Microwave Theory and Techniques, vol. 49, no. 5, pp. 1000-1003, 2001.

32. W. Kim, M. F. Iskander and W. D. Palmer, “An Integrated Phased Array Antenna Design Using Ferroelectric Materials and the Continuous Transverse Stub Technology,” IEEE Trasn. on Ant. And Propag., Vol. 54, No. 11, p. p. 3095-3105, 2006.

33. Y. Yashchyshyn, and J. W. Modelski, Rigorous analysis and investigations of the scan antennas on a ferroelectric substrate. IEEE Transactions on Microwave Theory and Techniques, vol. 53, No. 2, pp. 427-438, 2005.

34. A. Edalati and T. A. Denidni. Frequency selective surfaces for beam-switching applications. IEEE Transactions on Antennas and Propagation, 61(1):195–200, 2013.

35. M. Niroo-Jazi and T. A. Denidni. Electronically sweeping-beam antenna using a new cylindrical frequency-selective surface. IEEE Transactions on Antennas and Propagation, 61(2): 666–676, 2013.

36. Li Zhouyuan, E. Ahmed, A. M. Eltawil, and B. A. Cetiner. A beam-steering Reconfiguration antenna for WLAN applications. Antennas and Propagation," IEEE Transactions on Antennas and Propagation, 63(1): 24– 32, 2015.

37. L. Zhang, Q. Wu, and T. A. Denidni. Electronically radiation pattern steerable antennas using active frequency selective surfaces. IEEE Transactions on Antennas and Propagation,61(12):6000–6007, 2013.

38. J Chang won, L Ming-jer, G. P. Li, and F. De Flaviis. Reconfiguration scan-beam singlearm spiral antenna integrated with RF-MEMS switches. IEEE Transactions on Antennas and Propagation, 54(2):455–463, 2006.

39. A. Edalati and T. A. Denidni, "High-Gain Reconfiguration Sectoral Antenna Using an Active Cylindrical FSS Structure," IEEE Transactions on Antennas and Propagation, vol. 59, No. 7, pp. 2464-2472, July 2011.